MODELING AND OPTIMIZATION OF ACMV SYSTEMS FOR ENERGY EFFICIENT SMART BUILDINGS

DEQING ZHAI

2019

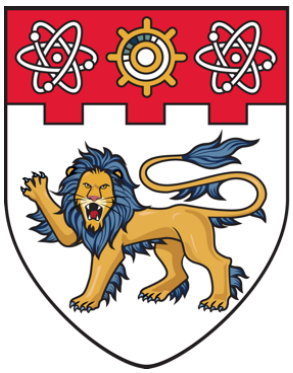

NANYANG TECHNOLOGICAL UNIVERSITY

SINGAPORE

MODELING AND OPTIMIZATION OF ACMV SYSTEMS FOR ENERGY EFFICIENT SMART BUILDINGS

DEQING ZHAI

SCHOOL OF ELECTRICAL AND ELECTRONIC ENGINEERING

2019

MODELING AND OPTIMIZATION OF ACMV SYSTEMS FOR ENERGY EFFICIENT SMART BUILDINGS

DEQING ZHAI

School of Electrical and Electronic Engineering

A thesis submitted to the Nanyang Technological University
in partial fulfilment of the requirement for the degree of
Doctorate of Philosophy

2019

Statement of Originality

I hereby certify that the work embodied in this thesis is the reearsult of original research, is free of plagiarised materials, and has not been submitted for a higher degree to any other University or Institution.

Deqing Zhai

28 March 2019

.....

Date

.....

Author

Supervisor Declaration Statement

I have reviewed the content and presentation style of this thesis and declare it is free of plagiarism and of sufficient grammatical clarity to be examined. To the best of my knowledge, the research and writing are those of the candidate except as acknowledged in the Author Attribution Statement. I confirm that the investigations were conducted in accord with the ethics policies and integrity standards of Nanyang Technological University and that the research data are presented honestly and without prejudice.

Yeng Chai Soh

28 March 2019

.....

Date

.....

Supervisor

Authorship Attribution Statement

This thesis contains material from six papers published in the following peer-reviewed journals and conferences where I was the first and/or corresponding author.

Chapter 4 is partially published as **D. Zhai**, T. Chaudhuri and Y. C. Soh, "Modeling and optimization of different sparse augmented firefly algorithms for acmv systems under two case studies," Building and Environment, vol. 125, pp. 129-142, 2017.

The contributions of the co-authors are as follows:
(1) Prof. Soh provided the initial research direction and suggestions to the manuscript.
(2) Chaudhuri provided comments on the manuscript and collaborated on the experiments.
(3) I conducted the indoor thermal comfort and energy consumption experiments, prepared and revised the manuscript.

Chapter 4 is partially published as **D. Zhai** and Y. C. Soh, "Balancing indoor thermal comfort and energy consumption of acmv systems via sparse swarm algorithms in optimizations," Energy and Buildings, vol.

149, pp. 1-15, 2017.

The contributions of the co-authors are as follows:
(1) Prof. Soh provided the initial research direction and suggestions to the manuscript.
(2) I conducted the different optimization schemes and modeling experiments, prepared and revised the manuscript.

Chapter 4 is partially published as **D. Zhai** and Y. C. Soh, "Balancing indoor thermal comfort and energy consumption of air-conditioning and mechanical ventilation systems via sparse Firefly algorithm optimization," IEEE 30th International Joint Conference on Neural Networks (IJCNN), pp. 1488-1494, Anchorage, Alaska, U.S.A., 2017.

The contributions of the co-authors are as follows:
(1) Prof. Soh provided the initial research direction and suggestions to the manuscript.
(2) I conducted experiments for energy consumption and thermal comfort evaluation of ACMV systems, prepared and revised the manuscript.

Chapter 4 is partially published as **D. Zhai**, Y. C. Soh and W. Cai,

"Operating points as communication bridge between energy evaluation with air temperature and velocity based on extreme learning machine (ELM) models," IEEE 11th International Conference on Industrial Electronics and Applications (ICIEA), pp. 712-716, Hefei, Anhui, China, 2016.

The contributions of the co-authors are as follows:
(1) Prof. Soh provided the initial research direction and suggestions to the manuscript.
(2) Prof. Cai provided experimental platform in school of electrical and electronic engineering.
(3) I conducted experiments for energy modeling of ACMV systems, prepared and revised the manuscript.

Chapter 5 is partially published as **D. Zhai**, T. Chaudhuri, Y. C. Soh, X. Ou and C. Jiang, "Improvement of Energy Efficiency of Markov ACMV Systems based on PTS Information of Occupants," IEEE World Congress on Computational Intelligence (WCCI), Rio de Janeiro, Brazil, 2018.

The contributions of the co-authors are as follows:

(1) Prof. Soh provided the initial research direction and suggestions to the manuscript.
(2) Chaudhuri conducted thermal comfort experiments.
(3) Ou and Jiang provided comments and suggestions on the manuscript.
(4) I conducted experiments of ACMV systems and modeling, prepared and revised the manuscript.

Chapter 5 is partially published as **D. Zhai**, T. Chaudhuri and Y. C. Soh, "Energy efficiency improvement with k-means approach to thermal comfort for acmv systems of smart buildings," IEEE Asian Conference on Energy, Power and Transportation Electrification (ACEPT), pp. 203-208, Singapore, 2017.

The contributions of the co-authors are as follows:
(1) Prof. Soh provided the initial research direction and suggestions to the manuscript.
(2) Chaudhuri conducted thermal comfort surveys, and modeled with k-menas approach.
(3) I conducted experiments of ACMV systems, prepared and revised the manuscript.

Deqing Zhai

28 March 2019

Date

Author

Acknowledgements

First and foremost, I would like to sincerely thank my supervisor, Prof. Soh Yeng Chai, for his guidance, advise and wisdom. He encouraged me to think independently and critically on research topics and projects, and he not only gave me precious opportunities to collaborate with Prof. Cai Wenjian in EEE-ERI@N Joint ACMV laboratory, and learn to work collaboratively with our collaborators, but also he provided me chances to attend international conferences. I also would like to give my thanks to Nanyang Technological University (NTU) for providing the financial support and training through the teaching assistant programme.

I also want to express my sincere thanks to my friends at NTU. Importantly, I shared my precious memories with my mates from Prof. Soh's group: Xu Jinming, Chen Zhenghua, Jiang Chaoyang. Mustafa Khalid Masood, Zhu Qingchang and Tanaya Chaudhuri. I especially would like to thank fellow researchers from Prof. Cai's group: Luo Yunhui, Yang Chao, Liu Mengchen, Huang Chongning, Wang Leyuan, Wang Xinli, Chen Can, Chen Haoran, Shen Suping, Ji Ke, Li Xian, Wu Bingjie, Cui Can, Xu Yingjun, Wu Qiong and Hong Wei in the EEE-ERI@N Joint ACMV laboratory at which I stayed for the last one year of my PhD candidature. I also had a wonderful time with my other labmates: Guan Zheming, Wei Zhe, Wei Chen, Zhao Wei, Zhang Shuai and Guo Huiting.

I am also greatly indebted to Prof. Li Hua and Prof. Ling Keck Voon, of the School of Mechanical and Aerospace Engineering and School of Electrical and Electronic Engineering respectively. They provided me many wonderful ideas and different ways of thinking in my research and studies in our annual Thesis Advisory Committee (TAC) meetings since my first year of PhD candidature. Especially, they discussed with me regarding my future endeavors, which encouraged and inspired me to do the very best possible. I also want to thank my apartment owners for their heartfelt care and support during my PhD candidature in Singapore over these years.

At last, special thanks must go to my dear parents and grandparents for their precious love and unconditional support. Moreover, I would like to thank my elder sister and younger brothers for their support and encouragement since my childhood time, and I also would like to express my special thanks to my fiancee Yang Fan for her perseverance in loving and supporting me during my whole PhD candidature.

Table of contents

Abstract

Modeling and optimization for energy efficient smart buildings are interesting and promising research areas. According to Paris Protocol signed in 2015, energy efficient, smart and green buildings are imperative concerns. Heating, ventilation and air-conditioning (HVAC) or air-conditioning and mechanical ventilation (ACMV) systems, consume around 40% of the total energy, and the systems also directly impact on the environmental conditions, especially the indoor environmental conditions, such as air temperature, air humidity, air velocity, air quality, etc. In this thesis, the main objective is to systematically optimize the ACMV systems to operate efficiently and maintain indoor environmental conditions as comfortable and healthy as possible for occupants. The thesis is organized into the following systematic three-phase methodology to enhance ACMV systems' energy efficiency and indoor occupants' thermal comfort in smart buildings:

- Phase 1: Modeling energy consumption of ACMV systems with machine learning techniques.
- Phase 2: Modeling thermal comfort sensations of occupants with passive and active approaches.
- Phase 3: Formulating and solving optimization problems to enhance smart

buildings' energy efficiency and maintaining indoor thermal comfort sensations of occupants under different algorithms.

Summary of key contributions:

- The author established an indoor environmental condition monitoring and data acquisition system in the thermal laboratory of Nanyang Technological University. The author has also completed a ML-based control algorithm for the ACMV systems of the laboratory. The details are discussed in Chapter 3.
- The author proposed and validated ML-based energy models of ACMV systems and ML-based thermal comfort models of occupants. The author firstly integrated both of these ML-based models for energy efficient smart buildings. The details are discussed in Chapter 5.
- The author proposed and validated nature inspired augmented firefly algorithm (AFA) on the laboratory platform for studying energy efficiency and thermal comfort, and has also examined and compared the AFA with other relevant algorithms, namely classic firefly algorithm (FA) and Bayesian Gaussian process optimization (BGPO). The details are discussed in Chapter 4 and Chapter 5.

Summary of key findings:

The proposed passive approach is largely based on environmental parameters under physical laws, while the proposed active approach is based on physiological parameters of occupants, both incorporated with machine learning techniques.

- The proposed passive approach of predicted mean vote method achieved an accuracy of 70% with about 15% energy saving on average.

- The proposed active approach of k-means method achieved an accuracy of 90% with about 21% energy saving on average.
- The proposed active approach of neural networks method achieved an accuracy of 98% with about 13.5% energy saving on average.
- Augmented firefly algorithm (AFA) outperformed classic firefly algorithm (FA) and Bayesian Gaussian processes optimization (BGPO) in terms of computational complexity and flexibility.

List of Figures

List of Tables

Nomenclature

The following tables describes nomenclatures used throughout this thesis.

Abbreviation	**Description**	**Unit**
ACMV	Air-Conditioning and Mechanical Ventilation	—
AHU	Air Handling Unit	—
AMV	Actual Mean Vote	—
CSE	Comfort Sensation Evaluation	—
EEE	Energy Efficiency Evaluation	—
ESR	Energy Saving Rate	—
HVAC	Heating and Ventilation Air-Conditioning	—
LDU	Liquid Dehumidification Unit	—
NN	Neural Networks	—
PMV	Predicted Mean Vote	—
PPD	Predicted Percentage Dissatisfied	—
PTS	Predictive Thermal State	—
WCU	Water Chilling Unit	—
λ	User-Preference Parameter	—
ϕ	Relative Humidity	%
A	Area	m^2
D	Diameter	m
E	Energy (Power) Consumption of ACMV Systems	kW
ω	Operating Frequency of ACMV Systems	Hz
F	Angle Factor between Occupant and Surface	—
M	Metabolic Rate	W/m^2
P	Pressure	Pa
Q	Heat Transfer Rate of Occupant	W/m^2
T	Temperature	$^\circ C$
V	Velocity	m/s
W	External Mechanical Work-done	W/m^2

The following tables describes nomenclatures used throughout this thesis.

Subscript		
a	Air	
atv	Active	
cl	Clothing	
$comp$	Compressor	
$cond$	Condenser	
$diff$	Diffusion	
du	DuBois	
$evap$	Evaporation	
g	Globe	
$grad$	Gradient	
mr	Mean Radiant	
$norm$	Normalized	
obj	Objective	
psv	Passive	
$pump$	Water Pump	
$resp$	Respiration	
saf	Supply-Air Fan	
sf	Surface	
sk	Skin	
Superscript		
$ambt$	Ambient	
$duct$	Duct	
$envt$	Environmental	
Special Term		
f_{cl}	Ratio of Surface Area of Clothed over Naked	—
h_c	Convection Heat Transfer Coefficient	$W/(Km^2)$
h_r	Radiant Heat Transfer Coefficent	$W/(Km^2)$
I_{cl}	Clothing Insulation Factor	m^2K/W or clo

Chapter 1

Introduction

1.1 Overview of ACMV Systems

This PhD study aims to enhance energy efficiency of centralized air-conditioning systems and indoor thermal comfort sensations of occupants in smart buildings. Since the energy efficiency and indoor thermal comfort are directly influenced by operating conditions of Air-Conditioning and Mechanical Ventilation (ACMV) systems, thus this study could have significant impacts on energy conservation, global warming gas (mainly CO_2) emission reduction and healthy indoor environment.

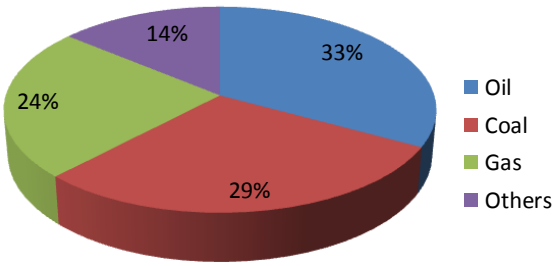

Figure 1.1: Percentages of Energy Resources Compositions 2016

According to World Energy Council report 2016, currently 86% of the current energy resources are still dependent on non-renewable fossil-fuel resources, such as coal, oil and natural gas. The other renewable energy resources (i.e. nuclear, hydro, wind and solar) only account for 14% to the current consumption of energy resources, as illus-

trated in Figure 1.1. However, according to the statistics from real-time meters, oil will be depleted in about 40-50 years, and about 160 years and 410 years respectively for natural gas and coals [37]. Therefore, the issues of diminishing energy resources have been gaining more and more attentions all over the world. The concept of energy efficiency has been applied into multiple fields, such as buildings, transportation, manufacture, industry and so forth in attempts to optimize energy usage. One of the major current concerns is the ever increasing number of buildings in cities. In the scope of my studies, the energy efficiency of smart buildings is the study focus. According to the statistical energy profiles of buildings, some of the major energy consuming parts are the Air-Conditioning and Mechanical Ventilation (ACMV) systems [56]. Generally, ACMV systems would account for 40% - 60% of the total energy consumed by buildings [56] as shown in Figures 1.2 and 1.3 for commercial and residential buildings respectively. The ACMV systems are represented by the portions of space heating, space cooling, ventilation, water heating and refrigeration for both commercial and residential buildings.

1.2 Motivations and Objectives

Based upon the agreed Paris Protocol in Paris Climate Conference 2015, global climate change targets were acknowledged worldwide. One of the targets is to keep a globally environmental temperature increment of below $2°C$ by year 2020 [1]. Singapore actively took part in this campaign and made a pledge with a target of "7% - 11%" emission reduction under the conditions of "business-as-usual" by the year of 2020 [37].

Based upon the statistics of European Union (EU) and the United States, buildings generally consume around 40% of the total energy generated from power plants

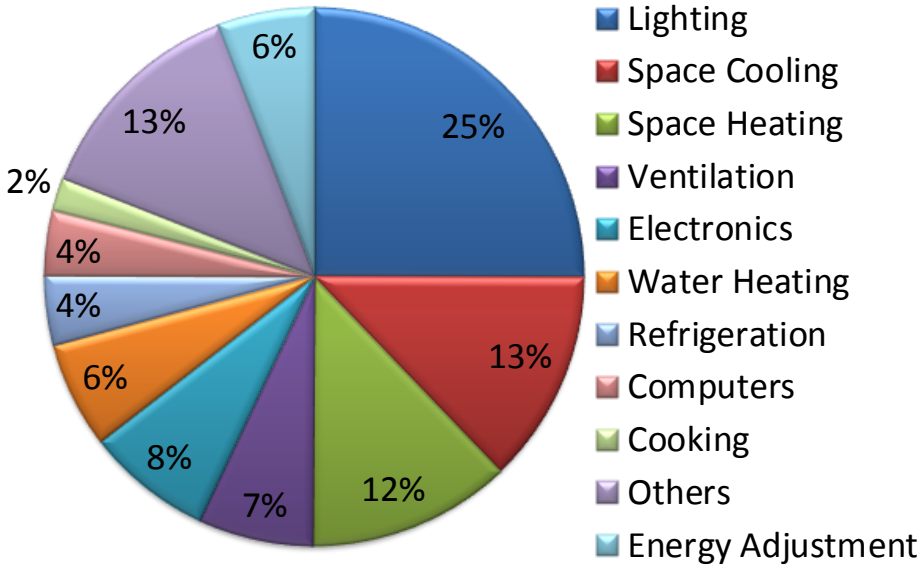

Figure 1.2: Percentages of Commercial Buildings Energy Compositions

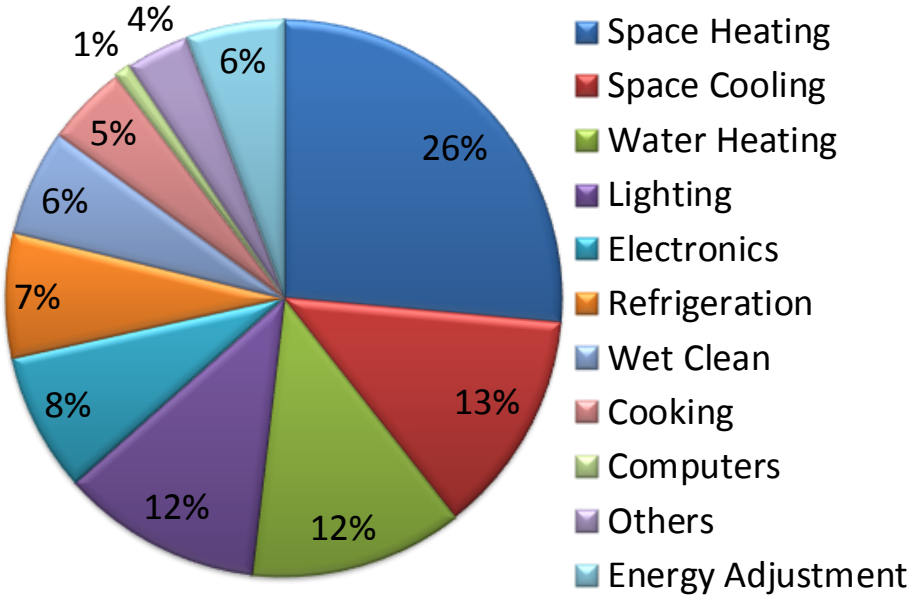

Figure 1.3: Percentages of Residential Buildings Energy Compositions

[46, 50]. Among the total energy consumed by buildings, Air-Conditioning and Mechanical Ventilation (ACMV) systems generally account for around 40%-60% [5, 46]. While consuming much energy, the ACMV systems significantly control the indoor environmental conditions, which can directly affect the productivity and health of indoor occupants as reported in the studies of Zhang et al. [98]. Moreover, according to the research from Berkeley National Laboratory, people generally spend an average of around 90% of the total time each day staying inside buildings [44]. Thus, it is important to optimally balance the ACMV systems' energy efficiency and occupants' indoor thermal comfort for the sake of energy saving, productivity and health.

Additionally, motivated by the current resource limitations and serious global environmental issues, the author aims to improve on buildings' energy efficiency and indoor environmental conditions for occupants by examining the operation of ACMV systems. Since ACMV systems have a significant role of consuming energy and maintaining indoor environmental conditions, the optimizations and balancing buildings' energy efficiency and indoor thermal comfort sensations of occupants will be promising and meaningful solutions to partly address the global environmental and diminishing energy resources issues. This is the motivation which drives the author to research and study the relevant problems. In order to better study the related topics, a thermal laboratory was built up at School of Electrical and Electronic Engineering, Nanyang Technological University, Singapore. This thermal laboratory is equipped with an isolated Air-Conditioning and Mechanical Ventilation (ACMV) systems. The ACMV systems consist of Air-Handling Unit (AHU), Liquid Dehumidification Unit (LDU), Water Chiller Unit (WCU) and all air ducts,water and refrigerant piping connections.

The objectives of this study can be divided into the following three steps:

- Phase 1: Modeling energy consumption of ACMV systems with machine learning data-driven approaches.

- Phase 2: Modeling indoor thermal comfort sensations of occupants with machine learning passive and active approaches. The passive approach is mainly based on environmental parameters, while the active approach directly focuses on physiological parameters of occupants.

- Phase 3: Formulating problems and optimizing on enhancing smart buildings' energy efficiency and maintaining indoor thermal comfort sensations of occupants.

To illustrate the thesis objectives and motivations clearly, Figure 1.4 presents a key overview flowchart of the study.

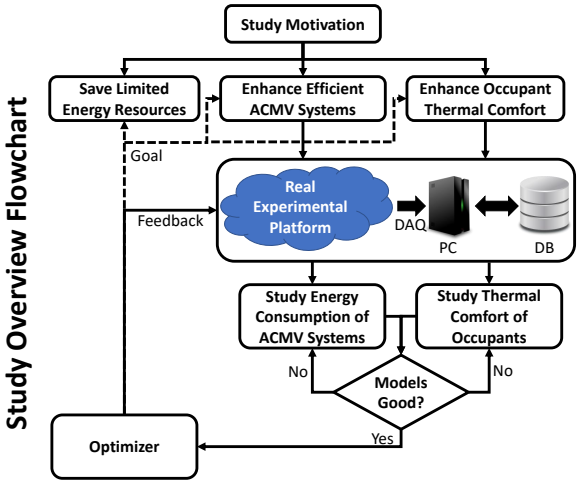

Figure 1.4: Study Overview Flowchart

For each of the phases mentioned above, specific methodologies are to be examined in subsequent chapters. The objective is to investigate a systematic way of modeling and optimizing the ACMV systems in thermal laboratory. Based upon the studies of

the ACMV systems, general solutions to modern smart buildings can be achieved by integrating energy models and indoor thermal comfort models. This systematic way of modeling and optimization can be utilized to improve buildings' energy efficiency and maintain occupants' indoor thermal comfort sensations.

1.3 Key Contributions

The objective of this thesis is to systematically model and optimize the operation of ACMV systems for enhancing smart buildings' energy efficiency and thermal comfort levels of occupants. Through innovations and experimental verifications, the key contributions of this thesis can be summarized as follows:

1. **Data Acquisition System of ACMV Systems**

   In order to model and optimize the operation of air-conditioning and mechanical ventilation (ACMV) systems, the author developed the necessary data acquisition system to monitor indoor environmental and occupant physiological parameters. The details are discussed in Chapter 3.

2. **Control System of ACMV Systems**

   In order to conduct experiments in the laboratory, the author also developed a machine learning based control algorithm for enhancing the energy efficiency of ACMV systems and thermal comfort of occupants. The details are discussed in Chapter 3, Chapter 4 and Chapter 5.

3. **Energy Model of ACMV Systems**

   The author proposed and applied machine learning (ML) approaches for the en-

ergy consumption prediction of the ACMV laboratory platform in the School of Electrical and Electronic Engineering, Nanyang Technological University. The energy model had inputs of supply air fan frequency, compressor frequency and water pump frequency, and output of energy consumption prediction. The energy model covered water chiller unit (WCU) and air handling unit (AHU). Traditionally, the energy consumption of AHU and WCU is examined by power meters measuring currents and voltages, which make them complex and not real-time. Therefore, an ML-based energy model has been proposed to predict energy consumption in real-time and without increasing the systems' complexity. Different from conventional approaches, the energy model was developed by a supervised data-driven method with a novel cost function proposed by the author. The datasets were randomly divided into two sub-datasets, namely training datasets (80%) and testing datasets (20%), and the random divisions of datasets were carried out 10 rounds for trainings and testings. The energy model was trained by back-propagation (BP) with a mean squared error (MSE) cost function Eq. 1.1 which introduced by the author. The final models were cross-validated with the 10 rounds of randomly divided testing datasets to avoid over-fitting and model-biasing. Further details are presented in Chapter 3.

Cost Function (Refer to Eq. 2.23 for details):

$$J(\mathbf{\Theta^{(2)}}, \mathbf{\Theta^{(1)}}|\mathbf{X}) = \frac{1}{m}\sum_{i=1}^{m}\sum_{j=1}^{p}(y_{i,j} - y_{i,j}^{*})^2 + \frac{\lambda}{m}\left(\sum_{u=0}^{n}\sum_{v=1}^{ka}(\theta_{u,v}^{(1)})^2 + \sum_{u=0}^{ka}\sum_{v=1}^{p}(\theta_{u,v}^{(2)})^2\right) \tag{1.1}$$

4. **Thermal Comfort Model of Indoor Occupants**

The author proposed and applied machine learning (ML) approaches for thermal comfort prediction of occupants. According to the sensory data sources,

the models had been classified into two categories, namely passive and active models. The passive model is largely based on environmental parameters, while the active model is focused on occupant physiological parameters. Further details are presented in Chapter 3, Chapter 4 and Chapter 5.

Passive Model: With the environmental sensory data of air temperature, pressure, humidity and velocity, and operating frequencies of supply air fan, compressor and water pump, supervised ML-based air temperature and velocity models were proposed and applied into Fangers predicted mean vote (PMV) model to estimate indoor thermal comfort levels of occupants. The models had inputs of supply air fan frequency, compressor frequency and water pump frequency, and outputs of air temperature and velocity. The training and testing processes followed the same procedures as energy models. The cost function also followed the MSE cost function Eq. 1.2 which is introduced by the author. The cross-validations were also carried out with 10 rounds of randomly divided datasets to avoid over-fitting and biasing.

Cost Function (Refer to Eq. 2.23 for details):

$$J(\mathbf{\Theta^{(2)}}, \mathbf{\Theta^{(1)}}|\mathbf{X}) = \frac{1}{m}\sum_{i=1}^{m}\sum_{j=1}^{p}(y_{i,j} - y_{i,j}^{*})^2 + \frac{\lambda}{m}\left(\sum_{u=0}^{n}\sum_{v=1}^{ka}(\theta_{u,v}^{(1)})^2 + \sum_{u=0}^{ka}\sum_{v=1}^{p}(\theta_{u,v}^{(2)})^2\right) \tag{1.2}$$

Active Model: With the recorded physiological data of occupant, namely skin temperature, height, weight and gender, occupants were asked to feedback on questionnaires under air-conditioned experiments. Supervised ML-based thermal comfort prediction models were then proposed and validated through physi-

ological parameters. The models had inputs of skin temperature, height, weight, gender and clothing factor, and output of thermal comfort levels based on 7-scale quantification. Through careful studies, the author proposed the following normalization method for standardizing the physiological parameters of different subjects as presented below (Refer to Eq. 2.43 and Eq. 2.44 for details).

$$\begin{aligned} T_{sk} &= T_{hand} \\ T_{sk,norm} &= \frac{T_{sk}}{A_{norm}} \end{aligned} \tag{1.3}$$

where

$$\begin{aligned} A_{norm} &= (1 - I_{cl}) \cdot A_{du} \\ A_{du} &= Weight^{0.425} \times Height^{0.725} \times 0.203 \end{aligned} \tag{1.4}$$

The training and testing processes followed the same procedures as energy models. The cost function also followed the MSE cost function Eq. 1.5 introduced by the author. The cross-validations were also carried out with 10 rounds of randomly divided datasets to make sure the models avoid over-fitting and biasing.

Cost Function (Refer to Eq. 2.23 for details):

$$J(\mathbf{\Theta^{(2)}}, \mathbf{\Theta^{(1)}}|\mathbf{X}) = \frac{1}{m}\sum_{i=1}^{m}\sum_{j=1}^{p}(y_{i,j} - y^*_{i,j})^2 + \frac{\lambda}{m}\left(\sum_{u=0}^{n}\sum_{v=1}^{ka}(\theta^{(1)}_{u,v})^2 + \sum_{u=0}^{ka}\sum_{v=1}^{p}(\theta^{(2)}_{u,v})^2\right) \tag{1.5}$$

The active models with different feature selections were also proposed and examined by the author in this PhD study. A total of 4 categories with 15 combinational features was proposed by the author and it is tabulated in Table 1.1.

Table 1.1: Feature Selection Study

Category	Features
1-Feature	T_{sk}
	T_{sk_grad}
	T_{sk_norm}
	$T_{sk\_grad\_norm}$
2-Feature	$T_{sk} + T_{sk\_grad}$
	$T_{sk\_norm} + T_{sk\_grad}$
	$T_{sk} + T_{sk\_grad\_norm}$
	$T_{sk} + T_{sk\_norm}$
	$T_{sk\_grad} + T_{sk\_grad\_norm}$
	$T_{sk\_norm} + T_{sk\_grad\_norm}$
3-Feature	$T_{sk} + T_{sk\_norm} + T_{sk\_grad}$
	$T_{sk} + T_{sk\_grad} + T_{sk\_grad\_norm}$
	$T_{sk} + T_{sk\_norm} + T_{sk\_grad\_norm}$
	$T_{sk\_norm} + T_{sk\_grad} + T_{sk\_grad\_norm}$
4-Feature	$T_{sk} + T_{sk\_norm} + T_{sk\_grad} + T_{sk\_grad\_norm}$

5. **Computational Optimization Algorithm**

The author proposed an augmented firefly algorithm (AFA), which was based on the concepts of Monte Carlo random process and computational intelligence. The AFA had also been compared and validated with other relevant algorithms, namely firefly algorithm (FA) and Bayesian Gaussian process optimization (BGPO), and six different schemes of AFA were also proposed and discussed by the author in this study. They are AFA-SRUW, AFA-SRGW-I, AFA-SRGW-II, AFA-LRUW, AFA-LRGW-I and AFA-LRGW-II. The key innovations and enhancements of AFA are summarized as follows:

(a) The inner for-loops were removed, so that the computational complexity is

reduced from $O(n^2)$ to $O(n)$. Please refer to Algorithm 8 and Algorithm 11. The computational efficiency was significantly enhanced.

(b) Distance coefficient (α), vortex coefficient (γ), randomness coefficient (β), randomness mode switch (ϵ) and searching mode switch (s) were introduced (Refer to Algorithm 11 for details) as presented below.

$$\mathbf{x}_i^{new} = \mathbf{x}_i^{old} + \alpha \cdot \gamma \left(\mathbf{x}_{max} - \mathbf{x}_i^{old} \right) + \beta \cdot \left[(\Delta B - 1) \cdot s + 1 \right] \cdot \epsilon$$

$$\mathbf{x}_i^{new} = \mathbf{x}_i^{old} + \beta \cdot \left[(\Delta B - 1) \cdot s + 1 \right] \cdot \epsilon$$

With the hyper-parameters α, γ, β, ϵ and s introduced, the algorithm was verified to be able to effectively locate high performance solutions without being trapped into sub-optima.

(c) The update of solutions were targeted on optimal solution directly with vortex linearized movements as shown below, instead of exponential movements in classic FA.

$$\mathbf{x}_i^{new} = \mathbf{x}_i^{old} + \alpha \cdot \gamma \left(\mathbf{x}_{max} - \mathbf{x}_i^{old} \right) + \beta \cdot \left[(\Delta B - 1) \cdot s + 1 \right] \cdot \epsilon$$

(d) A user-preference tuning parameter (λ) between energy efficiency and thermal comfort had been proposed by the author to allow for trade-off of energy efficiency and thermal comfort in smart buildings:

$$f_{obj}(\cdot) = \lambda \cdot EEE_{norm} + (1 - \lambda) \cdot CSE_{norm}$$

The above cost function served as the central objective function of optimization

algorithms of classic firefly algorithm, augmented firefly algorithm and Bayesian Gaussian process optimization. Further details are discussed in Chapter 4 and Chapter 5.

1.4 Organization of Thesis

The organization of this thesis is presented as follows:

- Chapter 2 presents the literature reviews on relevant research articles related to this study. In order to adequately and clearly understand the available results and developments relevant to the studies of energy efficiency and thermal comfort, this review is divided into 4 sub-areas. Firstly, different data-driven modeling techniques are examined. Secondly, different indoor thermal comfort evaluation techniques are presented. Thirdly, different optimization techniques for resolving the optimal solutions to the formulated problems are reviewed. Lastly, recent studies on balancing buildings' energy efficiency and indoor thermal comfort of occupants are presented.

- Chapter 3 briefly describes the methodologies on how to address the solutions to the formulated problem based on the objective of this study. There are four basic steps to resolve this problem. First, the methodologies of energy consumption modeling of buildings are presented. Second, the methodologies of indoor thermal comfort modeling of occupants are presented. Third, problem formulations with user-preference parameters are described with constraint boundaries. Lastly, different optimization algorithms are evaluated and compared based on benchmark testing functions.

- Chapter 4 proposes machine learning approaches for energy efficiency evaluations (EEE) under comfort sensation evaluations (CSE) with passive approaches. In the ACMV systems, there are four major energy consuming components that are examined in this study, which are the supply-air-fan motor in AHU; the compressor, the water pump and the condenser in WCU. The most well-known ASHRAE Standard 55 thermal comfort model is developed from P.O. Fanger's PMV model. The passive approaches use the environmental parameters to index thermal comfort of occupants. Three studies are covered in this chapter on energy efficiency and indoor thermal comfort evaluations. The different optimization algorithms are examined for energy efficiency evaluations.

- Chapter 5 proposes machine learning approaches for energy efficiency evaluations (EEE) under comfort sensation evaluations (CSE) with active approaches. The measurements of physiological parameters of occupants serve as models for thermal comfort sensations of occupants. Two studies are conducted in this chapter on energy efficiency and indoor thermal comfort evaluations with different optimization algorithms evaluated and compared.

- Chapter 6 draws conclusions based on the conducted studies, highlights existing limitations and outlines the future research directions of related studies.

Chapter 2

Preliminary

In this chapter, relevant literature and background knowledge are reviewed in details. The literature is classified into machine learning techniques, thermal comfort studies and optimization algorithms. Currently, there are many studies on energy efficiency improvements of buildings. For high latitude regions, the studies are based on heating capacity and demands to enhance energy efficiency of buildings. For medium latitude regions, the season-oriented heating and cooling capacity and demands are significantly differentiated. For low latitude regions, the weather is often rainy and cloudy. The climate is generally of high humidity and high temperature. The cooling capacity and demands are the most desired. Due to the geological constraints, different regions have different and specific cooling or heating profiles. So the gaps between different regions should be resolved with a more generic solution. Parallel to energy efficiency, there are also many studies on thermal comfort. There are three categories among the whole studies of thermal comfort in general, such as passive, active and hybrid thermal comfort evaluations. The passive thermal comfort evaluation is largely based on environmental parameters to predict thermal comfort levels of occupants, while an active thermal comfort evaluation depends on physiological parameters of occupants directly. The hybrid thermal comfort evaluation basically adopts both passive and active evaluations and may try to find a trade-off for implementation or accu-

racy. The active approach could be intrusive, while the passive approach could be time-consuming for implementation. Furthermore, the gaps between current energy efficiency improvement and thermal comfort are also not well addressed yet. Due to inherent complex coupling and correlations among energy consumption, environment control and occupant thermal comfort, there are various research gaps that require further examinations and studies in order to better understand and resolve the relationships within the complex coupling and correlations.

In the section on machine learning, literature on data-driven machine learning technique, such as neural networks back-propagation with batch/stochastic gradient descent, is reviewed. The theoretical backgrounds and applications are also discussed, such as learning strategies and optimizations for low cost functions.

In the section on thermal comfort studies, literature on passive and active approaches are discussed for evaluating the indoor thermal comfort sensations of occupants. The passive approaches basically utilize environmental parameters (i.e. air temperature, air velocity, air relative humidity, mean radiant temperature, etc.) and few occupant parameters (i.e. metabolic rate and clothing insulation factor, etc.) to predict thermal sensations of occupants, typically represented by Fanger's model. The active approaches directly make use of occupant physiological parameters (i.e. skin temperature, metabolic rate, heart rate, blood pressure, etc.) to investigate the predictive models for thermal sensations.

In the section on optimization algorithms, literature on certain typical optimization algorithms are reviewed. These optimization algorithms are grouped into three categories, which are nature-inspired algorithms, Bayesian optimizations and analytic algorithms. The nature-inspired algorithms are genetic algorithm, particle swarm optimization, firefly algorithm and augmented firefly algorithm. The Bayesian optimiza-

tions are governed by assumptions of Gaussian processes of sample distribution. The analytic algorithms are batch/stochastic gradient descent algorithms and quadratic programming for convex optimization problems.

2.1 Machine Learning

In this section, different modeling techniques are elaborated. In this study, data-driven machine learning models are applied. The basic idea of these models is to exploit big data and artificial intelligence. The models, trained by the collected big data, provide straight-forward and accurate solutions in our current studies.

2.1.1 Introduction

Since Frank Rosenblatt discovered the concept of perceptron to mimic neural neurons for computer sciences and engineering [63] in 1957, the dreams and efforts to achieve intelligence in machines since then have never stopped [45, 77]. Nowadays, the terms "artificial intelligence (AI)" or specifically "machine learning (ML)" are found everywhere in the fields of computer science studies. The effects were pushed even further when the AlphaGo Zero from Google DeepMind achieved a remarkable 100-0 competition result through reinforcement learning techniques [70] without prior knowledge of human inputs. The basic idea of reinforcement learning is to maximize reward function and minimize cost function after a long period of running. Since there are only regulations and rules declared without any prior knowledge, the learning processes of models are undertaken by numerous attempts to locate the best outcomes.

Besides reinforcement learning, there are two more machine learning categories, which are supervised learning and unsupervised learning. The main difference between these two learning ideologies is their training targets. For supervised learning, the training inputs and outputs are well labeled, however the unsupervised learning only uses training inputs without labeling. Therefore, the supervised learning can be more widely applicable for solving regression problems and classification problems. As for

regression problems, there are several methods such as neural networks, linear regression, logistic regression, non-parametric regression, etc. As for classification problems, some typical methods are neural networks, decision trees, support vector machine, etc. On the other hand, unsupervised learning mainly solves the classification problems by some typical methods, such as neural networks, clustering, k-means, hierarchical, principle component analysis, etc. Moreover, there is an in-between technique called semi-supervised learning. It attempts to draw on the benefits from supervised and unsupervised learnings. The basic idea is to label training inputs and output partially that could reduce the costs of labeling and training efforts with the benefits of unsupervised learning, and provide fairly low modeling errors with the guidance of supervised learning.

In this thesis, machine learning techniques are mainly investigated in detail for modeling energy consumption and environmental parameters of smart buildings and indoor thermal comfort sensations of occupants. Since it is important to balance indoor thermal comfort of occupants and energy-efficiency of ACMV systems, there is also a need to review different optimization algorithms in this study.

2.1.2 Supervised Learning

Currently, Artificial Intelligence (AI) has found wide applications in different fields from computer science to biological science [25], from chess games to AlphaGo. In addition, the core of artificial intelligence is originated from "machine learning" through a large number of training data or pre-defined regulations. The supervised learning is based on labeled training input and output pairs. The word "labeled" here means that the outputs of training inputs are validated by correct results from the perspective of human beings. It is often a laborious task to label large amount of

data, especially in the era of big data nowadays. For instance, the cat-dog problem is a supervised learning problem where a computer is to be trained to differentiate an image of a cat or a dog [59, 97]. The training inputs are numerous images of cats and dogs, but the training outputs are different. The training images of cats are labeled as 1s for the training outputs, while those of dogs are labeled as 0s. There are a number of state-of-the-art architectures and topologies of supervised learning, such as Neural Networks (NN), Convolution Neural Networks (CNN), Recurrent Neural Networks (RNN), Deep Learning (DL), Linear Regression (LinReg), Polynomial Regression (PolyReg), Logistic Regression (LogReg), Decision Tree, Random Forest, Naive Bayes, K Nearest Neighbors (KNN), etc. The supervised learning techniques are effectively and mostly applied for solving regression and classification problems. However, this mode of learning is not the same natural way as human being learning. Human beings can differentiate cat or dog by only learning a few pictures of cats and dogs in advance. Some key formulations of these topologies are summarized below.

Linear Regression (LinReg)

There are many problems that examine the relationships between one feature and another [84]. For instance, the corresponding relationship between the energy consumption of a city and its population is the kind of problem of linear regression study.

The data structure of linear regression is illustrated in detail below. The $\mathbf{X}$ is the m input datasets with n features. The $\mathbf{\Theta}$ is the model's weighted parameters for different features. The $\mathbf{Y}$ is the predicted output of linear regression model. The $\mathbf{Y}^*$ is the training output ground truth for training the model's weighted parameters [84].

Data Structure

$$\mathbf{X} = \begin{bmatrix} x_{1,0} & x_{1,1} & x_{1,2} & \cdots & x_{1,n} \\ x_{2,0} & x_{2,1} & x_{2,2} & \cdots & x_{2,n} \\ \vdots & \vdots & \vdots & \ddots & \vdots \\ x_{m,0} & x_{m,1} & x_{m,2} & \cdots & x_{m,n} \end{bmatrix}, \mathbf{Y} = \begin{bmatrix} y_1 \\ y_2 \\ \vdots \\ y_m \end{bmatrix}, \mathbf{Y}^* = \begin{bmatrix} y_1^* \\ y_2^* \\ \vdots \\ y_m^* \end{bmatrix}, \mathbf{\Theta} = \begin{bmatrix} \theta_0 \\ \theta_1 \\ \theta_2 \\ \vdots \\ \theta_n \end{bmatrix}$$

Model

- Element Form [84]

$$y_i = \theta_0 \cdot x_{i,0} + \theta_1 \cdot x_{i,1} + \cdots + \theta_n \cdot x_{i,n} \quad (i = 1, 2, 3, \cdots, m) \tag{2.1}$$

- Matrix Form [84]

$$\mathbf{Y} = \mathbf{X} \cdot \mathbf{\Theta} \tag{2.2}$$

In order to minimize the errors of models, the cost function is defined under the considerations of mean square error and parameter regularization below.

Cost Function

- Mean Squared Error and Regularization [57]

$$J(\mathbf{\Theta}|\mathbf{X}) = \frac{1}{2m} \sum_{i=1}^{m} (y_i - y_i^*)^2 + \frac{\lambda}{2m} \sum_{j=0}^{n} \theta_j^2 \tag{2.3}$$

- Error Difference

$$err_i = y_i - y_i^* \tag{2.4}$$

To locate the well-tuned parameters for minimizing the cost function, a gradient

descent algorithm is applied as follows by constructing a gradient matrix and updating model's parameters below.

Gradient Matrix

$$\frac{\partial J(\cdot)}{\partial \mathbf{\Theta}} = \begin{bmatrix} \frac{\partial J}{\partial \theta_0} \\ \frac{\partial J}{\partial \theta_1} \\ \frac{\partial J}{\partial \theta_2} \\ \vdots \\ \frac{\partial J}{\partial \theta_n} \end{bmatrix} = \frac{1}{m} \begin{bmatrix} \sum_{i=1}^{m} err_i \cdot x_{i,0} + \frac{\lambda}{m} \cdot \theta_0 \\ \sum_{i=1}^{m} err_i \cdot x_{i,1} + \frac{\lambda}{m} \cdot \theta_1 \\ \sum_{i=1}^{m} err_i \cdot x_{i,2} + \frac{\lambda}{m} \cdot \theta_2 \\ \vdots \\ \sum_{i=1}^{m} err_i \cdot x_{i,n} + \frac{\lambda}{m} \cdot \theta_n \end{bmatrix}$$

Update Model's Parameter $\mathbf{\Theta}$

$$\mathbf{\Theta^{new}} = \mathbf{\Theta^{old}} - \eta \cdot \frac{\partial J(\cdot)}{\partial \mathbf{\Theta}} \tag{2.5}$$

Polynomial Regression (PolyReg)

Similar to linear regression, the polynomial regression also focus on studying the relationships between input feature and another output target. However, many problems are not linear, but curvature in nature [62]. Therefore, there is a function needed to fit non-linear relationship accurately. Thus the main difference is that the input feature is not linear but polynomial terms as shown in the data structure below. That is the reason why it is called polynomial regression. The main objective of polynomial regression is to model the non-linear corresponding between independent and dependent parameters.

The data structure of polynomial regression is presented in detail below. The $\mathbf{X}$ is the m input datasets with n features. The $\mathbf{\Theta}$ is the model's weighted parameters for different features. The $\mathbf{Y}$ is the predicted output of linear regression model. The $\mathbf{Y}^*$

is the training output ground truth for training the model's weighted parameters.

Data Structure

$$\mathbf{X} = \begin{bmatrix} x_1^0 & x_1^1 & x_1^2 & \cdots & x_1^n \\ x_2^0 & x_2^1 & x_2^2 & \cdots & x_2^n \\ \vdots & \vdots & \vdots & \ddots & \vdots \\ x_m^0 & x_m^1 & x_m^2 & \cdots & x_m^n \end{bmatrix}, \mathbf{Y} = \begin{bmatrix} y_1 \\ y_2 \\ \vdots \\ y_m \end{bmatrix}, \mathbf{Y}^* = \begin{bmatrix} y_1^* \\ y_2^* \\ \vdots \\ y_m^* \end{bmatrix}, \mathbf{\Theta} = \begin{bmatrix} \theta_0 \\ \theta_1 \\ \theta_2 \\ \vdots \\ \theta_n \end{bmatrix}$$

Model

- Element Form [62]

$$y_i = \theta_0 + \theta_1 \cdot x_i + \theta_2 \cdot x_i^2 + \cdots + \theta_n \cdot x_i^n \quad (i = 1, 2, 3, \cdots, m) \tag{2.6}$$

- Matrix Form [62]

$$\mathbf{Y} = \mathbf{X} \cdot \mathbf{\Theta} \tag{2.7}$$

In order to minimize the errors of models, the cost function is defined under the considerations of mean square error and parameter regularization below.

Cost Function

- Mean Squared Error and Regularization [57]

$$J(\mathbf{\Theta}|\mathbf{X}) = \frac{1}{2m} \sum_{i=1}^{m} (y_i - y_i^*)^2 + \frac{\lambda}{2m} \sum_{j=0}^{n} \theta_j^2 \tag{2.8}$$

- Error Difference

$$err_i = y_i - y_i^* \tag{2.9}$$

To locate the well-tuned parameters for minimizing the cost function, a gradient descent algorithm is applied as follows by constructing a gradient matrix and updating model's parameters below.

Gradient Matrix

$$\frac{\partial J(\cdot)}{\partial \mathbf{\Theta}} = \begin{bmatrix} \frac{\partial J}{\partial \theta_0} \\ \frac{\partial J}{\partial \theta_1} \\ \frac{\partial J}{\partial \theta_2} \\ \vdots \\ \frac{\partial J}{\partial \theta_n} \end{bmatrix} = \frac{1}{m} \begin{bmatrix} \sum_{i=1}^{m} err_i \cdot x_i^0 + \frac{\lambda}{m} \cdot \theta_0 \\ \sum_{i=1}^{m} err_i \cdot x_i^1 + \frac{\lambda}{m} \cdot \theta_1 \\ \sum_{i=1}^{m} err_i \cdot x_i^2 + \frac{\lambda}{m} \cdot \theta_2 \\ \vdots \\ \sum_{i=1}^{m} err_i \cdot x_i^n + \frac{\lambda}{m} \cdot \theta_n \end{bmatrix}$$

Update Model's Parameter $\mathbf{\Theta}$

$$\mathbf{\Theta^{new}} = \mathbf{\Theta^{old}} - \eta \cdot \frac{\partial J(\cdot)}{\partial \mathbf{\Theta}} \tag{2.10}$$

Logistic Regression (LogReg)

Logistic regression uses a logistic function, or called sigmoid function, to transform inputs into a smooth binary-like outputs [39]. Unlike linear and polynomial regression, the logistic regression is a statistically model dealing with probability problems.

The $\mathbf{X}$ is the m input datasets with n features. The $\mathbf{\Theta}$ is the model's weighted parameters for different features. The $\mathbf{Y}$ is the predicted output of linear regression model. The $\mathbf{Y}^*$ is the training output ground truth for training the model's weighted parameters. $h_{\mathbf{\Theta}}(\cdot)$ is the transforming function, called sigmoid function or logistic function. The data structure of logistic regression is shown in detail below. The logistic regression model is presented in element-wise and matrix-wise afterward as well.

Data Structure

$$\mathbf{X} = \begin{bmatrix} x_{1,0} & x_{1,1} & x_{1,2} & \cdots & x_{1,n} \\ x_{2,0} & x_{2,1} & x_{2,2} & \cdots & x_{2,n} \\ \vdots & \vdots & \vdots & \ddots & \vdots \\ x_{m,0} & x_{m,1} & x_{m,2} & \cdots & x_{m,n} \end{bmatrix}, \mathbf{Y} = \begin{bmatrix} y_1 \\ y_2 \\ \vdots \\ y_m \end{bmatrix}, \mathbf{Y}^* = \begin{bmatrix} y_1^* \\ y_2^* \\ \vdots \\ y_m^* \end{bmatrix}, \mathbf{\Theta} = \begin{bmatrix} \theta_0 \\ \theta_1 \\ \theta_2 \\ \vdots \\ \theta_n \end{bmatrix}$$

Model

- Element Form

$$y_i = \frac{1}{1 + e^{-(\theta_0 \cdot x_{i,0} + \theta_1 \cdot x_{i,1} + \cdots + \theta_n \cdot x_{i,n})}} \tag{2.11}$$

- Matrix Form

$$\mathbf{Y} = h_{\mathbf{\Theta}}(\mathbf{x}) = \frac{1}{1 + e^{-\mathbf{X} \cdot \mathbf{\Theta}}} \tag{2.12}$$

Since the logistic function consists of highly non-linear exponential term, the cost function is different from those of linear and polynomial regressions with some mathematical manipulations illustrated below [57].

Cost Function

- Log Error and Regularization [57]

$$J(\mathbf{\Theta}|\mathbf{X}) = \frac{1}{m} \sum_{i=1}^{m} [C(h_{\mathbf{\Theta}}(\mathbf{x}_i), y_i^*)] + \frac{\lambda}{2m} \sum_{j=0}^{n} \theta_j^2 \tag{2.13}$$

where

$$C(h_{\mathbf{\Theta}}(\mathbf{x}_i), y_i^*) = \begin{cases} -\ln(h_{\mathbf{\Theta}}(\mathbf{x}_i)), & \text{if } y_i^* = 1 \\ -\ln(1 - h_{\mathbf{\Theta}}(\mathbf{x}_i)), & \text{if } y_i^* = 0 \end{cases} \tag{2.14}$$

Thus, Eq. 2.13 can be formulated as follows:

$$J(\mathbf{\Theta}|\mathbf{X}) = \frac{-1}{m}\sum_{i=1}^{m}[y_i^* \cdot \ln(h_{\mathbf{\Theta}}(\mathbf{x}_i)) + (1-y_i^*)\cdot\ln(1-h_{\mathbf{\Theta}}(\mathbf{x}_i))] + \frac{\lambda}{2m}\sum_{j=0}^{n}\theta_j^2 \quad (2.15)$$

Gradient Matrix

$$\frac{\partial J(\cdot)}{\partial \mathbf{\Theta}} = \begin{bmatrix} \frac{\partial J}{\partial \theta_0} \\ \frac{\partial J}{\partial \theta_1} \\ \frac{\partial J}{\partial \theta_2} \\ \vdots \\ \frac{\partial J}{\partial \theta_n} \end{bmatrix} = \frac{-1}{m}\begin{bmatrix} \sum_{i=1}^{m}[y_i^*\cdot(1-h_{\mathbf{\Theta}}(\mathbf{x}_i)) - (1-y_i^*)\cdot h_{\mathbf{\Theta}}(\mathbf{x}_i)]\cdot x_{i,0} + \frac{\lambda}{m}\cdot\theta_0 \\ \sum_{i=1}^{m}[y_i^*\cdot(1-h_{\mathbf{\Theta}}(\mathbf{x}_i)) - (1-y_i^*)\cdot h_{\mathbf{\Theta}}(\mathbf{x}_i)]\cdot x_{i,1} + \frac{\lambda}{m}\cdot\theta_1 \\ \sum_{i=1}^{m}[y_i^*\cdot(1-h_{\mathbf{\Theta}}(\mathbf{x}_i)) - (1-y_i^*)\cdot h_{\mathbf{\Theta}}(\mathbf{x}_i)]\cdot x_{i,2} + \frac{\lambda}{m}\cdot\theta_2 \\ \vdots \\ \sum_{i=1}^{m}[y_i^*\cdot(1-h_{\mathbf{\Theta}}(\mathbf{x}_i)) - (1-y_i^*)\cdot h_{\mathbf{\Theta}}(\mathbf{x}_i)]\cdot x_{i,n} + \frac{\lambda}{m}\cdot\theta_n \end{bmatrix}$$

Since $h_{\mathbf{\Theta}}(\mathbf{x}_i)$ is corresponding to y_i, we have:

$$\frac{\partial J(\cdot)}{\partial \mathbf{\Theta}} = \begin{bmatrix} \frac{\partial J}{\partial \theta_0} \\ \frac{\partial J}{\partial \theta_1} \\ \frac{\partial J}{\partial \theta_2} \\ \vdots \\ \frac{\partial J}{\partial \theta_n} \end{bmatrix} = \frac{-1}{m}\begin{bmatrix} \sum_{i=1}^{m}[y_i^*\cdot(1-y_i) - (1-y_i^*)\cdot y_i]\cdot x_{i,0} + \frac{\lambda}{m}\cdot\theta_0 \\ \sum_{i=1}^{m}[y_i^*\cdot(1-y_i) - (1-y_i^*)\cdot y_i]\cdot x_{i,1} + \frac{\lambda}{m}\cdot\theta_1 \\ \sum_{i=1}^{m}[y_i^*\cdot(1-y_i) - (1-y_i^*)\cdot y_i]\cdot x_{i,2} + \frac{\lambda}{m}\cdot\theta_2 \\ \vdots \\ \sum_{i=1}^{m}[y_i^*\cdot(1-y_i) - (1-y_i^*)\cdot y_i]\cdot x_{i,n} + \frac{\lambda}{m}\cdot\theta_n \end{bmatrix}$$

Update Model's Parameter Θ

$$\mathbf{\Theta}^{\mathbf{new}} = \mathbf{\Theta}^{\mathbf{old}} - \eta\cdot\frac{\partial J(\cdot)}{\partial \mathbf{\Theta}} \quad (2.16)$$

K Nearest Neighbors (KNN)

The K Nearest Neighbors (KNN) algorithm is a non-parametric method of supervised learning [9]. The KNN approach can be used for resolving both regression and

classification problems with prior knowledge of data that is unknown or difficult to acquire. Mostly, the KNN is a choice of classification for labeled training data [34]. Generally, the parameter "K" would be selected as an odd number, so that it can avoid the cases of tie classification from happening.

The training data $\mathbf{X}$ consists of m training data sets, and each training data set has n features with labeling $\mathbf{Y}$ as illustrated below. The training data outputs follow $y_i \in \{C_1, C_2, \cdots, C_s\}$, where $i \in [1, m]$ under $s - class$ labeled.

Data Structure

$$\mathbf{X} = \begin{bmatrix} x_{1,1} & x_{1,2} & \cdots & x_{1,n} \\ x_{2,1} & x_{2,2} & \cdots & x_{2,n} \\ \vdots & \vdots & \ddots & \vdots \\ x_{m,1} & x_{m,2} & \cdots & x_{m,n} \end{bmatrix}, \mathbf{Y} = \begin{bmatrix} y_1 \\ y_2 \\ \vdots \\ y_m \end{bmatrix}$$

Algorithm 1 K Nearest Neighbors (KNN)

1: *Input:* $\mathbf{X}, \mathbf{Y}, x_t$
2: *Output:* y_t
3: **for** $(u = 1; u \leq m; u++)$
4: $\quad d(x_u, x_t) = \sqrt{\sum_{k=1}^{n} (x_{u,k} - x_{t,k})^2}$
5: **endfor**
6: **Sort** $d(\mathbf{X}, x_t)$ **in ascending order up to K nearest neighbors.**
7: **Find the highest voted classification** (C^*) **in K nearest neighbors** $\left(\textbf{where } C^* \in \{C_1, C_2, \cdots, C_s\}\right)$**.**
8: $y_t \leftarrow C^*$
9: **Stop.**

The Euclidean distance of testing data is calculated for its K nearest neighbors to determine the final class of this particular testing data. For instance, a testing data is $x_u = [x_{u,1}, x_{u,2}, \cdots, x_{u,n}]$, and its neighboring data is $x_v = [x_{v,1}, x_{v,2}, \cdots, x_{v,n}]$. The

Euclidean distance between x_u and x_v is therefore given as follows:

$$d(x_u, x_v) = \sqrt{(x_{u,1} - x_{v,1})^2 + (x_{u,2} - x_{v,2})^2 + \cdots + (x_{u,n} - x_{v,n})^2} \tag{2.17}$$

Based on Eq. 2.17, the confusion matrix of testing data can be calculated against all training data. The class of testing data will be assigned as the most frequent class presented in the K nearest neighbor training data. The pseudo-code is presented in Algorithm 1. (x_t, y_t) are input and output data for testing, where $x_t = [x_{t,1}, x_{t,2}, \cdots, x_{t,n}]$ and $y_t \in \{C_1, C_2, \cdots, C_s\}$.

Neural Networks (NN)

Essentially, the learning principle is rooted in neural networks and they are widely adopted for solving regression and classification problems [38]. Therefore, the choice of neural networks modeling is selected and evaluated throughout the whole study.

Neural networks modeling is originated from Feed-Forward Back-Propagation networks. The "Feed-Forward" means that the output is the result of inputs fed with weight coefficients forwardly. The "Back-Propagation" means that the weight coefficients are trained according to the errors of outputs with respect to the associated neurons backwardly layer by layer. There are three important stages for training models generally. The first is to normalize the training data. The second is to formulate objective function (sometimes also called cost/loss function) that is to be minimized. The third is to derive the 1st-order differentiate equations of objective function with respect to associated neurons [9]. Then, the neural networks models can be trained according to the derived 1st-order differential equations and optimization algorithms can be applied to locate the weight coefficients that result in approaching

the minimum of the objective function. Generally, the optimal weight coefficients are located through gradient descent methods that utilize the 1st-order differential equations discussed previously [10].

Algorithm 2 Back Propagation (BP)

Input: $\mathbf{X}, \mathbf{Y}^*, \mathbf{\Theta^{(1)}}, \mathbf{\Theta^{(2)}}, \eta$
Output: $\mathbf{\Theta^{(1)}}, \mathbf{\Theta^{(2)}}$
while(stopping criteria not satisfied)
    Evaluate model output: $\mathbf{Y}$
    Evaluate cost function:
        $J(\mathbf{\Theta^{(2)}}, \mathbf{\Theta^{(1)}}|\mathbf{X}) = \frac{1}{m}\sum_{i=1}^{m}\sum_{j=1}^{p}(y_{i,j}-y^*_{i,j})^2 + \frac{\lambda}{m}\left(\sum_{u=0}^{n}\sum_{v=1}^{ka}(\theta^{(1)}_{u,v})^2 + \sum_{u=0}^{ka}\sum_{v=1}^{p}(\theta^{(2)}_{u,v})^2\right)$.
    Evaluate gradient matrix:
        $\frac{\partial J(\cdot)}{\partial \mathbf{\Theta^{(2)}}}$ and $\frac{\partial J(\cdot)}{\partial \mathbf{\Theta^{(1)}}}$.
    Update $\mathbf{\Theta^{(2)}}$ and $\mathbf{\Theta^{(1)}}$:
        $\mathbf{\Theta^{(2)}} = \mathbf{\Theta^{(2)}} - \eta \cdot \frac{\partial J(\cdot)}{\partial \mathbf{\Theta^{(2)}}}$, $\mathbf{\Theta^{(1)}} = \mathbf{\Theta^{(1)}} - \eta \cdot \frac{\partial J(\cdot)}{\partial \mathbf{\Theta^{(1)}}}$.
endwhile
Stop.

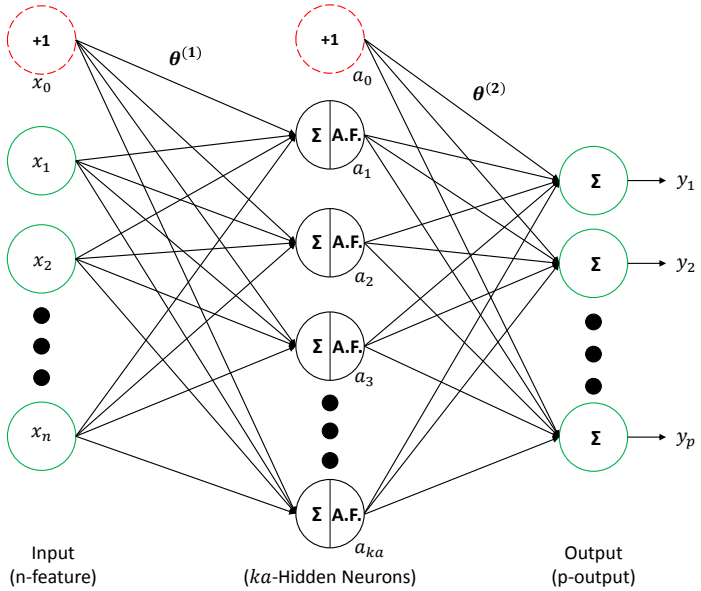

Figure 2.1: Topology of Neural Networks (1-Hidden Layer)-Regression

The topology of the regression neural networks as shown in Figure 2.1 above and neural networks (1-Hidden Layer)-Regression are mathematically formulated, and

the pseudo-code of back-propagation (BP) is provided in Algorithm 2 above. The data structures of the regression neural networks are illustrated below. The $\mathbf{X}$ is the m inputs with n features. The $\mathbf{Y}$ and $\mathbf{Y}^*$ are the predicted outputs from the neural networks and ground truth datasets respectively. The $\mathbf{A}^{(0)}$, $\mathbf{A}^{(1)}$ and $\mathbf{A}^{(2)}$ are intermediate matrices. The $\mathbf{\Theta}^{(1)}$ and $\mathbf{\Theta}^{(2)}$ are the weight parameters of neural networks.

Data Structure

$$\mathbf{X} = \begin{bmatrix} x_{1,0} & x_{1,1} & x_{1,2} & \cdots & x_{1,n} \\ x_{2,0} & x_{2,1} & x_{2,2} & \cdots & x_{2,n} \\ \vdots & \vdots & \vdots & \ddots & \vdots \\ x_{m,0} & x_{m,1} & x_{m,2} & \cdots & x_{m,n} \end{bmatrix}, \mathbf{Y} = \begin{bmatrix} y_{1,1} & y_{1,2} & y_{1,3} & \cdots & y_{1,p} \\ y_{2,1} & y_{2,2} & y_{2,3} & \cdots & y_{2,p} \\ \vdots & \vdots & \vdots & \ddots & \vdots \\ y_{m,1} & y_{m,2} & y_{m,3} & \cdots & y_{m,p} \end{bmatrix}$$

$$\mathbf{Y}^* = \begin{bmatrix} y^*_{1,1} & y^*_{1,2} & y^*_{1,3} & \cdots & y^*_{1,p} \\ y^*_{2,1} & y^*_{2,2} & y^*_{2,3} & \cdots & y^*_{2,p} \\ \vdots & \vdots & \vdots & \ddots & \vdots \\ y^*_{m,1} & y^*_{m,2} & y^*_{m,3} & \cdots & y^*_{m,p} \end{bmatrix}, \mathbf{A^{(0)}} = \begin{bmatrix} a_{1,0} \\ a_{2,0} \\ \vdots \\ a_{m,0} \end{bmatrix}, \mathbf{A^{(1)}} = \begin{bmatrix} a_{1,1} & a_{1,2} & \cdots & a_{1,ka} \\ a_{2,1} & a_{2,2} & \cdots & a_{2,ka} \\ \vdots & \vdots & \ddots & \vdots \\ a_{m,1} & a_{m,2} & \cdots & a_{m,ka} \end{bmatrix}$$

$$\mathbf{A^{(2)}} = \begin{bmatrix} A^{(0)} & A^{(1)} \end{bmatrix}, \text{ where } a_{i,0} = 1 \text{ for } \forall \text{ i} \in [1, m] \text{ and } i \in \mathbb{Z}^+$$

$$\mathbf{\Theta^{(1)}} = \begin{bmatrix} \theta^{(1)}_{0,1} & \theta^{(1)}_{0,2} & \theta^{(1)}_{0,3} & \cdots & \theta^{(1)}_{0,ka} \\ \theta^{(1)}_{1,1} & \theta^{(1)}_{1,2} & \theta^{(1)}_{1,3} & \cdots & \theta^{(1)}_{1,ka} \\ \vdots & \vdots & \vdots & \ddots & \vdots \\ \theta^{(1)}_{n,1} & \theta^{(1)}_{n,2} & \theta^{(1)}_{n,3} & \cdots & \theta^{(1)}_{n,ka} \end{bmatrix}, \mathbf{\Theta^{(2)}} = \begin{bmatrix} \theta^{(2)}_{0,1} & \theta^{(2)}_{0,2} & \theta^{(2)}_{0,3} & \cdots & \theta^{(2)}_{0,p} \\ \theta^{(2)}_{1,1} & \theta^{(2)}_{1,2} & \theta^{(2)}_{1,3} & \cdots & \theta^{(2)}_{1,p} \\ \vdots & \vdots & \vdots & \ddots & \vdots \\ \theta^{(2)}_{ka,1} & \theta^{(2)}_{ka,2} & \theta^{(2)}_{ka,3} & \cdots & \theta^{(2)}_{ka,p} \end{bmatrix}$$

Activation Function (Sigmoid Function)

$$h(x) = \frac{1}{1 + e^{(-x)}} \tag{2.18}$$

Model

- Element Form

$$a_{i,k} = \frac{1}{1 + e^{-(x_{i,0} \cdot \theta^{(1)}_{0,k} + x_{i,1} \cdot \theta^{(1)}_{1,k} + \cdots + x_{i,n} \cdot \theta^{(1)}_{n,k})}} \tag{2.19}$$

where $i = 1, 2, 3, \cdots, m$ and $k = 1, 2, 3, \cdots, ka$.

$$y_{i,j} = a_{i,0} \cdot \theta^{(2)}_{0,j} + a_{i,1} \cdot \theta^{(2)}_{1,j} + \cdots + a_{i,ka} \cdot \theta^{(2)}_{ka,j} \tag{2.20}$$

where $i = 1, 2, 3, \cdots, m$ and $j = 1, 2, 3, \cdots, p$.

- Matrix Form

$$\mathbf{A^{(1)}} = h\Big(\mathbf{X} \cdot \mathbf{\Theta^{(1)}}\Big) \tag{2.21}$$

$$\mathbf{Y} = \mathbf{A^{(2)}} \cdot \mathbf{\Theta^{(2)}} \tag{2.22}$$

Cost Function

$$J(\mathbf{\Theta^{(2)}}, \mathbf{\Theta^{(1)}} | \mathbf{X}) = \frac{1}{m} \sum_{i=1}^{m} \sum_{j=1}^{p} (y_{i,j} - y^*_{i,j})^2 + \frac{\lambda}{m} \Bigg(\sum_{u=0}^{n} \sum_{v=1}^{ka} (\theta^{(1)}_{u,v})^2 + \sum_{u=0}^{ka} \sum_{v=1}^{p} (\theta^{(2)}_{u,v})^2 \Bigg) \tag{2.23}$$

$$err_{i,j} = y_{i,j} - y^*_{i,j} \tag{2.24}$$

Gradient Matrix

$$\frac{\partial J(\cdot)}{\partial \mathbf{\Theta^{(2)}}} = \begin{bmatrix} \frac{\partial J}{\partial \theta^{(2)}_{0,1}} & \frac{\partial J}{\partial \theta^{(2)}_{0,2}} & \frac{\partial J}{\partial \theta^{(2)}_{0,3}} & \cdots & \frac{\partial J}{\partial \theta^{(2)}_{0,p}} \\ \frac{\partial J}{\partial \theta^{(2)}_{1,1}} & \frac{\partial J}{\partial \theta^{(2)}_{1,2}} & \frac{\partial J}{\partial \theta^{(2)}_{1,3}} & \cdots & \frac{\partial J}{\partial \theta^{(2)}_{1,p}} \\ \vdots & \vdots & \vdots & \ddots & \vdots \\ \frac{\partial J}{\partial \theta^{(2)}_{ka,1}} & \frac{\partial J}{\partial \theta^{(2)}_{ka,2}} & \frac{\partial J}{\partial \theta^{(2)}_{ka,3}} & \cdots & \frac{\partial J}{\partial \theta^{(2)}_{ka,p}} \end{bmatrix}, \frac{\partial J(\cdot)}{\partial \mathbf{\Theta^{(1)}}} = \begin{bmatrix} \frac{\partial J}{\partial \theta^{(1)}_{0,1}} & \frac{\partial J}{\partial \theta^{(1)}_{0,2}} & \frac{\partial J}{\partial \theta^{(1)}_{0,3}} & \cdots & \frac{\partial J}{\partial \theta^{(1)}_{0,ka}} \\ \frac{\partial J}{\partial \theta^{(1)}_{1,1}} & \frac{\partial J}{\partial \theta^{(1)}_{1,2}} & \frac{\partial J}{\partial \theta^{(1)}_{1,3}} & \cdots & \frac{\partial J}{\partial \theta^{(1)}_{1,ka}} \\ \vdots & \vdots & \vdots & \ddots & \vdots \\ \frac{\partial J}{\partial \theta^{(1)}_{n,1}} & \frac{\partial J}{\partial \theta^{(1)}_{n,2}} & \frac{\partial J}{\partial \theta^{(1)}_{n,3}} & \cdots & \frac{\partial J}{\partial \theta^{(1)}_{n,ka}} \end{bmatrix}$$

where

$$\frac{\partial J}{\partial \theta^{(2)}_{0,1}} = \frac{2}{m} \sum_{i=1}^{m} err_{i,1} \cdot a_{i,0} + \frac{2\lambda}{m} \cdot \theta^{(2)}_{0,1}$$

$$\cdots$$

$$\frac{\partial J}{\partial \theta^{(2)}_{0,p}} = \frac{2}{m} \sum_{i=1}^{m} err_{i,p} \cdot a_{i,0} + \frac{2\lambda}{m} \cdot \theta^{(2)}_{0,p}$$

$$\cdots$$

$$\frac{\partial J}{\partial \theta^{(2)}_{ka,1}} = \frac{2}{m} \sum_{i=1}^{m} err_{i,1} \cdot a_{i,ka} + \frac{2\lambda}{m} \cdot \theta^{(2)}_{ka,1}$$

$$\cdots$$

$$\frac{\partial J}{\partial \theta^{(2)}_{ka,p}} = \frac{2}{m} \sum_{i=1}^{m} err_{i,p} \cdot a_{i,ka} + \frac{2\lambda}{m} \cdot \theta^{(2)}_{ka,p}$$

and

$$\frac{\partial J}{\partial \theta^{(1)}_{0,1}} = \frac{2}{m} \sum_{i=1}^{m} \sum_{j=1}^{p} err_{i,j} \cdot \theta^{(2)}_{1,j} \cdot a_{i,1} \cdot (1 - a_{i,1}) \cdot x_{i,0} + \frac{2\lambda}{m} \cdot \theta^{(1)}_{0,1}$$

$$\cdots$$

$$\frac{\partial J}{\partial \theta^{(1)}_{0,ka}} = \frac{2}{m} \sum_{i=1}^{m} \sum_{j=1}^{p} err_{i,j} \cdot \theta^{(2)}_{ka,j} \cdot a_{i,ka} \cdot (1 - a_{i,ka}) \cdot x_{i,0} + \frac{2\lambda}{m} \cdot \theta^{(1)}_{0,ka}$$

$$\cdots$$

$$\frac{\partial J}{\partial \theta^{(1)}_{n,1}} = \frac{2}{m} \sum_{i=1}^{m} \sum_{j=1}^{p} err_{i,j} \cdot \theta^{(2)}_{1,j} \cdot a_{i,1} \cdot (1 - a_{i,1}) \cdot x_{i,n} + \frac{2\lambda}{m} \cdot \theta^{(1)}_{n,1}$$

$$\cdots$$

$$\frac{\partial J}{\partial \theta^{(1)}_{n,ka}} = \frac{2}{m} \sum_{i=1}^{m} \sum_{j=1}^{p} err_{i,j} \cdot \theta^{(2)}_{ka,j} \cdot a_{i,ka} \cdot (1 - a_{i,ka}) \cdot x_{i,n} + \frac{2\lambda}{m} \cdot \theta^{(1)}_{n,ka}$$

The topology of the classification neural networks as shown in Figure 2.2 with neural networks (1-Hidden Layer)-Classification are mathematically formulated. The data

structures of classification neural networks are illustrated below. The $\mathbf{X}$ is the m inputs with n features. The $\mathbf{Y}$ and $\mathbf{Y}^*$ are the predicted outputs from the neural networks and ground truth datasets respectively. The $\mathbf{A}^{(0)}$, $\mathbf{A}^{(1)}$ and $\mathbf{A}^{(2)}$ are intermediate matrices. The $\mathbf{\Theta}^{(1)}$ and $\mathbf{\Theta}^{(2)}$ are the weight parameters shown below.

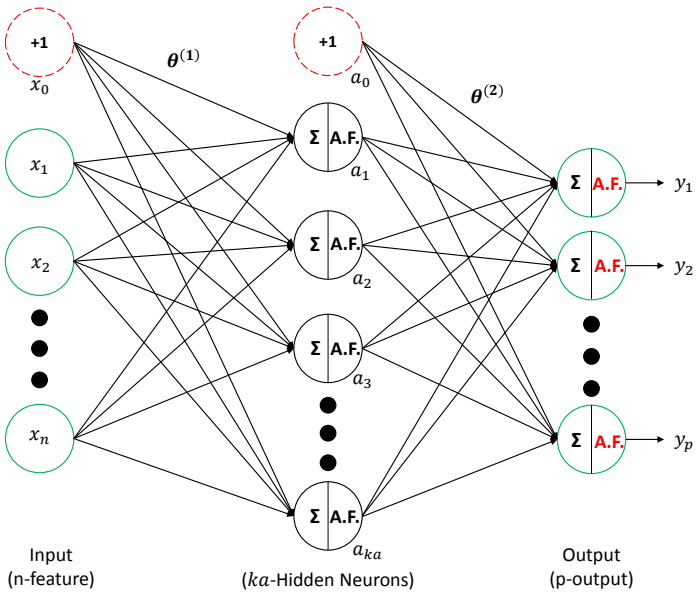

Figure 2.2: Topology of Neural Networks (1-Hidden Layer)-Classification

Data Structure

$$\mathbf{X} = \begin{bmatrix} x_{1,0} & x_{1,1} & x_{1,2} & \cdots & x_{1,n} \\ x_{2,0} & x_{2,1} & x_{2,2} & \cdots & x_{2,n} \\ \vdots & \vdots & \vdots & \ddots & \vdots \\ x_{m,0} & x_{m,1} & x_{m,2} & \cdots & x_{m,n} \end{bmatrix}, \mathbf{Y} = \begin{bmatrix} y_{1,1} & y_{1,2} & y_{1,3} & \cdots & y_{1,p} \\ y_{2,1} & y_{2,2} & y_{2,3} & \cdots & y_{2,p} \\ \vdots & \vdots & \vdots & \ddots & \vdots \\ y_{m,1} & y_{m,2} & y_{m,3} & \cdots & y_{m,p} \end{bmatrix}$$

$$\mathbf{Y}^* = \begin{bmatrix} y^*_{1,1} & y^*_{1,2} & y^*_{1,3} & \cdots & y^*_{1,p} \\ y^*_{2,1} & y^*_{2,2} & y^*_{2,3} & \cdots & y^*_{2,p} \\ \vdots & \vdots & \vdots & \ddots & \vdots \\ y^*_{m,1} & y^*_{m,2} & y^*_{m,3} & \cdots & y^*_{m,p} \end{bmatrix}, \mathbf{A^{(0)}} = \begin{bmatrix} a_{1,0} \\ a_{2,0} \\ \vdots \\ a_{m,0} \end{bmatrix}, \mathbf{A^{(1)}} = \begin{bmatrix} a_{1,1} & a_{1,2} & \cdots & a_{1,ka} \\ a_{2,1} & a_{2,2} & \cdots & a_{2,ka} \\ \vdots & \vdots & \ddots & \vdots \\ a_{m,1} & a_{m,2} & \cdots & a_{m,ka} \end{bmatrix}$$

$\mathbf{A^{(2)}} = \begin{bmatrix} A^{(0)} & A^{(1)} \end{bmatrix}$, where $a_{i,0} = 1$ for $\forall$ i $\in [1, m]$ and $i \in \mathbb{Z}^+$

$$\mathbf{\Theta^{(1)}} = \begin{bmatrix} \theta_{0,1}^{(1)} & \theta_{0,2}^{(1)} & \theta_{0,3}^{(1)} & \cdots & \theta_{0,ka}^{(1)} \\ \theta_{1,1}^{(1)} & \theta_{1,2}^{(1)} & \theta_{1,3}^{(1)} & \cdots & \theta_{1,ka}^{(1)} \\ \vdots & \vdots & \vdots & \ddots & \vdots \\ \theta_{n,1}^{(1)} & \theta_{n,2}^{(1)} & \theta_{n,3}^{(1)} & \cdots & \theta_{n,ka}^{(1)} \end{bmatrix}, \mathbf{\Theta^{(2)}} = \begin{bmatrix} \theta_{0,1}^{(2)} & \theta_{0,2}^{(2)} & \theta_{0,3}^{(2)} & \cdots & \theta_{0,p}^{(2)} \\ \theta_{1,1}^{(2)} & \theta_{1,2}^{(2)} & \theta_{1,3}^{(2)} & \cdots & \theta_{1,p}^{(2)} \\ \vdots & \vdots & \vdots & \ddots & \vdots \\ \theta_{ka,1}^{(2)} & \theta_{ka,2}^{(2)} & \theta_{ka,3}^{(2)} & \cdots & \theta_{ka,p}^{(2)} \end{bmatrix}$$

Activation Function (Sigmoid Function)

$$h(x) = \frac{1}{1 + e^{(-x)}} \tag{2.25}$$

Model

- Element Form

$$a_{i,k} = \frac{1}{1 + e^{-(x_{i,0} \cdot \theta_{0,k}^{(1)} + x_{i,1} \cdot \theta_{1,k}^{(1)} + \cdots + x_{i,n} \cdot \theta_{n,k}^{(1)})}} \tag{2.26}$$

where $i = 1, 2, 3, \cdots, m$ and $k = 1, 2, 3, \cdots, ka$.

$$y_{i,j} = \frac{1}{1 + e^{(a_{i,0} \cdot \theta_{0,j}^{(2)} + a_{i,1} \cdot \theta_{1,j}^{(2)} + \cdots + a_{i,ka} \cdot \theta_{ka,j}^{(2)})}} \tag{2.27}$$

where $i = 1, 2, 3, \cdots, m$ and $j = 1, 2, 3, \cdots, p$.

- Matrix Form

$$\mathbf{A^{(1)}} = h\left(\mathbf{X} \cdot \mathbf{\Theta^{(1)}}\right) \tag{2.28}$$

$$\mathbf{Y} = h\left(\mathbf{A^{(2)}} \cdot \mathbf{\Theta^{(2)}}\right) \tag{2.29}$$

Cost Function

$$J(\mathbf{\Theta^{(2)}}, \mathbf{\Theta^{(1)}}|\mathbf{X}) = \frac{1}{m}\sum_{i=1}^{m}\sum_{j=1}^{p}(y_{i,j}-y^*_{i,j})^2+\frac{\lambda}{m}\left(\sum_{u=0}^{n}\sum_{v=1}^{ka}(\theta^{(1)}_{u,v})^2+\sum_{u=0}^{ka}\sum_{v=1}^{p}(\theta^{(2)}_{u,v})^2\right) \quad (2.30)$$

$$err_{i,j} = y_{i,j} - y^*_{i,j} \quad (2.31)$$

Gradient Matrix

$$\frac{\partial J(\cdot)}{\partial \mathbf{\Theta^{(2)}}} = \begin{bmatrix} \frac{\partial J}{\partial \theta^{(2)}_{0,1}} & \frac{\partial J}{\partial \theta^{(2)}_{0,2}} & \frac{\partial J}{\partial \theta^{(2)}_{0,3}} & \cdots & \frac{\partial J}{\partial \theta^{(2)}_{0,p}} \\ \frac{\partial J}{\partial \theta^{(2)}_{1,1}} & \frac{\partial J}{\partial \theta^{(2)}_{1,2}} & \frac{\partial J}{\partial \theta^{(2)}_{1,3}} & \cdots & \frac{\partial J}{\partial \theta^{(2)}_{1,p}} \\ \vdots & \vdots & \vdots & \ddots & \vdots \\ \frac{\partial J}{\partial \theta^{(2)}_{ka,1}} & \frac{\partial J}{\partial \theta^{(2)}_{ka,2}} & \frac{\partial J}{\partial \theta^{(2)}_{ka,3}} & \cdots & \frac{\partial J}{\partial \theta^{(2)}_{ka,p}} \end{bmatrix}, \frac{\partial J(\cdot)}{\partial \mathbf{\Theta^{(1)}}} = \begin{bmatrix} \frac{\partial J}{\partial \theta^{(1)}_{0,1}} & \frac{\partial J}{\partial \theta^{(1)}_{0,2}} & \frac{\partial J}{\partial \theta^{(1)}_{0,3}} & \cdots & \frac{\partial J}{\partial \theta^{(1)}_{0,ka}} \\ \frac{\partial J}{\partial \theta^{(1)}_{1,1}} & \frac{\partial J}{\partial \theta^{(1)}_{1,2}} & \frac{\partial J}{\partial \theta^{(1)}_{1,3}} & \cdots & \frac{\partial J}{\partial \theta^{(1)}_{1,ka}} \\ \vdots & \vdots & \vdots & \ddots & \vdots \\ \frac{\partial J}{\partial \theta^{(1)}_{n,1}} & \frac{\partial J}{\partial \theta^{(1)}_{n,2}} & \frac{\partial J}{\partial \theta^{(1)}_{n,3}} & \cdots & \frac{\partial J}{\partial \theta^{(1)}_{n,ka}} \end{bmatrix}$$

where

$$\frac{\partial J}{\partial \theta^{(2)}_{0,1}} = \frac{2}{m}\sum_{i=1}^{m} err_{i,1}\cdot y_{i,1}\cdot(1-y_{i,1})\cdot a_{i,0} + \frac{2\lambda}{m}\cdot\theta^{(2)}_{0,1}$$

$\cdots$

$$\frac{\partial J}{\partial \theta^{(2)}_{0,p}} = \frac{2}{m}\sum_{i=1}^{m} err_{i,p}\cdot y_{i,p}\cdot(1-y_{i,p})\cdot a_{i,0} + \frac{2\lambda}{m}\cdot\theta^{(2)}_{0,p}$$

$\cdots$

$$\frac{\partial J}{\partial \theta^{(2)}_{ka,1}} = \frac{2}{m}\sum_{i=1}^{m} err_{i,1}\cdot y_{i,1}\cdot(1-y_{i,1})\cdot a_{i,ka} + \frac{2\lambda}{m}\cdot\theta^{(2)}_{ka,1}$$

$\cdots$

$$\frac{\partial J}{\partial \theta^{(2)}_{ka,p}} = \frac{2}{m}\sum_{i=1}^{m} err_{i,p}\cdot y_{i,p}\cdot(1-y_{i,p})\cdot a_{i,ka} + \frac{2\lambda}{m}\cdot\theta^{(2)}_{ka,p}$$

and

$$\frac{\partial J}{\partial \theta^{(1)}_{0,1}} = \frac{2}{m}\sum_{i=1}^{m}\sum_{j=1}^{p} err_{i,j}\cdot y_{i,j}\cdot(1-y_{i,j})\cdot\theta^{(2)}_{1,j}\cdot a_{i,1}\cdot(1-a_{i,1})\cdot x_{i,0} + \frac{2\lambda}{m}\cdot\theta^{(1)}_{0,1}$$

$\cdots$

$$\frac{\partial J}{\partial \theta^{(1)}_{0,ka}} = \frac{2}{m}\sum_{i=1}^{m}\sum_{j=1}^{p} err_{i,j}\cdot y_{i,j}\cdot(1-y_{i,j})\cdot\theta^{(2)}_{ka,j}\cdot a_{i,ka}\cdot(1-a_{i,ka})\cdot x_{i,0} + \frac{2\lambda}{m}\cdot\theta^{(1)}_{0,ka}$$

$$\cdots$$

$$\frac{\partial J}{\partial \theta^{(1)}_{n,1}} = \frac{2}{m} \sum_{i=1}^{m} \sum_{j=1}^{p} err_{i,j} \cdot y_{i,j} \cdot (1 - y_{i,j}) \cdot \theta^{(2)}_{1,j} \cdot a_{i,1} \cdot (1 - a_{i,1}) \cdot x_{i,n} + \frac{2\lambda}{m} \cdot \theta^{(1)}_{n,1}$$

$$\cdots$$

$$\frac{\partial J}{\partial \theta^{(1)}_{n,ka}} = \frac{2}{m} \sum_{i=1}^{m} \sum_{j=1}^{p} err_{i,j} \cdot y_{i,j} \cdot (1 - y_{i,j}) \cdot \theta^{(2)}_{ka,j} \cdot a_{i,ka} \cdot (1 - a_{i,ka}) \cdot x_{i,n} + \frac{2\lambda}{m} \cdot \theta^{(1)}_{n,ka}$$

Deep Learning (DL)

Aforementioned Neural Networks (NN) is a part of essential architectures for Deep Learning (DL) [33]. As its name implies, a deep learning architecture consists of deep hidden layers between inputs and outputs, which basically are deep neural networks. Among each layer, there are different types of topologies, such as partially or fully connected. Similarly, all data for training is labeled (i.e. a supervised learning with a large number of neurons and parameters to be tuned). Due to its complex layer architectures, each layer could learn some new abstract features from its inputs layer, and thus could generate more meaningful outputs for the next layer to process. Generally, deep learning has excellent performance in solving pattern recognition, classification, image processing and computer vision problems [33]. It can even be combined with reinforcement learning for competing chess games and artificial intelligence gaming strategy.

Moreover, traditional feature extractions of neural networks are on the basis of manual differentiations. After the features are extracted, the parameters of weights are trained so as to minimize the cost function. However, deep learning completes feature extraction within its deep hidden layers of neural networks without the prior knowledge of the facing problems. Many abstract features extracted are not identified by human beings after a series of complex computations and transformations. One of

the most commonly used networks in deep learning is Convolutional Neural Networks (CNN). Normally, a 2D filter is selected for the convolution computations, and the best application is for 2D data sets, such as image. For example, there is a picture of circle. The first layer could detect edges features, and deeper hidden layers could detect some more feature like eccentricity. Then the final layer could tell whether it is a square, rectangle, triangle or circle. Another example is shown in Figure 2.3 to illustrate the identification of a bird in an image. This model is fed and trained with many other labeled data sets, such as images of cats, dogs, etc [59, 97].

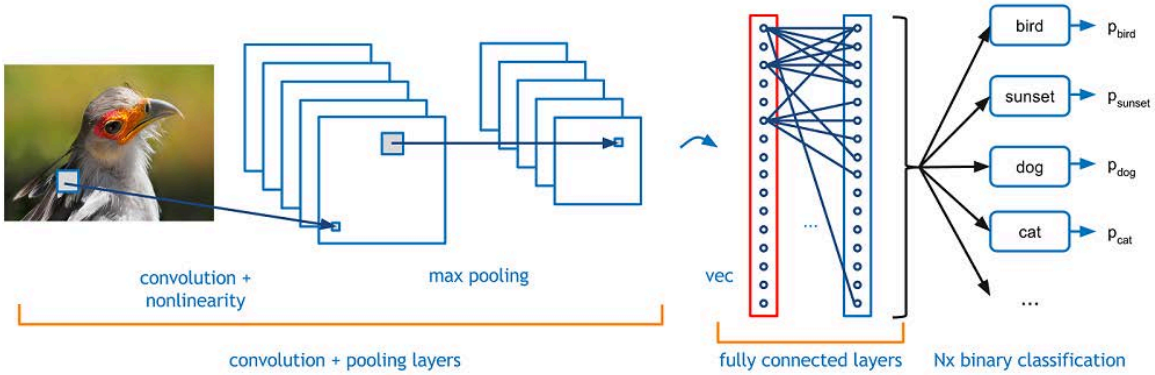

Figure 2.3: Convolutional Neural Networks (CNN) on Bird Classification

Besides the aforementioned applications, deep learning also performs excellently in many other fields, such as Natural Language Process (NLP), robotics, Computer Visions (CV), search engine, advertisement pop-up, medical diagnosis, financial prediction, etc.

2.1.3 Unsupervised Learning

Compared to supervised learning, unsupervised learning extracts information from unlabeled training data sets. Therefore, the unsupervised learning is mainly for clustering problem, while not for regression and classification problems like supervised

learning [13]. Unsupervised learning essentially analyzes the feature extractions and selections of unlabeled training data sets. There are many state-of-the-art unsupervised learning algorithms, such as K-Means, Hierarchical Clustering, Principal Component Analysis (PCA), Self Organization Maps (SOM), etc [10].

Hierarchical Clustering

There are three categories of clustering techniques, and they are hierarchical-based, partitional-based and Bayesian-based. In hierarchical clustering technique, successive clusters are determined by its previously established clusters. There are two kinds of sub-groups in hierarchical clustering based on propagation directions. One is called "Top-Bottom" architecture that means smaller successive clusters are further divided from larger previous clusters. Another architecture is followed as "Bottom-Top" that means larger successive clusters are aggregated from smaller previous clusters.

1. Top-Bottom:

   Start with all data in one cluster, the root.

   Split the root into several children clusters, and each child is further recursively divided.

   Stop when each cluster contains single data.

2. Bottom-Top:

   Start with bottom single data.

   Merge the most similar data into one cluster, and most similar clusters into a new cluster.

   Stop when all the data are merged into one single cluster.

The similarity of two adjacent data or clusters can be monitored by Euclidean distance, Manhattan distance or Minkowski distance. A larger distance means that the similarity is less between each other.

The Euclidean distance is defined as follows:

$$dist(x_i, x_j) = \sqrt{\sum_{k=1}^{n}(x_i^{(k)} - x_j^{(k)})^2} \tag{2.32}$$

The Manhattan distance is defined as follows:

$$dist(x_i, x_j) = \sum_{k=1}^{n}|x_i^{(k)} - x_j^{(k)}| \tag{2.33}$$

The Minkowski distance is defined as follows:

$$dist_p(x_i, x_j) = \left(\sum_{k=1}^{n}|x_i^{(k)} - x_j^{(k)}|^p\right)^{\frac{1}{p}} \tag{2.34}$$

where p is a positive integer.

K-Means

K-Means algorithm of clustering was first proposed by MacQueen in 1967, and it is a type of partitional clustering technique using the centroid approach. There are K centroids (i.e. K clustering) spread out in the data space, and each centre of one cluster is called a centroid, and it is calculated by the mean of this particular cluster of data among the data space [40], The pseudo-code is illustrated in Algorithm 3. There are some stopping criteria to be noted as well in the pseudo-code. In order to differentiate whether the iterations have converged, one uses the positions of centroids

to indicate. If the positions of centroids are not changing or changing at a very minimal level, then the iterations can be stopped and the clusters are indicated as having converged.

Similar to neural networks, the input training datasets $\mathbf{X}$ are following the data structure as below. There are m different datasets and each dataset consists of n features.

Data Structure

$$\mathbf{X} = \begin{bmatrix} x_{1,1} & x_{1,2} & \cdots & x_{1,n} \\ x_{2,1} & x_{2,2} & \cdots & x_{2,n} \\ \vdots & \vdots & \ddots & \vdots \\ x_{m,1} & x_{m,2} & \cdots & x_{m,n} \end{bmatrix}$$

Algorithm 3 K-Means

1: *Input:* $\mathbf{X}$
2: Choose $\mathbf{K}$ random data from $\mathbf{X}$ as initial centroids.
3: **while(stopping criteria not satisfied)**
4: Assign data into their nearest centroid clusters.
5: Euclidean distance can be calculated as follows:
6: $dist(x_i, x_j) = \sqrt{\sum_{k=1}^{n} (x_{i,k} - x_{j,k})^2}$
7: Re-calculate centroids with current data clusters.
8: **endwhile**
9: **Stop.**

There are many advantages in K-Means algorithm. First, it is a linear algorithm under $O(tkm)$, where t is the number of iterations, k is the number of clusters and m is the number of data points. Second, it is easy to implement due to its simplicity and efficiency. However, there are some limitations as well. For instance, the clustering results will be heavily impacted by outliers or mis-leading data, since the algorithm considers every single data for clustering. Moreover, the initial randomly selected centroids will be leading to significantly divergent clustering results. Even though

there are drawbacks in the K-Means algorithm, it is still the most popular clustering algorithm and there is no clear evidence showing that any other clustering algorithm performs better in general.

Principal Component Analysis (PCA)

Principal Component Analysis (PCA) is a statistical procedure that uses an orthogonal transformation to convert a set of observations of possibly correlated variables into a set of values of linearly uncorrelated variables [69], and the linearly uncorrelated variables are called principal components. The pseudo-code is presented in Algorithm 4.

Algorithm 4 Principal Component Analysis (PCA)

1: *Input:* $\mathbf{X}$
2: *Output:* $\mathbf{X}'$
3: Standardize $\mathbf{X}$ into $\mathbf{X_0}$ by means centering.
4: Compute covariance matrix ($\mathbf{C}$) of the standardized data $\mathbf{X_0}$.
5: Compute eigenvalues ($\mathbf{D}$) and eigenvectors ($\mathbf{V}$) of the covariance matrix.
6: Rank $\mathbf{D}$ and $\mathbf{V}$ in descending order of eigenvalues into $\mathbf{D}^*$ and $\mathbf{V}^*$.
7: Transpose $\mathbf{V}^*$ and reduce k rows from bottom into $\mathbf{V}_{PCA}$.
8: Calculate decomposed data: $\mathbf{X}' = \left(\mathbf{V_{PCA}} \cdot \mathbf{X}^T\right)^T$
9: **Stop.**

The m datasets with n features are formulated as matrix $\mathbf{X}$ below. The mean values of different features are calculated and presented in matrix $\boldsymbol{\mu}$, and the basic formulation is illustrated as follows [2].

Data Structure

$$\mathbf{X} = \begin{bmatrix} x_{1,1} & x_{1,2} & \cdots & x_{1,n} \\ x_{2,1} & x_{2,2} & \cdots & x_{2,n} \\ \vdots & \vdots & \ddots & \vdots \\ x_{m,1} & x_{m,2} & \cdots & x_{m,n} \end{bmatrix}, \boldsymbol{\mu} = \begin{bmatrix} \mu_1 & \mu_2 & \cdots & \mu_n \end{bmatrix}, \text{ where } \mu_k = \frac{1}{m}\sum_{i=1}^{m} x_{i,k}$$

$$\mathbf{X_0} = \begin{bmatrix} (x_{1,1} - \mu_1) & (x_{1,2} - \mu_2) & \cdots & (x_{1,n} - \mu_n) \\ (x_{2,1} - \mu_1) & (x_{2,2} - \mu_2) & \cdots & (x_{2,n} - \mu_n) \\ \vdots & \vdots & \ddots & \vdots \\ (x_{m,1} - \mu_1) & (x_{m,2} - \mu_2) & \cdots & (x_{m,n} - \mu_n) \end{bmatrix}$$

Covariance matrix of the standardized data $\mathbf{X_0}$:

$$\mathbf{C} = \frac{1}{m} \cdot \mathbf{X_0}^T \cdot \mathbf{X_0} \tag{2.35}$$

Eigenvalues and eigenvectors of covariance matrix $\mathbf{C}$:

$$\mathbf{D} = \begin{bmatrix} \lambda_1 & 0 & \cdots & 0 \\ 0 & \lambda_2 & \cdots & 0 \\ \vdots & \vdots & \ddots & \vdots \\ 0 & 0 & \cdots & \lambda_n \end{bmatrix}, \mathbf{V} = \begin{bmatrix} V_1^{(1)} & V_1^{(2)} & \cdots & V_1^{(n)} \\ V_2^{(1)} & V_2^{(2)} & \cdots & V_2^{(n)} \\ \vdots & \vdots & \ddots & \vdots \\ V_n^{(1)} & V_n^{(2)} & \cdots & V_n^{(n)} \end{bmatrix}$$

Rank $\mathbf{D}$ and $\mathbf{V}$ in descending order of eigenvalues, we get $\mathbf{D} \to \mathbf{D}^*$, $\mathbf{V} \to \mathbf{V}^*$.

Transpose the ranked eigenvectors $\mathbf{V}^*$ and reduce k rows of vectors from bottom:

$$\mathbf{V}^{*T} = \begin{bmatrix} V_1^{(1)} & V_2^{(1)} & \cdots & V_n^{(1)} \\ V_1^{(2)} & V_2^{(2)} & \cdots & V_n^{(2)} \\ \vdots & \vdots & \ddots & \vdots \\ V_1^{(n)} & V_2^{(n)} & \cdots & V_n^{(n)} \end{bmatrix} \Rightarrow \mathbf{V_{PCA}} = \begin{bmatrix} V_1^{(1)} & V_2^{(1)} & \cdots & V_n^{(1)} \\ V_1^{(2)} & V_2^{(2)} & \cdots & V_n^{(2)} \\ \vdots & \vdots & \ddots & \vdots \\ V_1^{(n-k)} & V_2^{(n-k)} & \cdots & V_n^{(n-k)} \end{bmatrix}$$

Reduce k features (dimensions) from n features ($\mathbf{X} \rightarrow \mathbf{X}^{'}$):

$$\mathbf{X}^{'} = \left(\mathbf{V_{PCA}} \cdot \mathbf{X}^{T} \right)^{T} \tag{2.36}$$

The data obtained in $\mathbf{X}^{'}$ is the standardized and linearly uncorrelated data with k feature reduced. The data $\mathbf{X}^{'}$ is orthogonally decomposed and transformed into a lower dimension space. Thus the PCA algorithm essentially achieves the purpose of features' dimension reduction.

2.1.4 Reinforcement Learning

Besides supervised and unsupervised learning techniques, another main branch of learning techniques is reinforcement learning (RL). The reinforcement learning is most similar to our natural processes of learning. There are agent and environment that will interact with each other [73]. The agent is like a human being, who is responsible to take actions towards the environment. The environment receives the corresponding actions and generates reward or penalty back to the agent, while it also changes its current state accordingly. It is like teaching a baby to perform correct doings by providing some candy or fruit as a reward, and punishing the baby by taking aways some candy or fruit as a penalty if some wrong deeds are conducted.

In the domain of reinforcement learning, returns are the summation of rewards. The agent will adjust its strategy accordingly to achieve maximum returns in the long-term [73]. The returns (R_t) at time t are defined as follows:

$$R_t = r_{t+1} + \gamma \cdot r_{t+2} + \gamma^2 \cdot r_{t+3} + \cdots = \sum_{k=0}^{\inf} \gamma^k \cdot r_{t+k+1} \tag{2.37}$$

where γ is the discount rate in the range of $[0, 1]$.

There are three classifications regarding on different ranges of γ. For $\gamma = 0$, the agent is called "myopic agent" that only maximizes immediate rewards. For $0 < \gamma < 1$, R_t is a finite sum as long as the series $\{r_k\}$ is bounded. For $\gamma \to 1$, the agent is a farsighted agent that takes future long-term rewards more strongly into account.

According to the theory of reinforcement learning rooted in Markov Decision Process (MDP), a policy $(\pi(s, a))$ is a probability distribution with respect to action (a) under state (s). The State-Value function under policy π is shown as follows:

$$\begin{aligned} V^{\pi}(s) &= E_{\pi}\Big\{ R_t | s_t = s \Big\} \\ &= E_{\pi}\Big\{ \sum_{k=0}^{\inf} \gamma^k \cdot r_{t+k+1} | s_t = s \Big\} \\ &= \sum_{a} \pi(s, a) \sum_{s'} P^{a}_{ss'} \Big(R^{a}_{ss'} + \gamma \cdot V^{\pi}(s') \Big) \end{aligned} \tag{2.38}$$

The Action-Value function under policy π is presented as follows:

$$\begin{aligned} Q^{\pi}(s, a) &= E_{\pi}\Big\{ R_t | s_t = s, a_t = a \Big\} \\ &= E_{\pi}\Big\{ \sum_{k=0}^{\inf} \gamma^k \cdot r_{t+k+1} | s_t = s, a_t = a \Big\} \\ &= \sum_{s'} P^{a}_{ss'} \Big(R^{a}_{ss'} + \gamma \cdot V^{\pi}(s') \Big) \end{aligned} \tag{2.39}$$

In reinforcement learning, an optimal solution is obtained if there is a policy (π) found that it can achieve the maximum level of rewards over a long-term running. Therefore, the optimal State-value is $V^*(s) = \max_{\pi} V^{\pi}(s)$ for $\forall s \in S$, and the optimal Action-value is $Q^*(s, a) = \max_{\pi} Q^{\pi}(s, a)$ for $\forall s \in S, \forall a \in A(s)$ [73].

In order to locate an optimal policy solution, there are a series of policy iterations to be conducted. It consist of policy evaluation and policy improvement in each time of iteration. The pseudo-code [73] of policy iteration is illustrated in Algorithm 5.

Algorithm 5 Policy Iteration

1: **1. Initialization:**
2: $V(s) \in R$, $\pi(s) \in A(s)$ arbitrarily $\forall s \in S$.
3: **2. Policy Evaluation:**
4: Repeat
5: $\Delta \leftarrow 0$
6: for each $s \in S$:
7: $v \leftarrow V(s)$
8: $V(s) \leftarrow \sum_{s'} P_{ss'}^{\pi(s)} \left(R_{ss'}^{\pi(s)} + \gamma \cdot V(s') \right)$
9: $\Delta \leftarrow \max(\Delta, |v - V(s)|)$
10: Until $\Delta < \theta$, where θ is a small positive number
11: **3. Policy Improvement:**
12: policy stable $\leftarrow$ true
13: for each $s \in S$:
14: $b \leftarrow \pi(s)$
15: $\pi(s) \leftarrow \arg\max_a \sum_{s'} P_{ss'}^{a} \left(R_{ss'}^{a} + \gamma \cdot V(s') \right)$
16: If $b \neq \pi(s)$, then policy stable $\leftarrow$ false.
17: If policy stable is true, then stop;
18: Else go to section 2.
19: **Stop.**

2.1.5 Summary

In this section, we have examined different and widely applied machine learning techniques, such as supervised learning, unsupervised learning and reinforcement learning. The supervised learning mainly covers linear regression, polynomial regression, logistic regression, k nearest neighbors, neural networks, etc. The supervised learning can provide a higher accuracy in labeled data sets for training, compared to unsupervised learning in classification or clustering problems. It is mainly discussed over hierarchi-

cal clustering, k means, principal component analysis, etc in unsupervised learning. As for the reinforcement learning, the basic principles of policy evaluation, policy improvement and policy determination are illustrated, and agent-environment loops of action-reward are discussed. The theory and application methods of different machine learning techniques are elaborated with respect to different types of problems.

2.2 Thermal Comfort

In this section, different approaches of evaluating indoor thermal comfort sensations are examined. The approaches examined are based on environmental and physiological occupant models, and also data-driven machine learning models. The data-driven models can be further divided into three groups. The first group uses only the environmental parameters to train thermal comfort models [26]. The second group uses only occupant parameters to train thermal comfort models [21]. The last group is a hybrid model that can be trained by environmental and occupant parameters [95]. The environmental parameters in the hybrid models are to be used as a tuning factor to adjust thermal comfort model more accurately. In this study, only the first and second groups are elaborated and discussed in details.

2.2.1 Introduction

Generally, people spend about 90% of their time staying in indoor environment [56]. A thermally comfortable environment would make occupants more productive and healthier for both workplace and home. According to the ISO 7730 standard, the definition of "thermal comfort" is that of "the condition of mind which expresses satisfaction with the thermal environment" [6]. However, the evaluations of thermal comfort are far more complex than this simple definition.

There are many parameters to be considered environmentally and physiologically in order to thoroughly describe the conditions of thermal comfort in an environment [6]. Environmentally, there are parameters such as air flow rate, temperature, humidity, pressure, velocity, solar radiation, light, air quality, noise, etc. Physiologically, the condition of occupants matters and it can impact their thermal comfort satisfactions.

These include the activity levels of occupants, clothing status, genders, etc [74].

2.2.2 Passive Approach

The passive approach to explore thermal comfort sensations is by using objective environmental conditions. The environmental conditions generally consist of air field conditions, radiation conditions and occupant objective conditions. As for air field conditions, there are many parameters to be considered, such as air flow rate, air temperature, air relative humidity, air quality, air pressure, air velocity, etc [6]. The radiation conditions are basically the result of solar radiation of the day. Thus, there is a need to also include the occupant objective parameters, such as clothing factor, metabolic rate, activity level, etc [6].

The most famous and well adopted approach was originated from P. O. Fanger in 1970s [26, 42, 72]. He proposed innovative Predicted Mean Vote (PMV) model and Predicted Percentage of Dissatisfied (PPD) model to predict thermal comfort sensations of occupants from a series of physical laws and large amount of occupant surveys [26]. Based on the study, there are two conditions to be satisfied so as to be thermally comfortable for occupants. Condition 1 is a sense of thermal neutrality achieved from skin temperature and the body's core temperature. Condition 2 is the heat balance of a body, which means the heat generated by metabolic processes of the body is equal to the heat lost from the body [76].

According to ISO-7730:2005, the Fanger's PMV model [75] is elaborated as follows:

$$PMV = \left(0.303 \cdot e^{-0.036M} + 0.028\right) \cdot \left(M - W - Q\right) \tag{2.40}$$

where

$$Q = Q_{diff} + Q_{evap} + Q_{resp},$$

$$Q_{diff} = 3.05 \times 10^{-3} \cdot \Big[5733 - 6.99 \cdot (M - W) - P_a\Big] - \tfrac{1}{I_{cl}} \Big[T_{cl} - 35.7 + 0.028 \cdot (M - W)\Big],$$

$$Q_{evap} = 0.42 \cdot (M - W - 58.15),$$

$$Q_{resp} = 1.71 \times 10^{-5} \cdot M \cdot (5869 - P_a) + 0.0014 \cdot M \cdot (34 - T_a),$$

$$T_{cl} = 35.7 - 0.028 \cdot (M - W) - I_{cl} \Big\{ 3.96 \times 10^{-8} \cdot f_{cl} \cdot \Big[(T_{cl} + 273)^4 - (T_{mr} + 273)^4\Big] + f_{cl} \cdot h_c \cdot (T_{cl} - T_a) \Big\},$$

$$h_c = \max \begin{cases} 2.38 \cdot |T_{cl} - Ta|^{1/4} \\ 12.1 \cdot \sqrt{V_a} \end{cases}$$

$$f_{cl} = \begin{cases} 1.00 + 1.29 \cdot I_{cl}, & (I_{cl} \leq 0.078 m^2 K/W.) \\ 1.05 + 0.645 \cdot I_{cl}, & (I_{cl} > 0.078 m^2 K/W.) \end{cases}$$

$$P_a = 6.11 \cdot \tfrac{RH}{100} \cdot 10^{\frac{7.5 \cdot T_a}{237.7 + T_a}}.$$

$$PPD = 100 - 95 \cdot e^{-(0.03353 \cdot PMV^4 + 0.2179 \cdot PMV^2)} \tag{2.41}$$

In Eq. 2.40 of the PMV model, Q_{diff} is the heat loss by diffusion of an occupant, and Q_{evap} and Q_{resp} are the heat losses by evaporation and respiration processes respectively. The Predicted Percentage of Dissatisfied (PPD) model in Eq. 2.41 is highly related to the PMV model. However, due to different people and environmental conditions, the models of PMV and PPD have to be calibrated so as to achieve better performance.

2.2.3 Active Approach

The active approach to examine thermal comfort sensations is through the evaluations of subjective occupant conditions [21, 71, 83]. The information of subjective occupant conditions are gender, clothing, skin temperatures of different spots of the body, blood pressure, etc. Furthermore, the gradient of such physiological parameters can also be parts of the important information [16, 32]. After a large amount of research [52], it has been shown that skin temperature is the most significant physiological parameter to the thermal comfort sensations of occupants [19]. In addition, its first order gradient is also an important input for providing the rate of change and its changing trends.

There are many skin spots that have been evaluated for thermal comfort sensations in the previous studies and they are as shown in Figure 2.4. According to the figure, each spot of the skin is labeled as "A: forehead, B: chest, C: upper arm, D: back, E: abdomen, F: elbow, G: hand, H: anterior thigh, I: anterior calf, J: foot" correspondingly.

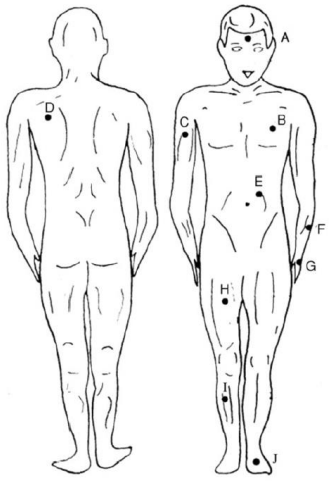

Figure 2.4: Human Skin Spots for Thermal Comfort Sensation Evaluations [53]

For the active approaches, they can be further divided into two general groups of multiple skin-spot and single skin-spot approaches [17]. The multiple skin-spot approach basically transfers multiple skin temperature into a single weighted average of skin temperature [89]. For example, Liu et. al. [53] had used this approach via Eq. 2.42:

$$\begin{aligned} T_{sk} &= 0.06T_{forehead} + 0.08T_{upperarm} + 0.06T_{elbow} \\ &+ 0.05T_{hand} + 0.12T_{back} + 0.12T_{chest} \\ &+ 0.12T_{abdomen} + 0.19T_{thigh} + 0.13T_{calf} + 0.07T_{foot} \end{aligned} \tag{2.42}$$

The single skin-spot approach is normally utilizing the skin temperatures of wrist or the hand's back parts and their corresponding gradients as research had shown the significant improvements on thermal comfort sensation modelings. Besides skin temperature, there are many other physiological parameters to be addressed, such as hight, weight, gender, etc [74]. These parameters are used to further standardize skin temperature and to keep the features more generally comparable.

Since some physiological parameters (i.e. height and weight) are also important to skin temperature, a normalization factor is developed as well for better data representations as Eq. 2.44 shows, and the normalized skin temperature is calculated as Eq. 2.43:

$$\begin{aligned} T_{sk} &= T_{hand} \\ T_{sk,norm} &= \frac{T_{sk}}{A_{norm}} \end{aligned} \tag{2.43}$$

where

$$\begin{aligned} A_{norm} &= (1 - I_{cl}) \cdot A_{du} \\ A_{du} &= Weight^{0.425} \times Height^{0.725} \times 0.203 \end{aligned} \tag{2.44}$$

2.2.4 Summary

In this section, different approaches for thermal comfort evaluations are examined. There are two approaches to evaluate thermal comfort levels, namely passive and active approaches. The passive approaches extract the information largely from environmental parameters, such as air temperature, air flow rate, air velocity, air relative humidity, air pressure, etc. The active approaches predict thermal comfort sensations by measuring the physiological parameters of occupants directly. The passive approaches are non-intrusive to occupants, however, they generally involve high cost of sensory implementation and measurement. The active approaches are easy to implement, but the personal physiological data of occupants may be at risk of exposure. But this cannot prevent the active approaches from becoming a promising and feasible technology in real applications, especially when one can proposed a simple and easily implementable physiological measurement through secure data channels.

2.3 Optimization Algorithms

In this section, different optimization algorithms are examined and discussed. The optimization algorithms are grouped into three categories, namely nature-inspired, Bayesian-based and analytical algorithms. In the category of nature-inspired algorithms, some famous algorithms examined are the genetic algorithm, particles swarm optimization and augmented firefly algorithm [85]. In the category of Bayesian-based algorithm, a special Bayesian Gaussian Process optimization are evaluated [61]. Lastly, the analytical method algorithms such as gradient descent methods, quadratic optimization are examined [11].

2.3.1 Introduction

There are many optimization theory and algorithms for solving optimization problems. Most of practical problems that we face are not solvable through analytical methods [11, 23]. Therefore, probability-based and numerical-based methods can be used as alternative approaches for solving highly non-linear, discrete or continuous optimization problems [81].

2.3.2 Genetic Algorithm

The genetic algorithm (GA) that was developed by John H. Holland and his colleagues in 1970s [38] is one of the most widely applied algorithms. The basic idea of genetic algorithm is based on the evolutionary theory of Charles Darwin's natural selection. According to Darwin's theory, the biological evolution consists of operators like crossover, mutation, recombination and selection. These operators in genetic algorithms are essential components to mimic the natural process of biology.

According to the schemes of genetic algorithm, the procedures can be briefly illustrated as follows: 1) define cost function, 2) define fitness function, 3) create initial population, 4) perform iteration or evolution to generate new population by crossover, mutation and recombination, 5) decode the final solution based on selection criteria. To be more specific, the pseudo-code is as presented in Algorithm 6.

Algorithm 6 Genetic Algorithm

Define objective function
    $f(\mathbf{x})$, $\mathbf{x} = (x_1, x_2, \cdots, x_d)^T$
Encode solutions into chromosomes
Define fitness function
    $F \propto f(\mathbf{x})$ for maximization problems
Generate initial population
Initialize crossover(p_c) and mutation(p_m) probabilities
    while $t \leq Max\_Generation$:
        Generate new solutions by crossover and mutation
        Accept the new solutions if fitness values increase
        Select current best solution for the next generation (elitism)
        Update $t \leftarrow t + 1$
    endwhile
Visualization results
Stop.

As mentioned previously, there are three main essential operators and they are crossover, mutation and selection. For crossover, it operates the swapping between chromosomes which means mixing partial solutions happen over this operation under a probability p_c. Similarly for mutation, it performs the information changes of chromosomes which means solutions change randomly under a probability p_m. This operation can avoid being trapped into a local optimum. Moreover, the selection operator follows the principle of Darwin's "fittest of the survival", and it operates as a natural selection process over the population or solutions. The fittest solutions will be the survival into the next generation. After a few number of generations, solutions will be converging to the final output results.

2.3.3 Particle Swarm Optimization

Particle swarm optimization (PSO) was firstly developed from nature inspiration by Kennedy and Eberhart in 1995 [41]. The PSO is inspired by swarm behaviors in biological activities, such as fish and bird schooling [85]. According to many reviews, PSO has been applied into almost every field of optimizations, and there are many transformed and hybrid versions of PSO as well, and the pseudo-code for particle swarm optimization is illustrated in Algorithm 7.

Algorithm 7 Particle Swarm Optimization

Define objective function
    $f(\mathbf{x})$, $\mathbf{x} = (x_1, x_2, \cdots, x_d)^T$
Initialize locations $\mathbf{x}_i$ and velocity $\mathbf{v}_i$ of n particles
Find $\mathbf{g}^*$ from $\min\left\{f(\mathbf{x_1}), \cdots, f(\mathbf{x_n})\right\}$ (at $t = 0$)
while (criteria):
    for loop all n particles and all d dimensions:
        Generate new velocity
            $\mathbf{v}_i^{t+1} = \mathbf{v}_i^t + \alpha \cdot \epsilon_1(\mathbf{g}^* - \mathbf{x}_i^t) + \beta \cdot \epsilon_2(\mathbf{x}_i^{*(t)} - \mathbf{x}_i^t)$
        Calculate new location
            $\mathbf{x}_i^{t+1} = \mathbf{x}_i^t + \mathbf{v}_i^{t+1}$
        Evaluate new locations $\mathbf{x}_i^{t+1}$ by objective function
        Find the current best for each particle $\mathbf{x}_i^*$
    endfor
    Find the current global best g^*
    Update $t \leftarrow t + 1$
endwhile
Visualize results $\mathbf{x}_i^*$ and g^*
Stop.

The particle swarm optimization considers each particle as a solution to the particular optimization problem. The particles (i.e. solutions) will be swarming or converging into optima after numerous iterations. As Figure 2.5 shows, the particle i will proceed on many possible directions. However, it may be going toward current optimum x_i^*,

but it eventually will approach g^* (i.e. global optimum).

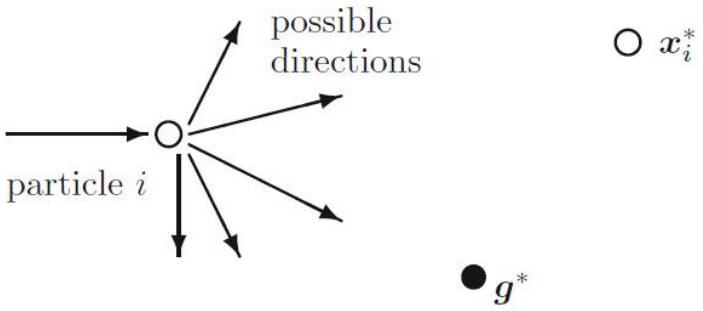

Figure 2.5: Particle Swarm Optimization Principle

Based on the studies of X. S. Yang [87], particle swarm optimization can perform outstandingly over many other optimization algorithms, such as genetic algorithm and other conventional algorithms. However, there are still drawbacks, such as premature convergence and trapped into local optima. As mentioned by X. S. Yang [87] in the book, many other methods, namely cuckoo search method and firefly algorithms, also outperform PSO algorithms in many applications.

2.3.4 Firefly Algorithm

The study of nature-inspired optimization algorithms has been surging over the last 10-15 years. In the meantime, firefly algorithms (FA) have emerged since 2008 [87]. Due to their properties of efficiency and fast convergence, the research under this topic has been very popular and have drawn significant attentions.

The first firefly algorithm is described in the published papers of X. S. Yang in 2008 [85, 86]. For simplicity, some rules are to be defined as follows: 1) All fireflies are unisex, so the attractiveness of each other is regardless of sex; 2) Attractiveness is proportional to the brightness of firefly. The brightness is decreasing as the distance between each other increases. If there is no brighter one, fireflies will be wandering

randomly; 3) The brightness is governed by the objective function. The pseudo-code of firefly algorithm is presented in Algorithm 8.

Algorithm 8 Firefly Algorithm

Define objective function
    $f(\mathbf{x})$, $\mathbf{x} = (x_1, x_2, \cdots, x_d)^T$
Initialize population of n fireflies $\mathbf{x}_i$ $(i = 1, 2, \cdots, n)$
Determine light intensity I_i at $\mathbf{x}_i$ by $f(\mathbf{x}_i)$
Define light absorption coefficient γ
while $(t < Max\_Generation)$:
    for $i = 1 : n$ (all n fireflies):
        for $j = 1 : n$ (all n fireflies):
            if $(I_i < I_j)$
                Move firefly i to j
                $\mathbf{x}_i^{t+1} = \mathbf{x}_i^t + \beta_0 \cdot e^{-\gamma \cdot r_{ij}^2} \cdot (\mathbf{x}_j^t - \mathbf{x}_i^t) + \alpha \cdot \epsilon_i^t$
            endif
            Vary attractiveness with distance r by $e^{-\gamma \cdot r^2}$
            Evaluate new solutions and update new light intensity
        endfor j
    endfor i
    Rank fireflies and find current global best g^*
endwhile
Visualize results global best g^*
Stop.

Since the firefly algorithm belongs to swarm intelligence, it has similar advantages and disadvantages as well. The firefly algorithm has two major advantages compared with other swarm intelligence algorithms. These are 1) Firefly algorithm is based on attractiveness, so the population can be automatically sub-divided into sub-populations. Among each sub-population, the local optimum can be obtained. Moreover, the global optimum can be further located among all local optima in sub-populations [86]; 2) Theoretically, all the local and global optima can be simultaneously located as long as the population size is large enough for the problem [87].

With the above features, the firefly algorithm is particularly suitable for solving high-

ly non-linear, multi-mode optimization problems. With these features, the firefly algorithm can deal with clustering, classification, discrete, continuous and combinatorial optimizations, and there are numerous extension versions of firefly algorithms including the augmented firefly algorithms (AFA), which is proposed by the author and will be further elaborated in later chapters to avoid duplication here.

2.3.5 Bayesian Optimization

Besides nature-inspired optimization algorithms as discussed above, Bayesian approach is another direction for solving optimization problems [12]. Bayesian optimization has remarkable advantages in the objective functions that are expensive to evaluate, especially in reinforcement learning and fields of planning [12]. This is an optimization technique that looks for global optima through a black-box scenario. Based on statistical probability and assumption of Gaussian random processes of observed samples, Bayesian optimization can then be implementable. Bayesian optimization applies the Bayesian technique of defining a prior over the objective function and combining it with observed samples to get a posterior [12]. This technique utilizes a utility-based selection of the next observation position, which considers both exploration and exploitation. With the traits of Gaussian processes, it is suitable to predict output based only on limited observed samples instead of know the knowledge of analytical functions. The definition and derivations are presented as follows:

A Prior P on a function $f(\cdot)$ is a Gaussian Process prior, with mean function $\mu_0(\cdot)$ and covariance function $k_0(\cdot)$. Thus, for any given set of j observed samples, $\mathbf{X} =$

$\left\{\mathbf{x}_1, \mathbf{x}_2, ..., \mathbf{x}_j\right\}$ under P, we have

$$\begin{bmatrix} f(\mathbf{x}_1) \\ f(\mathbf{x}_2) \\ \vdots \\ f(\mathbf{x}_j) \end{bmatrix} \sim N\Bigg(\begin{bmatrix} \mu_0(\mathbf{x}_1) \\ \mu_0(\mathbf{x}_2) \\ \vdots \\ \mu_0(\mathbf{x}_j) \end{bmatrix}, \begin{bmatrix} k_0(\mathbf{x}_1, \mathbf{x}_1) & k_0(\mathbf{x}_1, \mathbf{x}_2) & ... & k_0(\mathbf{x}_1, \mathbf{x}_j) \\ k_0(\mathbf{x}_2, \mathbf{x}_1) & k_0(\mathbf{x}_2, \mathbf{x}_2) & ... & k_0(\mathbf{x}_2, \mathbf{x}_j) \\ \vdots & \vdots & \ddots & \vdots \\ k_0(\mathbf{x}_j, \mathbf{x}_1) & k_0(\mathbf{x}_j, \mathbf{x}_2) & ... & k_0(\mathbf{x}_j, \mathbf{x}_j) \end{bmatrix} \Bigg) \tag{2.45}$$

where the mean function is defined as:

$$\begin{bmatrix} \mu_0(\mathbf{x}_1) \\ \mu_0(\mathbf{x}_2) \\ \vdots \\ \mu_0(\mathbf{x}_j) \end{bmatrix} = \begin{bmatrix} 0 \\ 0 \\ \vdots \\ 0 \end{bmatrix} = [0] \tag{2.46}$$

and the covariance (kernel) function is defined:

$$k_0(\mathbf{x}_i, \mathbf{x}_j) = exp(-\frac{1}{2\theta_h}||\mathbf{x}_i - \mathbf{x}_j||^2) \tag{2.47}$$

Let

$$[K] = \begin{bmatrix} k_0(\mathbf{x}_1, \mathbf{x}_1) & k_0(\mathbf{x}_1, \mathbf{x}_2) & ... & k_0(\mathbf{x}_1, \mathbf{x}_j) \\ k_0(\mathbf{x}_2, \mathbf{x}_1) & k_0(\mathbf{x}_2, \mathbf{x}_2) & ... & k_0(\mathbf{x}_2, \mathbf{x}_j) \\ \vdots & \vdots & \ddots & \vdots \\ k_0(\mathbf{x}_j, \mathbf{x}_1) & k_0(\mathbf{x}_j, \mathbf{x}_2) & ... & k_0(\mathbf{x}_j, \mathbf{x}_j) \end{bmatrix} \tag{2.48}$$

Thus, Eq. 2.45 can be further simplified as:

$$[f] \sim \mathcal{N}([0], [K]) \tag{2.49}$$

where

$$[f] = \begin{bmatrix} f(\mathbf{x}_1) \\ f(\mathbf{x}_2) \\ \vdots \\ f(\mathbf{x}_j) \end{bmatrix} \tag{2.50}$$

Since Gaussian distribution applies to all in *Domain*, any given $\mathbf{x}^* \in Domain$ satisfies:

$$\begin{bmatrix} [f] \\ f(\mathbf{x}^*) \end{bmatrix} \sim \mathcal{N}\left(\begin{bmatrix} [0] \\ \mu^* \end{bmatrix}, \begin{bmatrix} [K] & [k] \\ [k^T] & k^* \end{bmatrix} \right) \tag{2.51}$$

where

$$[k] = \begin{bmatrix} k_0(\mathbf{x}_1, \mathbf{x}^*) \\ k_0(\mathbf{x}_2, \mathbf{x}^*) \\ \cdots \\ k_0(\mathbf{x}_j, \mathbf{x}^*) \end{bmatrix}, k^* = k_0(\mathbf{x}^*, \mathbf{x}^*) \tag{2.52}$$

Given Eq. 2.51, the solution $f(\mathbf{x}^*)$ follows a Gaussian distribution using Sherman-Morrison-Woodbury formula [61] as given below:

$$f(\mathbf{x}^*) \sim \mathcal{N}(\mu^*, \Sigma^*) \tag{2.53}$$

where

$$\begin{aligned} \mu^* &= [k^T] \cdot [K^{-1}] \cdot [g] \\ \Sigma^* &= k^* - [k^T] \cdot [K^{-1}] \cdot [k] \end{aligned} \tag{2.54}$$

Based on Eq. 2.53, the solution $f(\mathbf{x}^*)$ can be determined with the observed samples. The pseudo-code of Bayesian optimization is presented in Algorithm 9. Since

Bayesian optimization is rooted only from observed samples, and it provides solutions according to Gaussian processes without knowledge of the prior probability distribution of population, it has great advantages over other optimization algorithms with the help of data increments [61].

Algorithm 9 Bayesian Optimization

1: **Obtain** initial observed samples $(\mathbf{x}, f(\mathbf{x}))$
2: **while** (stopping criteria not satisfied):
3: a) **Calculate** Bayesian posterior distribution from $(\mathbf{x}, f(\mathbf{x}))$
4: b) **Estimate** the next observation using posterior distribution
5: **endwhile**
6: **Report** the point with the best estimation $(\mathbf{x}^*, f(\mathbf{x}^*))$ based on the most recent posterior distribution
7: **Stop.**

2.3.6 Gradient Descent Algorithm

Different from previous nature-inspired and Bayesian optimization algorithms, gradient descent (GD) algorithms utilize the gradient property of function analytically to slide into smooth optima [80]. Since this analytical algorithm knows the exact direction of the next movement with the knowledge of its gradient, the algorithm can converge remarkably fast. For the gradient descent algorithm given in Algorithm 10, the stopping criteria generally follows the format of $\|\nabla f(\mathbf{x})\|_2 \leq \epsilon$, where ϵ is user-defined small and positive number.

Due to the particular starting point defined, some drawback are introduced as well. First, the converging process would be relatively slow. For instance, if the starting point is selected very far from the optimum and the step size is relatively small, then the updating process would take a much longer time to finally converge. Second, if the step size is too large, then the solution would not be able to converge, and it

would be oscillating over a domain. Third, if the optimization problem has more than one optima (i.e. existing local optima and global optimum), and the starting point is not well defined, then the final converging solution would be trapped into local optima easily.

Algorithm 10 Gradient Descent Algorithm

1: **Define** function $f(\mathbf{x})$
2: **Define** starting point $\mathbf{x}^* = \mathbf{x}_0$
3: **Define** step size η
4: **while** (stopping criteria not satisfied):
5: a) **Calculate** gradient at starting point: $\Delta\mathbf{x} = \nabla f(\mathbf{x})|_{\mathbf{x}=\mathbf{x}^*}$
6: b) **Update** the point: $\mathbf{x}^* = \mathbf{x}^* - \eta \cdot \Delta\mathbf{x}$
7: **endwhile**
8: **Report** the point with the best solution $(\mathbf{x}^*, f(\mathbf{x}^*))$
9: **Stop.**

2.3.7 Quadratic Optimization

In quadratic optimization problems, general constrained problems can be formulated into the following matrix form [11]:

$$\begin{aligned} &\min_{\mathbf{x}\in\Omega} f(\mathbf{x}) = \mathbf{c}\mathbf{x} + \mathbf{x}^T\mathbf{D}\mathbf{x} \\ &s.t. \quad \mathbf{A}\mathbf{x} \leq \mathbf{b} \\ &\qquad \mathbf{x} \geq \mathbf{0} \end{aligned} \tag{2.55}$$

where $\mathbf{x} \in \mathbb{R}^n$ and $\mathbf{A} \in \mathbb{R}^{m\times n}$, and the objective function $f(\cdot) : \mathbb{R}^n \to \mathbb{R}$ is over a defined domain Ω.

In order to search for optimal solutions in quadratic optimization problems, the Karush-Kuhn-Tucker conditions must be satisfied. The constrained conditions are formulated as a conditional function, $g(\mathbf{x}) = \mathbf{A}\mathbf{x} - \mathbf{b}$. Here, a Lagrangian function is

stated as follows:

$$\begin{aligned} L(\mathbf{x}, \mathbf{\Lambda}) &= f(\mathbf{x}) - \mathbf{\Lambda} g(\mathbf{x}) \\ &= f(\mathbf{x}) - \Lambda_1 g_1(\mathbf{x}) - \Lambda_2 g_2(\mathbf{x}) - \cdots - \Lambda_m g_m(\mathbf{x}) \end{aligned} \tag{2.56}$$

where $\mathbf{\Lambda}$ is a set of Lagrangian multipliers along with constraints.

Due to Lagrangian multipliers, the optimal solutions $\mathbf{x}^*$ have to satisfy the conditions with corresponding optimal $\mathbf{\Lambda}^*$ as follows:

$$\begin{aligned} \nabla_{\mathbf{x}} L(\mathbf{x}^*, \mathbf{\Lambda}^*) &= 0 \\ \nabla_{\mathbf{\Lambda}} L(\mathbf{x}^*, \mathbf{\Lambda}^*) &= 0 \\ \mathbf{\Lambda}^* &\geq 0 \end{aligned} \tag{2.57}$$

In matrix form, the optimal solutions ($\mathbf{x}^*$) and the corresponding Lagrangian multipliers ($\mathbf{\Lambda}^*$) can be obtained as follows [11]:

$$\begin{bmatrix} \mathbf{x}^* \\ \mathbf{\Lambda}^* \end{bmatrix} = \begin{bmatrix} 2\mathbf{D} & \mathbf{A}^T \\ \mathbf{A} & 0 \end{bmatrix} \cdot \begin{bmatrix} \mathbf{c}^T \\ \mathbf{b} \end{bmatrix}$$

2.3.8 Summary

In this section, different categories of optimization algorithms are examined. There are nature-inspired algorithms, which include genetic algorithm, particle swarm optimization, firefly algorithm and the newly proposed augmented firefly algorithm. The genetic algorithm is based on three operators of crossover, mutation, recombination and selection. The existence of these operators can prevent the solutions from being

trapped into sub-optima. The particle swarm optimization outperforms genetic algorithm and other conventional algorithms in terms of computation complexity. However, it can be easily trapped into sub-optima. The firefly algorithm and augmented firefly algorithm can perform even better on highly non-linear, multi-mode optimization problems. It can automatically divide the population into sub-populations due to its unique property of attractiveness. Bayesian optimization approaches can solve for solutions without the knowledge of analytical functions. The observed data is assumed to follow Gaussian processes, and the optimization can be used as a real-time data-driven optimization approach, and its accuracy increases as the prior observed data increases. The gradient descent algorithm is one of the most commonly used analytic methods in solving convex optimizations. It has its own traits namely fast convergent, easily implementable, while it also has drawbacks which are over-shooting oscillation and sub-optima trap.

To better understand and address the complex coupling and correlations of energy consumption of buildings with environmental condition control of buildings and thermal comfort of occupants, there is a need to deploy an array of practical approaches to tackle the issues of modeling, control and optimization. It is believed that machine learning can provide effective perspectives for modeling physically complex and multiply coupled systems, and air-conditioning and mechanical ventilation (ACMV) system is one of such system. Thermal comfort studies with machine learning will also provide new approaches to examine suitable comfort levels. Thermal comfort models optimized with machine learning can be readily utilized together for high performance of predicting thermal comfort levels of occupants. Optimization algorithms contribute to the location of solutions in the domain of complex coupling, and they can be realized in real applications and not just restricted to mathematical proof of

effectiveness.

Based on state-of-the-art studies of machine learning, thermal comfort and optimization algorithms, the thesis attempts to push the study boundaries forward and reduces the gaps in the understanding and realizations of modeling, control and optimization of complex ACMV systems. Then, the objectives of realizing smart and energy efficient buildings can be achieved.

Chapter 3

Methodology

- Modeling/Optimization of Energy Consumption and Thermal Comfort

3.1 Introduction

Heating, ventilation and air-conditioning (HVAC) systems are necessary apparatuses and they are widely used in modern commercial and residential buildings [31, 56, 64, 65, 78]. Bearing to meet different outdoor environmental conditions, the HVAC systems are deployed from the arctic to equatorial regions all over the world with different capacities from heating to cooling respectively. While in tropical regions, such as Singapore, heating capacity is not a necessary demand compared with cooling. Therefore, air-conditioning and mechanical ventilation (ACMV) systems are adopted in this thesis study. Statistically, energy consumption of ACMV systems is about $40\% - 60\%$ of the total electricity generated from power plants [3, 43, 51, 79, 88]. Under current huge demands of ACMV systems, it would significantly impact on the worldwide climate change and put great stress on currently available energy resources. Therefore, it is imperative to develop energy-efficient ACMV systems through accurate modeling and optimization [7, 14, 99], so that the available energy resources can be more efficiently utilized.

People are spending about more than 90% of their time indoors these days and the in-

door environmental conditions directly affect occupants' thermal comfort [44]. The indoor environmental conditions are maintained by ACMV systems throughout. Thus, the relationship between ACMV systems and occupants' thermal comfort should be examined thoroughly through various evaluation techniques. However, the thermal comfort is a very subjective term that differs from person to person. Therefore, suitable quantification of the subjective occupants' thermal comfort is a definite path to achieve good evaluations.

In this chapter, the methodologies of modeling energy consumption and indoor thermal comfort will be presented, and the balancing problem of energy consumption and thermal comfort will be formulated into a multiple-objective optimization problem [61, 66]. On energy consumption models, several data-driven approaches are discussed. They are essentially different Neural Networks (NN) [29, 49, 50]. The theoretical backgrounds and applications are analyzed, so that the optimizations for low cost functions can yield good evaluation results for energy saving [48].

In order to model energy consumption and indoor thermal comfort, a data acquisition system and a control system have been developed. The systems are presented in Figure 3.1. For the data acquisition system, the air related sensors are mounted to the air duct and ambient environment, and building wall surface sensor and occupant sensors are mounted to the wall of thermal laboratory and the back of the hand of occupant, respectively. The aggregated sensory data are collected through multiple Arduino Uno boards. The Arduino Uno boards can convert analog sensory signals to digital signals and transmit the sensory signals through serial ports to stand-alone computers, Raspberry Pis. The stand-alone computers can visualize and store the real-time sensory data for further model trainings and control algorithm implementations. For the control system, the main PC runs control algorithms to control

the operations of air-conditioning and mechanical ventilation (ACMV) systems by signaling the variable frequency drives (VFD) of supply air fan motor, water pump and compressor. The VFDs drive the corresponding electric appliances by altering the supply voltage frequency. Since the condenser operates constantly at its rated operating condition once it starts, it is just controlled by on/off modes.

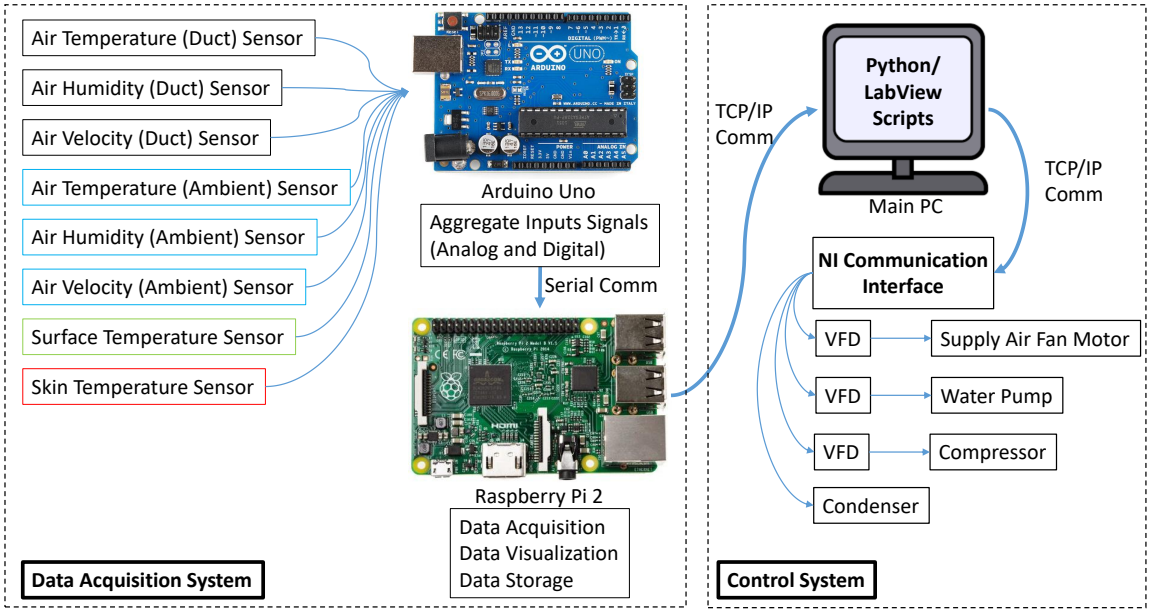

Figure 3.1: Data Acquisition System and Control System

In the section on constructing the indoor thermal comfort models, two different types of methodologies are illustrated, namely passive and active approaches. The passive approaches are mainly based on the studies of P.O. Fanger [6] and many great successors [44, 68, 82]. The quantifications of thermal comfort are based on physical laws of heat transfer. The heat transfer can be calculated through environmental parameters and some occupant parameters. The environmental parameters cover ambient air temperature, ambient air velocity, air relative humidity and mean radiant temperature, while occupant parameters are metabolic rate and clothing insulation

factor [6, 98]. The active approaches directly utilize occupants' physiological parameters to predict their indoor thermal sensations [21]. The physiological parameters consist of hight, weight, gender, age, metabolic rate, exposed skin surface area, skin temperature, blood pressure, etc [20, 60, 74, 96].

In the section on problem formulation and optimization, the main objective is to formulate and optimize cost functions or objective functions with goals of enhancing the performance of ACMV systems and the thermal comfort levels of occupants [8, 22, 28, 30, 47, 55]. Therefore, the objective functions for smart buildings will utilize the knowledge of energy consumption of ACMV systems and indoor thermal comfort sensations [4, 15, 18, 24, 27, 36, 58]. Plus, a user-preference coefficient is proposed for adjusting the objective functions according to different user preferences in real applications [35, 54, 67]. Different optimization algorithms have been investigated. There are three categories of algorithms discussed, namely nature-inspired algorithms, Bayesian optimization and analytical algorithms.

Before model methodologies of energy consumption and thermal comfort, a general experimental procedure is described. For experiments of evaluating energy consumption of ACMV systems, the operating frequencies of supply air fan motor, compressor and water pump were tuned and recorded from 30 Hz to 50 Hz. The VFDs are configured to vary frequencies from 0 Hz to 50 Hz. While the frequencies below 30 Hz are not operable to drive apparatuses in thermal laboratory. The energy consumption of ACMV systems was recorded correspondingly by a power meter. In addition, the ambient/duct air temperature, ambient/duct air relative humidity and ambient/duct air velocity were also recorded concurrently in data acquisition system. For experiments of evaluating thermal comfort of occupants, the subjects were asked to follow a standard activity level, either general offices duty (case 1) or lec-

ture theatres/conference rooms (case 2). The experiments were carried out for 40 minutes for each experimental subject in thermal laboratory. The first 20 minutes were cooling experiments (duct air temperature around 18 $^{\circ}C$), and the second 20 minutes were normal experiments (duct air temperature around 24 $^{\circ}C$). The occupants were given questionnaires to reflect their thermal comfort sensations every 10 minutes. Throughout the experiments, the environmental parameters (ambient air temperature, ambient air relative humidity, ambient air velocity and clothing insulation factor) and the physiological parameters (activity level, skin temperature, height and weight) were concurrently collected in data acquisition system for further data analysis and modeling.

Since the ACMV systems are set up in Singapore (a tropical country), the experiments mainly focus on cooling capacity of ACMV systems. The latent cooling load basically refers to the wet bulb temperature of the building, and the sensible cooling load refers to the dry bulb temperature of the building. The sensible heat profile of the thermal laboratory can be calculated as follows:

$$h_s = c_p \rho q \Delta T \tag{3.1}$$

where c_p is the specific heat of air (1.006 $kJ/kg^{\circ}C$), ρ is the density of air (1.202 kg/m^3), q is the air flow rate (m^3/s), ΔT is the temperature difference ($^{\circ}C$).

The rated RPM of supply air fan motor is 3000 rpm, and the variable frequency drive (VFD) adjusts the speed of motor by operating frequency linearly, thus the RPM of motor is between 1800 rpm and 3000 rpm (30 Hz to 50 Hz). The rated air flowrate is about 640 cfm (0.302 m^3/s). According to the thermal laboratory profile during

experiments and fan laws, the air flow rate follows the rule below:

$$\frac{q_{unknown}}{q_{known}} = \frac{VFD_{unknown}}{VFD_{known}} \tag{3.2}$$

Therefore the air flow rate is between 0.1812 m^3/s and 0.302 m^3/s. The temperature of the thermal laboratory varies between 16 $°C$ to 24 $°C$, thus the profile of sensible heat profile is between 1.753 kW and 2.921 kW.

In addition, the latent heat profile of the thermal laboratory can be examined as follows:

$$h_s = \rho q h_{we} d_{wkg} \tag{3.3}$$

where ρ is the density of air (1.202 kg/m^3), q is the air flow rate (m^3/s), h_{we} is the latent heat evaporation water (generally 2454 kJ/kg at air atmospheric condition, 20 $°C$), d_{wkg} is the humidity ratio difference (kg_water/kg_dryair), which can be determined by Mollier diagram presented in Figure 3.2.

According to the experimental conditions, the h_{we} is selected as 2454 kJ/kg as the condition is a general air atmospheric pressure (Singapore at sea level). The temperature is cooled from 24 $°C$ to 16 $°C$ in cooling process, and the specific humidity is between 0.011 kg_water/kg_dryair and 0.0067 kg_water/kg_dryair by checking the Mollier Diagram. With the range of air flow rate of 0.1812 m^3/s and 0.302 m^3/s as calculated above, the latent heat profile is between 2.298 kW and 3.83 kW. The above calculations demonstrate the sensible and latent heat profiles in the thermal laboratory.

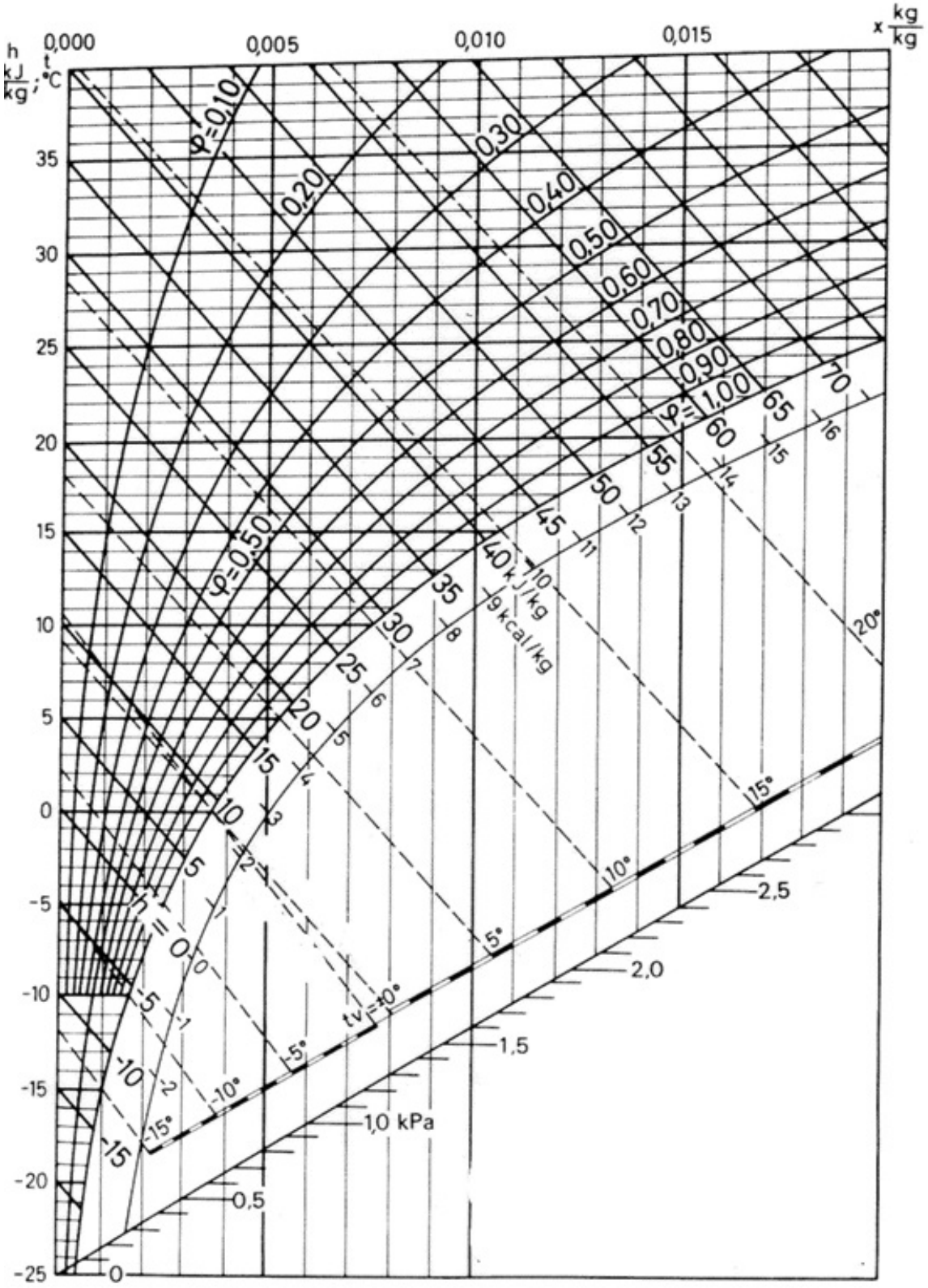

Figure 3.2: Mollier Diagram

3.2 ACMV Energy Consumption Modeling

In this section, the modeling of energy consumption of ACMV systems is presented. Since the operation conditions of ACMV systems have direct impacts on the energy consumption as well as the built environment, the correlation study between operation conditions and energy consumption will offer an important perspective. The operation data of ACMV systems were collected and recorded through experiments. The ACMV systems consist of the following units: Air Handling Unit (AHU), Water Chiller Unit (WCU) and Liquid Dehumidification Unit (LDU) as shown in Figure 3.3. The main energy consuming apparatuses are supply air fan motor (AHU), compressor (WCU), water pump (WCU) and condenser (WCU). In this study, the physical systems of AHU and WCU are illustrated in Figure 3.4, and LDU is presented in Figure 3.5.

In order to operate ACMV systems versatilely, Variable Frequency Drives (VFD) are applied to supply air fan motor, compressor and water pump. The condenser is not operated by variable frequency drives (VFD), and it works continuously at its rated operating condition once started. Traditionally, the energy consumption of AHU and WCU is examined by power meters measuring currents and voltages, which make the systems complex and not real-time. Therefore, an ML-based energy model has been proposed to predict energy consumption in real-time and without increasing the systems' complexity. Thus, the whole study are centered around the key control parameters which are the operating conditions of three components, namely the supply air fan motor, compressor and water pump. In addition, the models of supply air fan motor, compressor, water pump, condenser and power meter are listed in Table 3.1, and the corresponding VFD devices are given in Table 3.2:

The thermal laboratory is the place where experiments were conducted, and it was

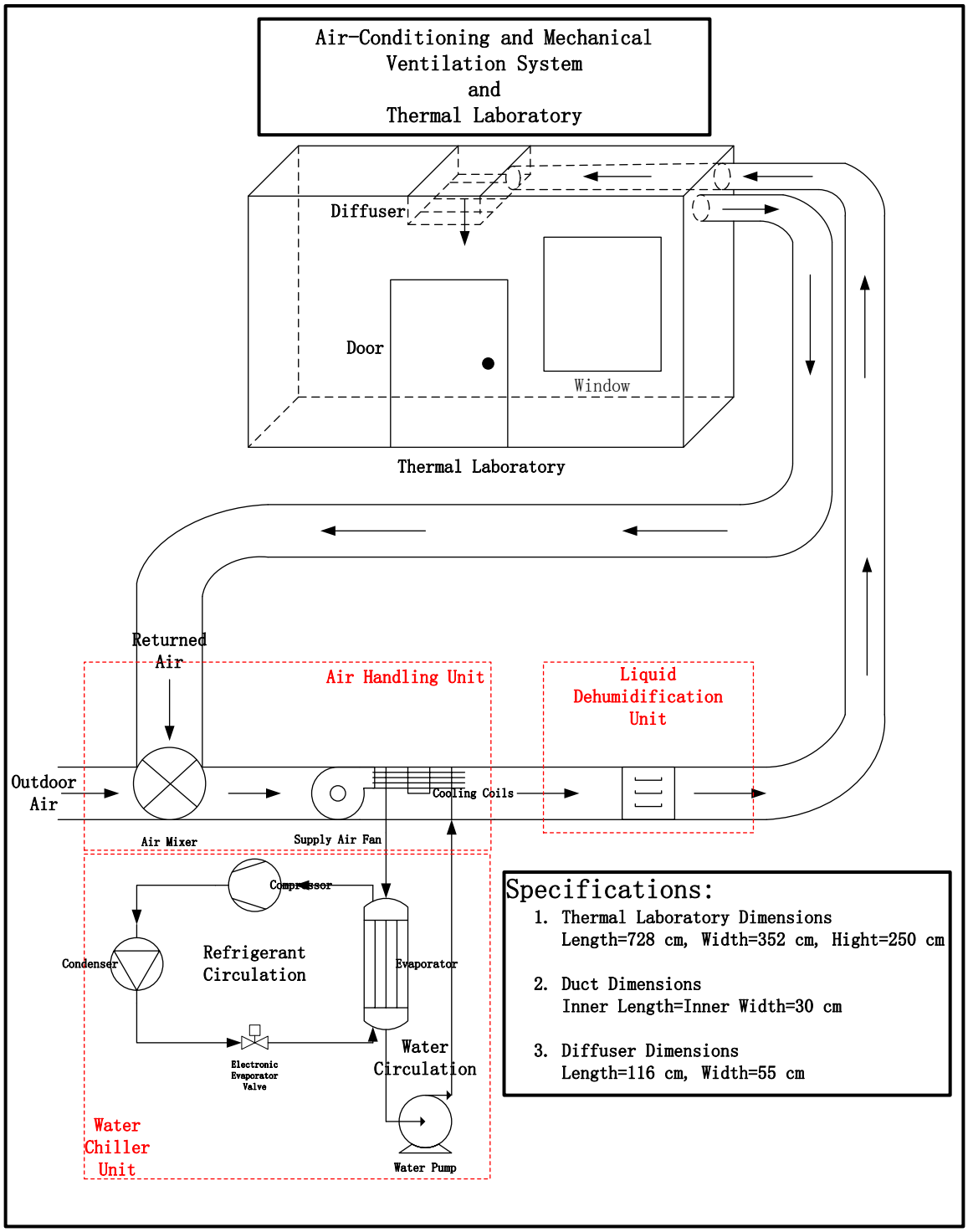

Figure 3.3: Air-Conditioning and Mechanical Ventilation Systems

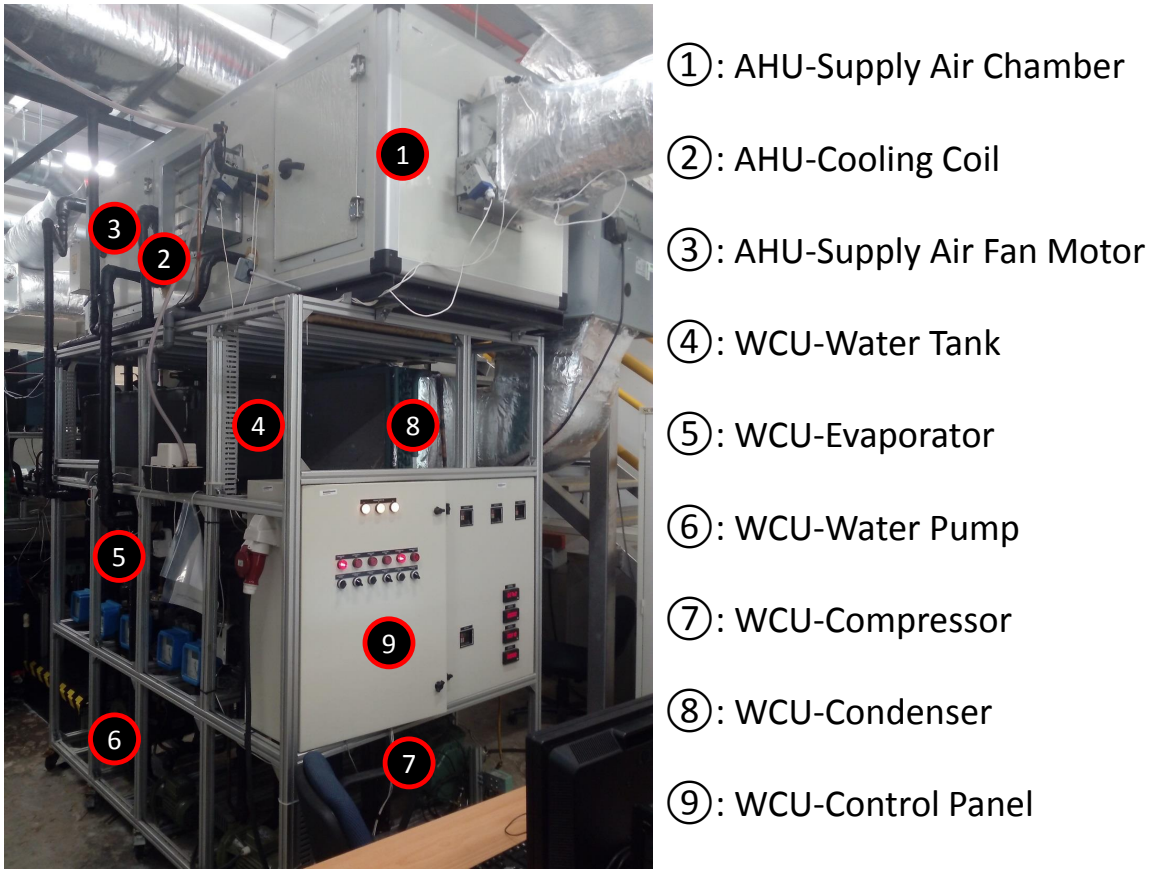

Figure 3.4: Air-Handling Unit and Water Chiller Unit

Table 3.1: Electric Appliances of ACMV Systems

Appliance	**Model**	**Specification**
Supply Air Fan Motor	TECO INVERTER MOTOR AEHLVS	3P: 0.75 kW (Rated)
Compressor	BITZER 4CES-6Y-40S	3P: 9.7 kW (Rated)
Water Pump	SAER ELETTROPOMPE CMP/76	3P: 0.76 kW (Rated)
Condenser	WOLTER EKH 400-4	1P: 0.47 kW (Rated)
Power Meter	YOKOGAWA IM CW240E	3P3W/1P2W

Table 3.2: Electric Appliances VFD of ACMV Systems

Appliance	**Model**	**Specification**
Supply Air Fan Motor VFD	ABB ACS510	3P: $380 - 480$ V, $1.1 - 160$ kW
Compressor VFD	OMRON 3G3MX2-A4055	3P: 400 V, 5.5 kW
Water Pump VFD	OMRON 3G3MX2-A4040	3P: 400 V, 4.0 kW

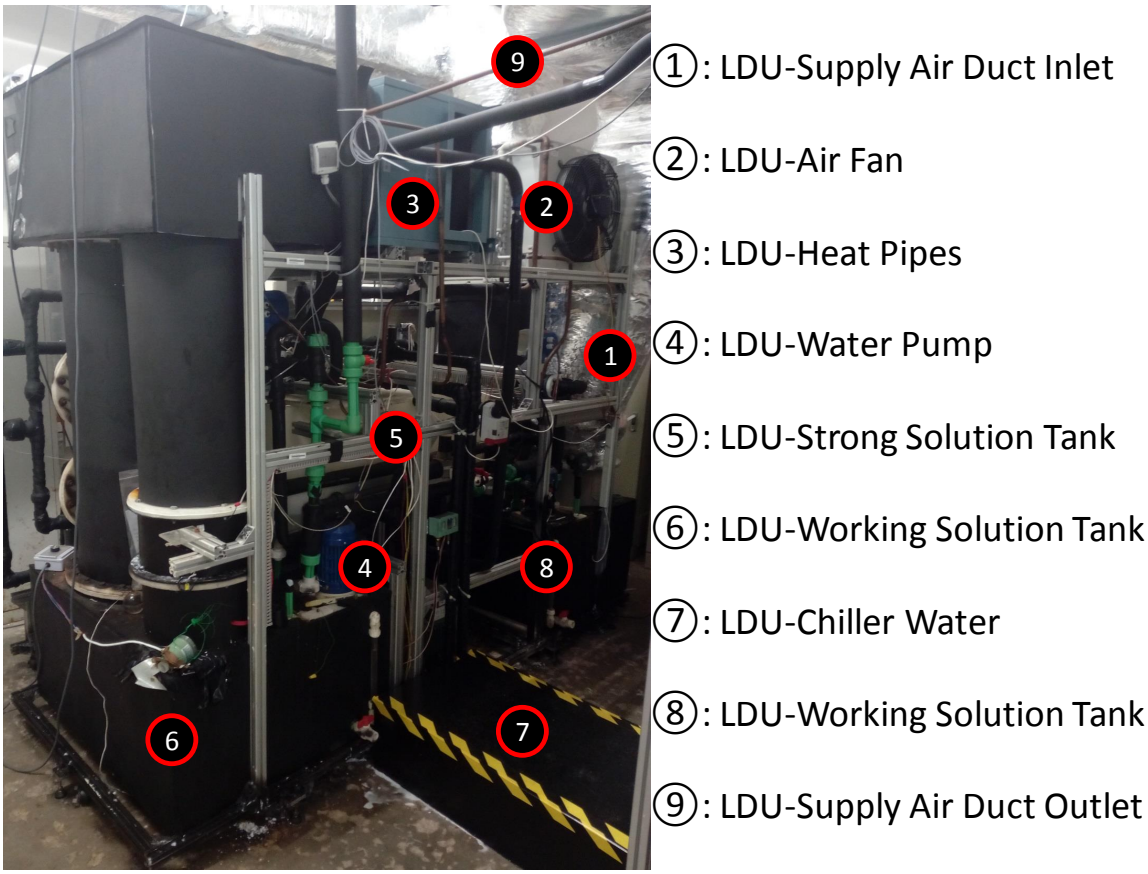

Figure 3.5: Liquid Dehumidification Unit

also one of the main set-ups in the School of Electrical and Electronic Engineering, Nanyang Technological University, Singapore for studying the performance of ACMV systems. The thermal laboratory has a dimension of $7.28m \times 3.52m \times 2.50m$ (length, width and height). The thermal laboratory is isolated from the outside environment, and air-conditioned solely by ACMV systems in the laboratory. Environmental sensors are installed inside the thermal laboratory, and they monitor the environmental conditions, such as air temperature, air velocity and air relative humidity, etc.

The models of energy consumption of ACMV systems are based on supervised learning. The model topology of neural networks (NN) is shown in Figure 3.6.

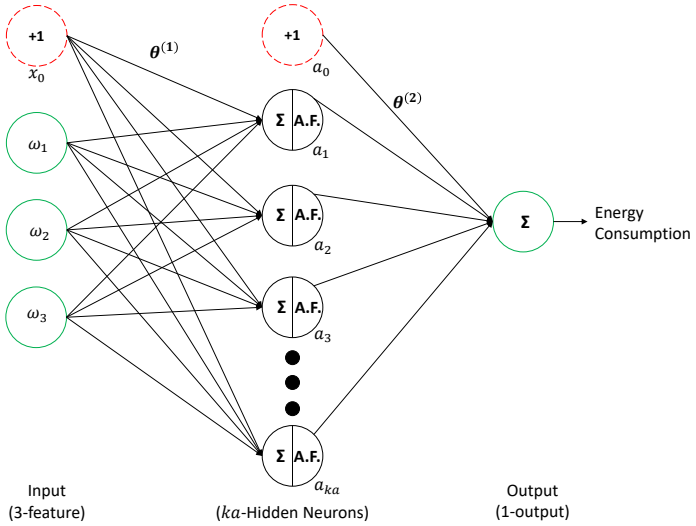

Figure 3.6: Neural Networks - Energy Consumption

The models are established for monitoring and predicting energy consumption of ACMV systems. The training of neural networks is based on back-propagation and convex optimization (basically batch/stochastic gradient descent approaches). The objective is to minimize the cost function or loss function (i.e. mean squared errors between model results and ground truth results) with respect to feature weights that will be continuously tuned through back-propagation iterations as mentioned in

Chapter 2. The parameter tuning process is basically solving a convex optimization problem. Generally, Lagrange multiplier, Newton's method and quadratic programming can also be applied to solve this problem in the mathematics point of view.

Based on experimental data, the energy consumption of partially loaded chiller (i.e. compressor and water pump) is analyzed. The visualization of experimental data is presented in Figure 3.7. The experimental data shows that the energy consumption of partially loaded chiller does not always increase with the increase of system operations. This phenomenon is due to the coupling effects of compressor, water pump and supply air fan motor.

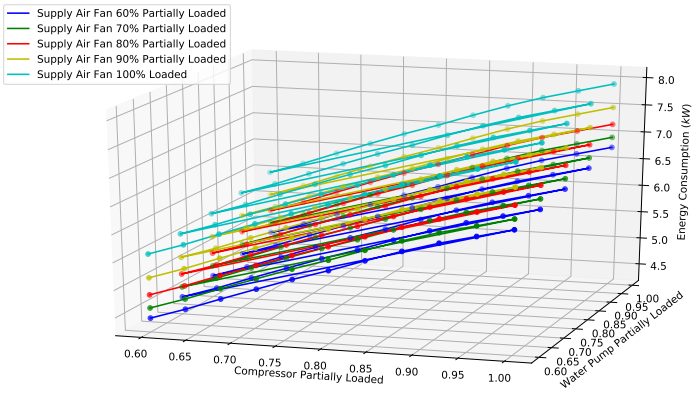

Figure 3.7: Partially Loaded Chiller Energy Profiles

For the models of energy consumption aforementioned, some key assumptions of these models are listed as follows:

- The models are merely associated with the operation conditions of ACMV systems.
- The weather conditions are not incorporated in the models of this study.
- The models are based on an assumption of uniformly distributed environment.

3.3 Indoor Thermal Comfort Modeling

In this section, different approaches of evaluating on indoor thermal comfort sensations are illustrated. These approaches are based on physical laws and data-driven machine learning techniques. The first group of approaches is largely using environmental parameters to train the thermal comfort models. The second group of approaches is only using physiological parameters to train the thermal comfort models. The last group of approaches is a hybrid one that can be trained by both environmental and physiological parameters. In this thesis, only the first and second groups are discussed in details. To be consistent throughout the thesis, the approaches largely based on environmental parameters are called passive approaches, while the approaches based on physiological parameters are called active approaches.

Figure 3.8: Thermal Laboratory (Left: Inside, Right: Outside)

The experiments were conducted in the thermal laboratory, located at School of Electrical and Electronic Engineering, Nanyang Technological University, Singapore. The views of inside and outside the thermal laboratory are illustrated in Figure 3.8.

The experimental transducers are installed and utilized to acquire real time data. The information of transducers is tabulated in the Table 3.3.

Table 3.3: Experimental Transducers

Parameter	**Model**	**Specification**
Air Temperature - Duct	EE21-FT3B56/T07	Range: $0 - 60\ ^{\circ}C$, $\pm\ 0.2\ ^{\circ}C$
Air Temperature - Ambient	AOSONG AM2302	Range: -40 $-$ 80 $^{\circ}C$, $\pm$ 0.5 $^{\circ}C$
Air Relative Humidity - Duct	EE21-FT3B56/T07	Range: 0 $-$ 100 %, $\pm$ 2 %
Air Relative Humidity - Ambient	AOSONG AM2302	Range: 0 $-$ 99.9 %, $\pm$ 2-5 %
Air Velocity - Duct	TSI 8455	Range: $0.125 - 50\ m/s$, $\pm$ 2 %
Air Velocity - Ambient	TSI 8475	Range: $0.05 - 0.5\ m/s$, $\pm$ 1 %
Skin Temperature	Exacon D-S18JK	Range: $0 - 50\ ^{\circ}C$, $\pm\ 0.1\ ^{\circ}C$
Surface Temperature	PT-1000 RTD	Range: -200 $-$ 850 $^{\circ}C$, $\pm$ 0.3 $^{\circ}C$

For the models of thermal comfort (passive and active approaches) aforementioned, some key assumptions of these models are listed as follows:

- The environmental parameters (ambient air temperature and ambient air velocity and ambient air humidity) in passive approach are treated as uniformly distributed for simplifying the models.
- The metabolic rate in passive approach is determined by checking activity-metabolic rate table.
- The skin temperature in active approach is represented by the skin temperature of the back of the hand.
- The questionnaires for the occupants are assumed to naturally reflect the subjective feelings which are not biased by the bulky and messy experimental devices.

The experiments are carried out in the thermal laboratory along with questionnaires for the occupants. The questionnaire is attached in Figure 3.9. The feedbacks of

occupants are treated as ground truths for evaluating and validating the models of passive and active approaches.

Thermal Comfort Questionnaire

This questionnaire is part of study aiming to evaluate thermal comfort levels of occupant in the experimental indoor environment. **We appreciate your feedback, and keep your feedback confidential**. Please fill up and tick appropriately in the form.

1. Name:	Gender:	□ Male	□ Female	
2. Age:	Height:	(m)	Weight:	(kg)
3. Clothing Please tick the corresponding wearing as you fill up this questionnaire in the Table 1 below. If your wearing is not listed in Table 1, please describe in the blank space provided below. Clothing Description:				
4. Activity Level Please tick the most suitable activity as you fill up this questionnaire. □ Seated / Writing, 1 met □ Typing, 1.1 met □ Standing Relaxed, 1.2 met □ Walking About, 1.7 met □ Light Machine Work, 2.2 met □ Heavy Machine Work, 4 met				
5. Thermal Comfort Level Please tick the most suitable level as you fill up this questionnaire. □ +3 Hot □ +2 Warm □ +1 Slightly Warm □ 0 Neutral □ -1 Slightly Cool □ -2 Cool □ -3 Cold				

Clothing Description	**Remark** (Please tick appropriately)
Trousers + Short-sleeve shirt	
Trousers + Long-sleeve shirt	
Trousers + Long-sleeve shirt + Suit jacket	
Trousers + Long-sleeve shirt + Suit jacket + Vest + T-shirt	
Trousers + Long-sleeve shirt + Long-sleeve sweater + T-shirt	
Knee length skirt + Short-sleeve shirt	
Knee length skirt + Long-sleeve shirt	
Knee length skirt + Long-sleeve shirt + Long-sleeve sweater	
Angle-length skirt + Long-sleeve shirt + Suit jacket	
Walking shorts + Short-sleeve shirt	
Long-sleeve overalls + T-shirt	
Overalls + Long-sleeve shirt + T-shirt	
Sweat pants + Sweat shirt	

Table 1: Clothing Description

Figure 3.9: Thermal Comfort Questionnaire

3.3.1 Passive Approach

In passive approaches, the widely-adopted Predicted Mean Vote (PMV) model has been implemented as thermal comfort sensation indicators. According to the PMV model, there are seven parameters to predict thermal comfort sensations, and these parameters are ambient air temperature, ambient air relative humidity, ambient air velocity, mean radiant temperature, metabolic rate, clothing insulation and external mechanical work done.

Table 3.4: Angle Factor Coefficients

State	**Position**	F_{max}	A	B	C	D	E
Seated	Wall or Window facing person	0.118	1.216	0.169	0.717	0.087	0.052
	Floor or Ceiling facing person	0.116	1.396	0.13	0.951	0.08	0.055
Standing	Wall or Window facing person	0.12	1.242	0.167	0.616	0.082	0.051
	Floor or Ceiling facing person	0.116	1.595	0.128	1.226	0.046	0.044

The parameters of ambient air temperature, ambient air relative humidity and ambient air velocity can be obtained directly by transferring raw analogue voltage signals into real physical terms, and they are further logged into database with respect to corresponding operating conditions of ACMV systems for neural networks modeling. The mean radiant temperature is defined as uniform temperature of a black imaginary enclosure that leads to same heat loss by radiant of the occupant. There are two ways to determine this parameter.

The first method uses surface temperatures and angle factors to estimate the mean radiant temperature [6]. The angle factors are calculated through the occupant states (i.e. seated or standing) and dimensions of space according to REHVA Guidebook No.7 [6]. The angle factor coefficients are shown in Table 3.4.

The equations of calculating angle factors are presented as follows:

$$
\begin{aligned}
&T_{mr} = \sqrt[4]{\sum_{i=1}^{n} F_i \cdot (T_{sf_i} + 273)^4} - 273 \\
&\sum_{i=1}^{n} F_i = 1 \\
&\tau_{(p)} = A + B \cdot \left(\frac{a}{c}\right)_{(p)} \\
&\gamma_{(p)} = C + D \cdot \left(\frac{b}{c}\right)_{(p)} + E \cdot \left(\frac{a}{c}\right)_{(p)} \\
&F_{i(p)} = F_{max} \cdot \left(1 - \exp\left(-\frac{a}{c \cdot \tau}\right)_{(p)}\right) \cdot \left(1 - \exp\left(-\frac{b}{c \cdot \gamma}\right)_{(p)}\right) \\
&F_i = \sum_{p=1}^{4} F_{i(p)}
\end{aligned}
\tag{3.4}
$$

According to the dimensions of experimental zone (i.e. thermal laboratory), the calculation matrix of six surface angle factors are given in Table 3.5 and Table 3.6, where a, b and c are the corresponding surfaces of the experimental space. Therefore, the mean radiant temperatures can be calculated correspondingly as Eq. 3.4.

The second method is based on air velocity, globe and air temperatures to estimate mean radiant temperature. A series of equations estimate the mean radiant temper-

Table 3.5: Calculations of Angle Factor (Occupant State: Seated)

	Subsurface	a	b	c	a/c	b/c	τ	γ	$F_{i(p)}$	F_i
Left Wall	1	1.76	1.9	3.64	0.483516	0.521978	1.297714	0.787555	0.017786	0.049945
	2	1.76	1.9	3.64	0.483516	0.521978	1.297714	0.787555	0.017786	
	3	1.76	0.6	3.64	0.483516	0.164835	1.297714	0.756484	0.007186	
	4	1.76	0.6	3.64	0.483516	0.164835	1.297714	0.756484	0.007186	
Right Wall	1	1.76	1.9	3.64	0.483516	0.521978	1.297714	0.787555	0.017786	0.049945
	2	1.76	1.9	3.64	0.483516	0.521978	1.297714	0.787555	0.017786	
	3	1.76	0.6	3.64	0.483516	0.164835	1.297714	0.756484	0.007186	
	4	1.76	0.6	3.64	0.483516	0.164835	1.297714	0.756484	0.007186	
Front Wall	1	3.64	1.9	1.76	2.068182	1.079545	1.565523	0.918466	0.059806	0.176549
	2	3.64	1.9	1.76	2.068182	1.079545	1.565523	0.918466	0.059806	
	3	3.64	0.6	1.76	2.068182	0.340909	1.565523	0.854205	0.028469	
	4	3.64	0.6	1.76	2.068182	0.340909	1.565523	0.854205	0.028469	
Back Wall (Window @ 0.6 m)	1	3.64	1.9	1.76	2.068182	1.079545	1.565523	0.918466	0.059806	0.176549
	2	3.64	1.9	1.76	2.068182	1.079545	1.565523	0.918466	0.059806	
	3	3.64	0.6	1.76	2.068182	0.340909	1.565523	0.854205	0.028469	
	4	3.64	0.6	1.76	2.068182	0.340909	1.565523	0.854205	0.028469	
Ceiling	1	3.64	1.76	1.9	1.915789	0.926316	1.645053	1.130474	0.044634	0.178534
	2	3.64	1.76	1.9	1.915789	0.926316	1.645053	1.130474	0.044634	
	3	3.64	1.76	1.9	1.915789	0.926316	1.645053	1.130474	0.044634	
	4	3.64	1.76	1.9	1.915789	0.926316	1.645053	1.130474	0.044634	
Floor	1	3.64	1.76	0.6	6.066667	2.933333	2.184667	1.519333	0.093003	0.37201
	2	3.64	1.76	0.6	6.066667	2.933333	2.184667	1.519333	0.093003	
	3	3.64	1.76	0.6	6.066667	2.933333	2.184667	1.519333	0.093003	
	4	3.64	1.76	0.6	6.066667	2.933333	2.184667	1.519333	0.093003	

Table 3.6: Calculations of Angle Factor (Occupant State: Standing)

	Subsurface	a	b	c	a/c	b/c	τ	γ	$F_{i(p)}$	F_i
Left Wall	1	1.76	1.3	3.64	0.483516	0.357143	1.322747	0.669945	0.015182	0.058998
	2	1.76	1.3	3.64	0.483516	0.357143	1.322747	0.669945	0.015182	
	3	1.76	1.2	3.64	0.483516	0.32967	1.322747	0.667692	0.014317	
	4	1.76	1.2	3.64	0.483516	0.32967	1.322747	0.667692	0.014317	
Right Wall	1	1.76	1.3	3.64	0.483516	0.357143	1.322747	0.669945	0.015182	0.058998
	2	1.76	1.3	3.64	0.483516	0.357143	1.322747	0.669945	0.015182	
	3	1.76	1.2	3.64	0.483516	0.32967	1.322747	0.667692	0.014317	
	4	1.76	1.2	3.64	0.483516	0.32967	1.322747	0.667692	0.014317	
Front Wall	1	3.64	1.3	1.76	2.068182	0.738636	1.587386	0.782045	0.053406	0.208884
	2	3.64	1.3	1.76	2.068182	0.738636	1.587386	0.782045	0.053406	
	3	3.64	1.2	1.76	2.068182	0.681818	1.587386	0.777386	0.051036	
	4	3.64	1.2	1.76	2.068182	0.681818	1.587386	0.777386	0.051036	
Back Wall (Window @ 0.6 m)	1	3.64	1.3	1.76	2.068182	0.738636	1.587386	0.782045	0.053406	0.208884
	2	3.64	1.3	1.76	2.068182	0.738636	1.587386	0.782045	0.053406	
	3	3.64	1.2	1.76	2.068182	0.681818	1.587386	0.777386	0.051036	
	4	3.64	1.2	1.76	2.068182	0.681818	1.587386	0.777386	0.051036	
Ceiling	1	3.64	1.76	1.3	2.8	1.353846	1.9534	1.411477	0.054484	0.217935
	2	3.64	1.76	1.3	2.8	1.353846	1.9534	1.411477	0.054484	
	3	3.64	1.76	1.3	2.8	1.353846	1.9534	1.411477	0.054484	
	4	3.64	1.76	1.3	2.8	1.353846	1.9534	1.411477	0.054484	
Floor	1	3.64	1.76	1.2	3.033333	1.466667	1.983267	1.426933	0.058358	0.233431
	2	3.64	1.76	1.2	3.033333	1.466667	1.983267	1.426933	0.058358	
	3	3.64	1.76	1.2	3.033333	1.466667	1.983267	1.426933	0.058358	
	4	3.64	1.76	1.2	3.033333	1.466667	1.983267	1.426933	0.058358	

ature as follows:

$$
\begin{aligned}
T_{mr} &= \sqrt[4]{(T_g + 273)^4 + \frac{h_{c,g}}{h_r} \cdot (T_g - T_a)} - 273 \\
h_r &= \epsilon \cdot \sigma = 0.95 \times 5.67 \times 10^{-8} = 5.38 \times 10^{-8} \\
h_{c,g} &= \begin{cases} 6.3 \cdot \frac{(V_a)^{0.6}}{D_g^{0.4}}, & \text{(Forced convection)} \\ 1.4 \cdot \left(\frac{|T_g - T_a|}{D_g} \right)^{0.25}, & \text{(Free convection)} \end{cases}
\end{aligned}
\tag{3.5}
$$

Compared with the first method, this method is much easier to estimate the mean radiant temperature with less measurement costs. However, it has drawbacks since it does not consider the 3 dimensional conditions in space. Therefore, it also normally results in larger errors in predictions with respect to the first method.

3.3.2 Active Approach

Many researchers have shown that the skin temperatures have the most correlation with thermal comfort sensations of occupants. In this study, our proposed approach directly uses physiological parameters to model thermal comfort sensations of occupants. According to the thermal comfort guidelines of ASHRAE Standard 55 2013, the comfortable guideline of air temperature is between 19.4 $^{\circ}C$ and 27.8 $^{\circ}C$, and the comfortable guideline of air humidity is no more than 65%, and the comfortable guideline of air velocity is between 0.05 m/s and 0.23 m/s [6]. The questionnaire also follows the ASHRAE's standard 7 categories of thermal comfort levels, namely -3 (cold), -2 (cool), -1 (slightly cool), 0 (neutral comfort), 1 (slightly warm), 2 (warm) and 3 (hot).

The experiments in this study were carried out to examine 20 occupant subjects one-by-one, and each subject had an monitoring period of 40 minutes. The environmental parameters, physiological parameters and thermal comfort feedbacks of occupants were recorded concurrently. During the first 20 minutes (cold scenario), the supply-air temperature of ACMV systems was set at 16 $^{\circ}C$ with normal ventilations. During the second 20 minutes (general scenario), the supply-air temperature was switched to 24 $^{\circ}C$ with normal ventilations. Before each experiment starts, the experimental room had been prepared at the corresponding temperature for half an hour, so that the room condition was considered as a suitable steady-state for conducting experiments.

The skin temperatures of occupant subjects were recorded every second, and their gradients were calculated accordingly for training models of thermal comfort. Besides skin temperature and its gradient, there are other physiological parameters to be addressed, such as height, weight, gender, etc. These parameters are used to normalize the recorded skin temperatures and corresponding gradients. Since physiological parameters of height, weight and clothing factor (I_{cl}) impact on skin temperature from person to person, a normalization factor is proposed by as follows:

$$\begin{aligned} A_{norm} &= (1 - I_{cl}) \cdot A_{du} \\ A_{du} &= Weight^{0.425} \times Height^{0.725} \times 0.203 \end{aligned} \tag{3.6}$$

where A_{du} is the Du Bois's body surface area.

Hereby the normalized skin temperature is derived as follows for later data analyses

and modeling:

$$T_{sk,norm} = \frac{T_{sk}}{A_{norm}} \tag{3.7}$$

In addition to the many results showing the significant correlations between the skin temperature of the back of the hand and thermal comfort sensation, the gradient of skin temperature is also a promising information that can significantly leads to different thermal comfort sensations. Thus, the normalized gradient of skin temperature is also derived as follows for later data analyses and modeling:

$$T_{sk,grad,norm} = \frac{\nabla_t T_{sk}}{A_{norm}} \tag{3.8}$$

3.4 Problem Formulation and Optimization

In this section, optimization problems are described, and mathematical formulations of the optimization problems are defined. In this thesis, the optimization problems basically involve energy efficiency evaluations (EEE) and comfort sensation evaluations (CSE) for smart buildings in Singapore. Furthermore, the energy are mainly consumed by the centralized air-conditioning and mechanical ventilation (ACMV) systems. Furthermore, the ACMV systems also control and maintain the guaranteed indoor air quality that significantly influences the health and productivity of occupants. Therefore, the optimization problems are narrowed down to balancing the energy efficiency of air-conditioning and mechanical ventilation (ACMV) systems and thermal comfort sensations of occupants.

The optimization problems are classified as multiple-objective non-linear discrete optimizations without the knowledge of analytic mathematical expressions for both objectives. According to the literature on optimization techniques in Chapter 2, the nature-inspired algorithms and Bayesian optimizer have better advantages in solving this type of real application optimizations.

The multiple-objective problems are formulated into two parts. The first part is energy efficiency evaluation (EEE) of air-conditioning and mechanical ventilation (ACMV) systems, and the second part is comfort sensation evaluation (CSE) of occupants. For the first part, the EEE is determined by supply-air fan motor, compressor, water pump and condenser of ACMV systems as formulated in Eq. 3.9:

$$\begin{aligned} EEE &= \sum_{i=1}^{4} E_i(\omega_i) \\ \omega_i &= \left(\omega_1, \omega_2, \omega_3, \omega_4\right)^T, i = 1, 2, 3 \text{ and } 4 \\ \omega_1 &= \omega_{saf}, E_1 = E_{saf} \\ \omega_2 &= \omega_{comp}, E_2 = E_{comp} \\ \omega_3 &= \omega_{pump}, E_3 = E_{pump} \\ \omega_4 &= \omega_{cond}, E_4 = E_{cond} \end{aligned} \tag{3.9}$$

For the second part, the CSE will depend upon the approaches used, so it can be formulated in Eq. 3.10:

$$\begin{aligned} CSE_{psv} &= f_{psv}(M, W, Q) \\ CSE_{atv} &= f_{atv}(T_{sk}, I_{cl}, Height, Weight) \end{aligned} \tag{3.10}$$

With EEE of ACMV systems and CSE of occupants, the optimization problems can

be established by integrating these two components. Since the components have different numerical scales, the normalizations of EEE and CSE are required before formulating the objective functions, and the normalizations are shown in Eq. 3.11:

$$\begin{aligned} EEE_{norm} &= \frac{EEE - EEE_{min}}{EEE_{max} - EEE_{min}} \\ CSE_{norm} &= \frac{CSE - CSE_{min}}{CSE_{max} - CSE_{min}} \end{aligned} \tag{3.11}$$

The normalized EEE and CSE are further formulated as weighted multiple-objective functions by introducing a user-preference tuning parameter (λ) as shown in Eq. 3.12:

$$f_{obj}(\cdot) = \lambda \cdot EEE_{norm} + (1 - \lambda) \cdot CSE_{norm} \tag{3.12}$$

The optimization algorithms are applied to the formulated objective function in order to search for the specific optimal solutions. The optimization algorithms were examined using different algorithms from swarm intelligence to Bayesian. In this thesis, a novel Augmented Firefly Algorithm (AFA) has been proposed and evaluated. It has been compared with other optimization algorithms, namely classic Firefly Algorithm (FA), Bayesian optimization, etc. The pseudo-code of AFA is illustrated in Algorithm 11. The innovations and novelties of the proposed AFA algorithm has already been discussed in Chapter 1.

The evaluation results of computational complexity of classic FA and AFA are illustrated in Figure 3.10. The evaluations are based on a standard 2D optimization function, namely four-peak function. Based on the computation time experiments, AFA outperforms classic FA in both studies of iteration and firefly population.

Algorithm 11 Augmented Firefly Algorithm

Define objective function
    $f(\mathbf{x})$, $\mathbf{x} = (x_1, x_2, \cdots, x_d)^T$
Initialize population of n fireflies $\mathbf{x}_i$ $(i = 1, 2, \cdots, n)$
Determine light intensity I_i at $\mathbf{x}_i$ by $f(\mathbf{x}_i)$
while (not reach stopping criteria):
    for $i = 1 : n$ (all n fireflies):
        if $(I_i < I_{max})$
            $\mathbf{x}_i^{new} = \mathbf{x}_i^{old} + \alpha \cdot \gamma \left(\mathbf{x}_{max} - \mathbf{x}_i^{old} \right) + \beta \cdot \left[(\Delta B - 1) \cdot s + 1 \right] \cdot \epsilon$
            Update new intensity I_i by $f(\mathbf{x}_i)$
        else
            $\mathbf{x}_i^{new} = \mathbf{x}_i^{old} + \beta \cdot \left[(\Delta B - 1) \cdot s + 1 \right] \cdot \epsilon$
            Update new intensity I_i by $f(\mathbf{x}_i)$
    endfor i
endwhile
Visualize population fireflies and obtain global optimum g^*
Stop.

Notes:
$\alpha \in (0, 1]$: Distance Coefficient
$\beta \in [0, 1]$: Randomness Coefficient
$\gamma \in [0, 1]$: Vortex Coefficient
ϵ: Uniform Distribution $(-1, 1)$ / Gaussian Distribution $\mathcal{N}(0, 1)$
ΔB: Maximum Boundary Difference
$s = \begin{cases} 0, & \text{(Small Region Wandering)} \\ 1, & \text{(Large Region Wandering)} \end{cases}$

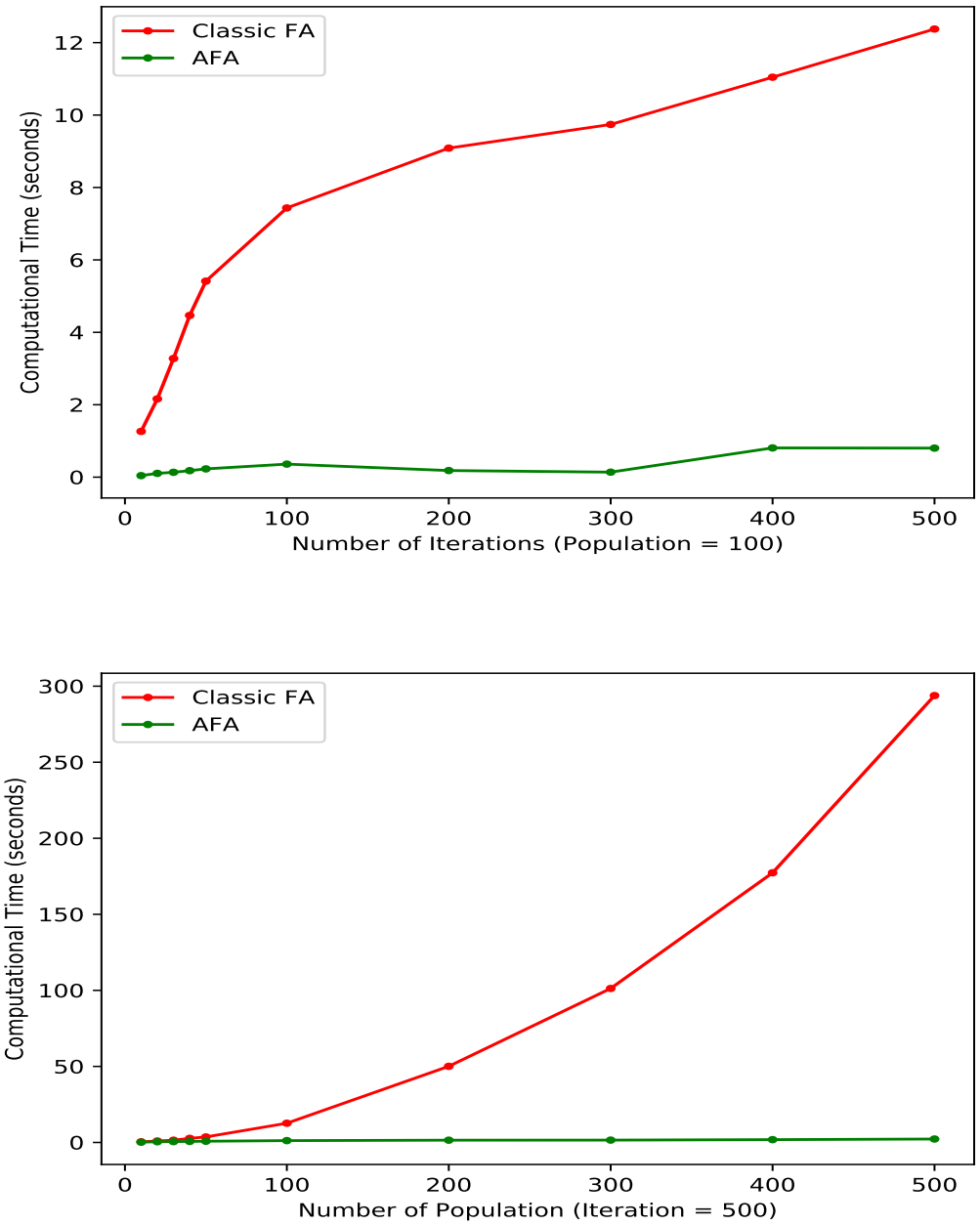

Figure 3.10: Computational Complexity Analysis

In the study of iteration, the computation time is within a range of 0.04s to 0.8s for AFA. While the computation time is between 1.2s and 12s for classic FA. The computation time of classic FA is more than 10 times that of AFA. In the study of population, the computation time is within a range of 0.2s to 2.2s for AFA. However, the computation time varies between 0.4s to 293s for classic FA. The computation time increases exponentially for classic FA with the increase of population.

3.5 Summary

In this chapter, the methodologies of modeling and optimization are presented for energy consumption and thermal comfort sensations. First, the data acquisition system and control system of air-conditioning and mechanical ventilation (ACMV) are designed and implemented so as to enable the evaluations of subsequent studies on energy efficiencies and thermal comfort. Second, the different component units of ACMV systems are introduced in details. The machine learning models of energy consumption of ACMV systems are described through the neural networks topology. Third, the models of thermal comfort sensation are described through the use of passive and active approaches and verified with 20 experimental occupants. Fourth, the optimization formulation is described in details, and the justifications of improvement of classic Firefly Algorithm (FA) to yield the proposed Augmented Firefly Algorithm (AFA) are illustrated and demonstrated through computational complexity evaluations. In the next two chapters, the optimization evaluations between energy efficiency evaluations (EEE) and comfort sensation evaluations (CSE) are discussed using passive and active approaches, respectively.

Chapter 4

Energy Efficiency Evaluation

- Using Passive Approaches

4.1 Introduction

The very subjective term of "thermal comfort" could have different "quantifications" for different environmental conditions and occupants. A significant milestone on its definition can be dated back to 1970s when Fanger developed a way of quantifying thermal comfort through environmental and occupant parameters [6]. He derived a term called "Predicted Mean Vote (PMV)" [26] for evaluating thermal comfort levels of occupants. Based on the conversion from a subjective term to a quantified term, it is applicable to evaluate the multiple-objective problem of energy efficiency and indoor thermal comfort. In this chapter, machine learning modeling and experimental results are presented for energy efficiency evaluations (EEE) based on passive approaches of thermal comfort sensation evaluations (CSE).

Table 4.1: Two Scenarios in Experiments

Case 1 General Offices	**Case 2** Lecture Theatres/Conference Rooms
$M = 70W/m^2$ $I_{cl} = 0.08Km^2/W$ $\phi = 58\%$	$M = 93W/m^2$ $I_{cl} = 0.1Km^2/W$ $\phi = 58\%$

4.2 Method - Passive Approaches

In this section, the methodologies of modeling and optimizations of ACMV systems are presented. One of supervised learning techniques, Neural Networks, is selected as the modeling technique for energy consumption, ambient air temperature, ambient air velocity, and mean radiant temperature. Two case studies are focused, and the non-parameterized conditions (i.e. metabolic rate, clothing insulation and relative humidity) are tabulated in Table 4.1. The overall analytic diagram of modeling and optimization is presented in Figure 4.1 with the controllable variables of ω_1 (operating frequency of supply air fan motor), ω_2 (operating frequency of compressor) and ω_3 (operating frequency of water pump). Throughout the whole experiments, the environmental data were monitored and recorded every second for further analysis and modeling.

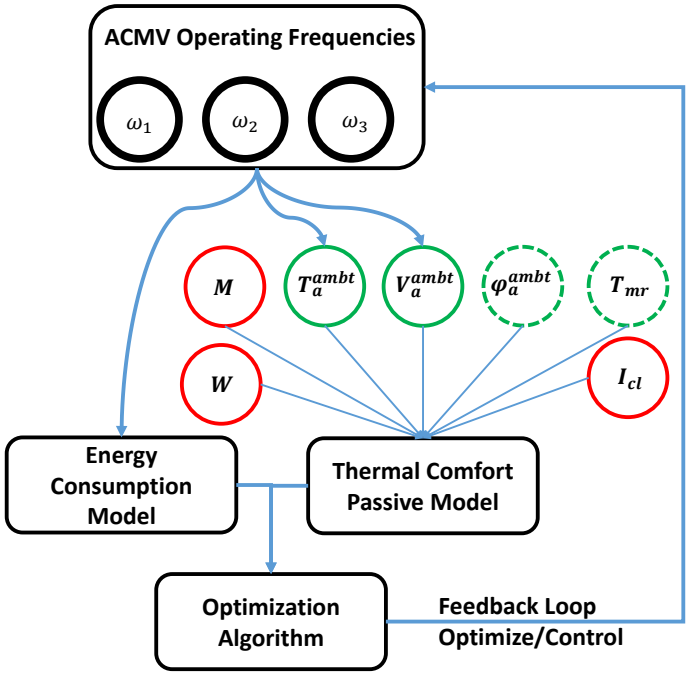

Figure 4.1: Overall Analytic Diagram for Passive Approaches

The external work done (W) is defaulted as zero. The indoor thermal comfort model is presented in a series of equations shown in Eq. 4.1 below:

$$PMV = \left(0.303 \cdot e^{-0.036M} + 0.028\right) \cdot \left(M - W - Q\right) \tag{4.1}$$

where

$Q = Q_{diff} + Q_{evap} + Q_{resp}$,

$Q_{diff} = 3.05 \times 10^{-3} \cdot \left[5733 - 6.99 \cdot (M - W) - P_a\right] - \frac{1}{I_{cl}}\left[T_{cl} - 35.7 + 0.028 \cdot (M - W)\right]$,

$Q_{evap} = 0.42 \cdot (M - W - 58.15)$,

$Q_{resp} = 1.71 \times 10^{-5} \cdot M \cdot (5869 - P_a) + 0.0014 \cdot M \cdot (34 - T_a)$,

$T_{cl} = 35.7 - 0.028 \cdot (M - W) - I_{cl}\left\{3.96 \times 10^{-8} \cdot f_{cl} \cdot \left[(T_{cl} + 273)^4 - (T_{mr} + 273)^4\right] + f_{cl} \cdot h_c \cdot (T_{cl} - T_a)\right\}$,

$$h_c = \max \begin{cases} 2.38 \cdot |T_{cl} - Ta|^{1/4} \\ 12.1 \cdot \sqrt{V_a} \end{cases}$$

$$f_{cl} = \begin{cases} 1.00 + 1.29 \cdot I_{cl}, & (I_{cl} \leq 0.078 m^2 K/W.) \\ 1.05 + 0.645 \cdot I_{cl}, & (I_{cl} > 0.078 m^2 K/W.) \end{cases}$$

$P_a = 6.11 \cdot \frac{\phi}{100} \cdot 10^{\frac{7.5 \cdot T_a}{237.7 + T_a}}$.

4.3 Experimental Result and Discussion

Based on numerous experiments, the final models of energy consumption are trained by assigning 1000 hidden neurons, 500 iterations and 0.1 learning rate; the final models of ambient air temperature are trained by assigning 500 hidden layer neurons, 500 iterations and 0.1 learning rate; the final models of ambient air velocity are trained by assigning 500 hidden layer neurons, 500 iterations and 0.01 learning rate. The

transfer function or activation function of neurons is sigmoid function. According to the training results shown in Figure 4.2, the training costs of models are significantly reduced as the number of hidden layer neurons and the number of iterations increase. But the increase of the number of neurons and iterations will lead to time-consuming training processes. There are trade-offs whenever training processes take place. In order to perform a trade-off between training time and cost, the training costs of energy approach zero when the number of hidden neurons reaches 1000, while the training costs of air temperature and velocity approach zero when the number of hidden neurons reaches 500. Moreover, the training costs of iterations are almost zero when the number of iterations is greater than 500. The valleys of training costs on learning rates are different for energy consumption, air temperature and velocity. It is better to choose a learning rate within the valley, so that the models can be properly trained. The valleys of training costs of energy consumption and air temperature are within a closed interval of [0.01, 0.1]. While the valley of training cost of air velocity is within a closed interval of [0.001, 0.5]. Based on the above results and analysis, the final models of energy consumption, air temperature and velocity are trained according to the aforementioned parameters, and the models are adopted for further implementation and integration.

The passive approaches of thermal comfort evaluations are based on the simplified Fanger's predicted mean vote (PMV) method. Based on the experiments, the evaluations and validations of models established with thermal comfort feedbacks of occupants are presented in Figure 4.3. The PMV model validations show that the prediction accuracies of PMV in cooling and neutral modes are 70% and 75%, respectively. The feedbacks of occupants are treated as the ground truth data.

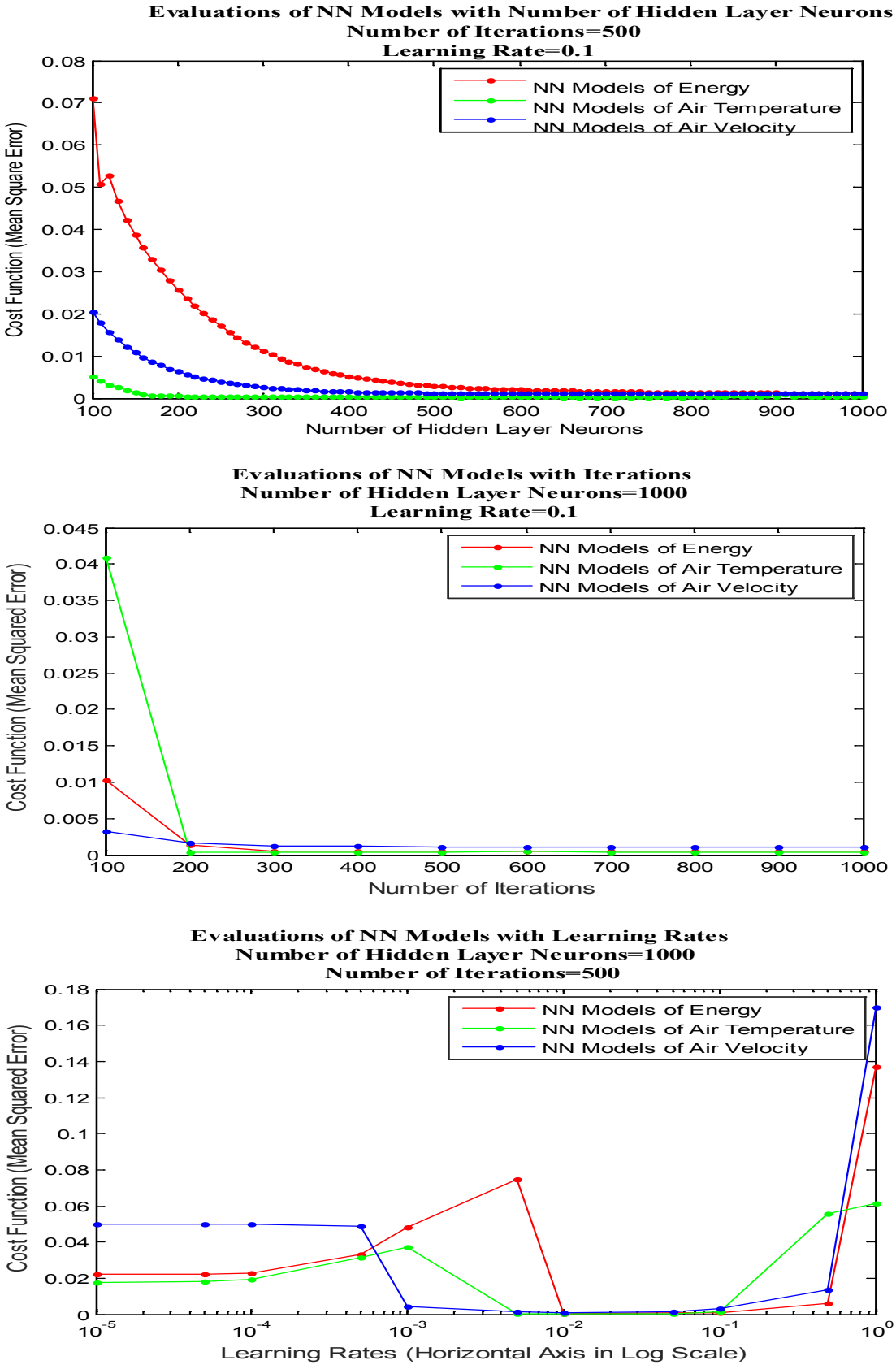

Figure 4.2: Evaluations of NN Models on Neuron, Iteration and Learning Rate

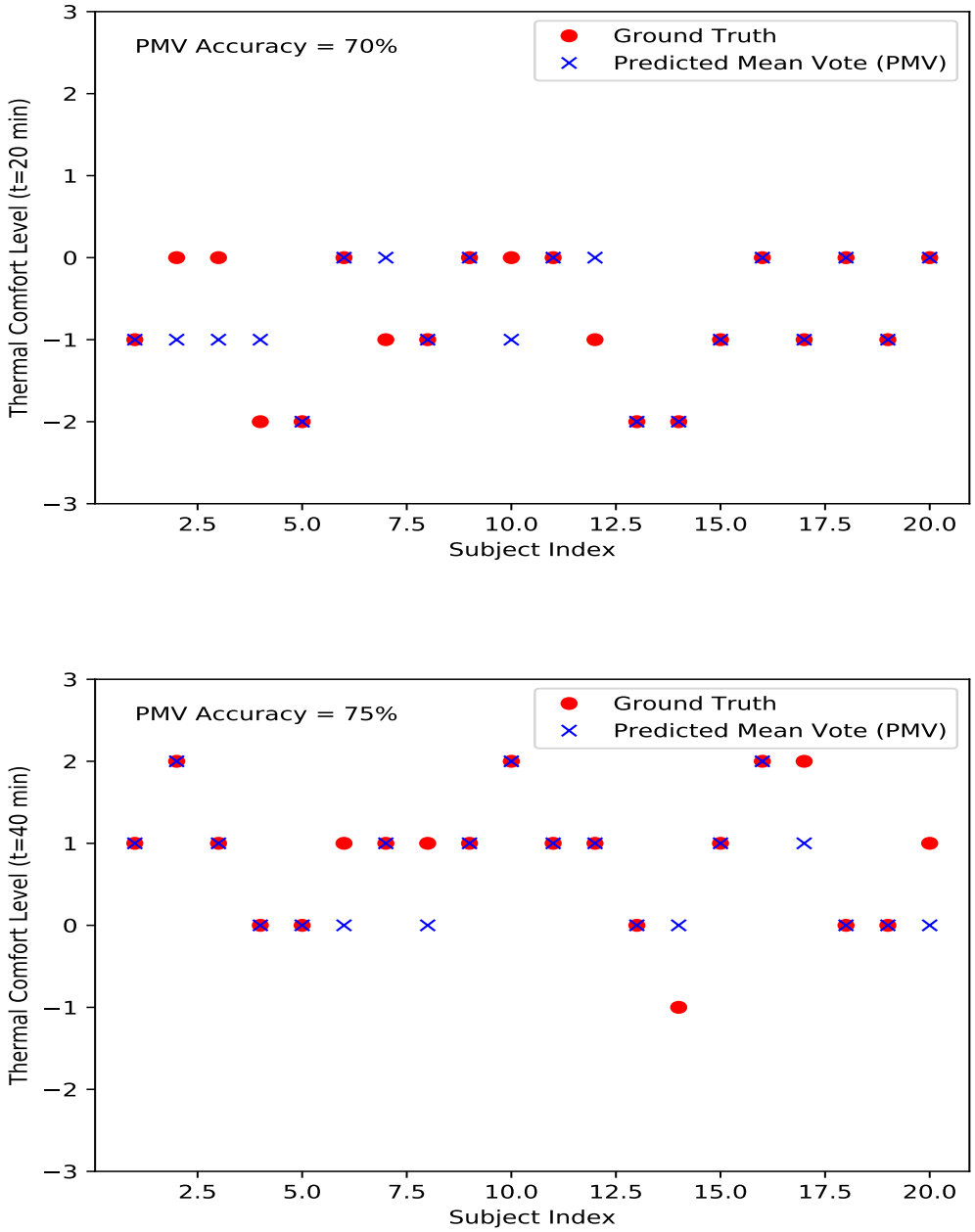

Figure 4.3: PMV Model Validation

4.3.1 Study 1: EEE under Six Schemes of Augmented Firefly Algorithms with Passive PMV CSE

Comprehensive studies of six schemes of Augmented Firefly Algorithms (AFA) based optimizations have been carried out. The discrete optimal solutions can be identified by AFA optimizations. The experiments were carried out with discrete integer operating states (e.g. integer 35 Hz), while the real operating states can be continuously adjusted (e.g. decimal 35.3 Hz). Thus, it is imperative to fill up these gaps, and parameterized 3rd-order polynomial interpolation have been introduced. For the ease of reference, the six different schemes of AFA optimizations with corresponding performance figures are tabulated in Table 4.2, and the performance figures are presented in Figures A1.1 - A1.12 in Appendix A1.

Table 4.2: Tabulation of Six Schemes of AFA with Performance Figures

Scheme	Case 1	Case 2
AFA-SRUW	Figure A1.1	Figure A1.2
AFA-SRGW-I	Figure A1.5	Figure A1.6
AFA-SRGW-II	Figure A1.9	Figure A1.10
AFA-LRUW	Figure A1.3	Figure A1.4
AFA-LRGW-I	Figure A1.7	Figure A1.8
AFA-LRGW-II	Figure A1.11	Figure A1.12

To get visualizations on how the different schemes perform, the evaluations are divided into two groups, which are thermal comfort preferred (TCP) (i.e. $\lambda \leq 0.3$) and energy efficiency preferred (EEP) (i.e. $\lambda \geq 0.7$) according to Eq. 3.12. The statistical analyses of the experimental results in terms of ESR means and ESR standard deviations are presented in Tables 4.3 and 4.4, respectively. According to the thermal comfort guidelines of ASHRAE Standard 55 2013, the comfortable guideline of air temperature is between 19.4 $^{\circ}C$ and 27.8 $^{\circ}C$, and the comfortable guideline of air hu-

midity is no more than 65%, and the comfortable guideline of air velocity is between 0.05 m/s and 0.23 m/s [6]. The questionnaire also follows the ASHRAE's standard 7 categories of thermal comfort levels, namely -3 (cold), -2 (cool), -1 (slightly cool), 0 (neutral comfort), 1 (slightly warm), 2 (warm) and 3 (hot).

According to the statistical analysis of ESR means in Table 4.3, the Large Region Gaussian Wandering (LRGW) has better ESR than the Small Region Gaussian Wandering (SRGW), which means that the ACMV systems can be made more energy efficient on average for both Case 1 and Case 2 over the whole search space.

Table 4.3: Comparisons between Six AFA Schemes on ESR Means

Schemes	**ESR Means (Case 1)**		**ESR Means (Case 2)**	
	$\lambda \leq 0.3$	$\lambda \geq 0.7$	$\lambda \leq 0.3$	$\lambda \geq 0.7$
AFA-SRUW	-9.25%	-23.25%	6.38%	-7.63%
AFA-SRGW-I	-17.75%	-24.78%	**2.5%**	-7.13%
AFA-SRGW-II	-12%	-25.75%	**2.5%**	-8%
AFA-LRUW	-8%	-23.5%	5%	-6%
AFA-LRGW-I	**-19.63%**	**-26.5%**	2.75%	-7.5%
AFA-LRGW-II	-17.75%	-24.75%	3.93%	**-9.83%**

Note: The best results are highlighted in bold font.

Based on Table 4.3, the ESRs of Case 1 are generally much higher than those of Case 2. The main reason behind this observed phenomenon is that the condition of Case 2 has higher metabolic rates and heavier clothing insulations. The ACMV systems have to increase the cooling capacities to balance this expanded cooling demand so as to compensate the required indoor thermal comfort of occupants. The ways of increasing cooling capacity are to raise the operating frequencies of apparatuses according to the developed models. In addition, the statistical analysis of the ESR standard deviations in Table 4.4 demonstrates that the LRGW has relatively less variations than the other schemes, and it is also validated to be relatively more consistent generally.

The reason for good consistency of LRGW is due to its ability to locate the global optimal solutions instead of the local optimal solutions obtained from SRGW. Therefore, the results of LRGW are relatively more consistent than those of SRGW. Based on the experimental results of six different schemes of AFA, we can draw the following conclusions.

Table 4.4: Comparisons between Six AFA Schemes on ESR Standard Deviations

Schemes	**ESR Std Dev (Case 1)**		**ESR Std Dev (Case 2)**	
	$\lambda \leq 0.3$	$\lambda \geq 0.7$	$\lambda \leq 0.3$	$\lambda \geq 0.7$
AFA-SRUW	0.0350	0.0096	0.0382	0.0125
AFA-SRGW-I	0.0222	**0.0022**	0.0342	0.0144
AFA-SRGW-II	0.0440	0.0126	0.0311	0.0091
AFA-LRUW	0.0337	0.0100	**0.0220**	0.0071
AFA-LRGW-I	0.0189	0.0041	0.0377	**0.0000**
AFA-LRGW-II	**0.0104**	0.0029	0.0761	0.0379

Note: The best results are highlighted in bold font.

First, Large-Region Wandering (LRW) performs slightly better than Small-Region Wandering (SRW) based on the continuous regression optimal solutions in Case 1 and Case 2.

Second, Gaussian distribution Wandering (GW) presents better solutions than Uniform distribution Wandering (UW) based on the continuous regression optimal solutions in Case 1 and Case 2. The Gaussian distribution examines two settings in this study, namely $(\mu = 0, \sigma = 0.1)$ and $(\mu = 0, \sigma = 1)$, whereas the Uniform distribution only covers a range of $(-0.5, +0.5)$.

Third, the experimental results show that the Gaussian distribution with $\sigma = 0.1$ provides better solutions than the Gaussian distribution with $\sigma = 1$. Given the experimental results, the average maximum potential Energy Saving Rates (ESRs) are identified at about -26.5% in Case 1 and -9.83% in Case 2, respectively.

Given the three points highlighted above, it is clear that the proposed Large-Region Gaussian Wandering (LRGW) scheme could effectively achieve a better strategy for energy efficiency improvement while maintaining satisfactory indoor thermal comfort conditions in buildings. Besides the technical conclusions drawn, the practical operations of ACMV systems can also be guided by the real-time optimal solutions on site (i.e. operating frequencies feedbacks from AFA optimization solutions) obtained by the proposed models and optimization schemes of AFA. In this way, buildings can perform more energy efficient and environmental-friendly, while maintaining the indoor conditions in pre-defined comfort zones. Besides the aforementioned, there are several limitations that should be noted:

- The thermal laboratory is located in a tropical country. Therefore, the ACMV systems only provide the cooling capacity, which is not a general Heating and Ventilation Air-Conditioning (HVAC) system for all four seasons.
- There is an assumption that the rooms in the buildings are identical for the purpose of experimental simplicity. However, in real applications, each room is different according to its facing, location inside the building and many other factors. Therefore, there is a need for room classifications if we aim to comprehensively improve the energy efficiency of the whole building.

4.3.2 Study 2: EEE under Classic Firefly Algorithm and Augmented Firefly Algorithm with Passive PMV CSE

The experimental results from classic FA and AFA optimizations are presented in Figures A2.1 - A2.6 in Appendix A2, and the experimental results are based on the well-trained models defined from the previous section. According to the experimental

results, the AFA optimizations generally present better results than the classic FA optimizations for both Case 1 and Case 2 when the weight coefficient (λ) increases from 0 to 1. The trend of energy consumption has been shown to decrease when weight coefficient (λ) increases from 0 to 1. One should note that the discrete actual optimized results are plotted and based on the experimental data-driven models, however, the continuing regression results are interpolated and based on the discrete actual optimized results shown from Figure A2.1 to Figure A2.6 in details.

Moreover, the indoor thermal comfort is also optimized via classic FA and AFA optimization algorithms for Case 1 and Case 2. The experimental results are presented in Figure A2.3 and A2.4. The trend of indoor thermal comfort has been shown to approach the neutral standard when the weight coefficient (λ) decreases from 1 to 0.

On the Energy Saving Rate (ESR) evaluations, the benchmarks of the energy consumption of the ACMV is followed at a median operating points. The ESR experimental results are presented in Figure A2.5 and Figure A2.6. The results of AFA optimization are better than those of classic FA optimization in both Case 1 and Case 2. In Case 1, the ESRs of classic FA and AFA optimizations are within intervals $[-25\%, -16\%]$ and $[-24\%, -17\%]$ respectively ($\lambda = 1$) among all different generations at the maximum level of capability as shown in Figure A2.5. In Case 2, the ESRs of classic FA and AFA optimizations are within intervals $[-30\%, -18\%]$ and $[-31\%, -18\%]$ respectively ($\lambda = 1$) among all different generations at the maximum level of capability as shown in Figure A2.6. The negative values of intervals mean that the ACMV system operates at a condition of energy efficiency with respect to median operating conditions.

Based on the experimental evaluations on the optimization algorithms of classic FA and AFA, the AFA is more efficient in comparison to classic FA. Since the complexity

of FA is $O(n^2)$ as shown in classic FA pseudo-code (Algorithm 8) and the complexity of AFA is $O(n)$ as shown in AFA pseudo-code (Algorithm 11), the accuracy of AFA is not only better than that of classic FA, but also the computational complexity of AFA is far less than that of classic FA especially for large population cases.

Based on the results in Figure A2.5 and A2.6, the maximum prediction of potential ESR can be -30% and -31% via the AFA optimizations for Case 1 and Case 2 while maintaining indoor thermal comfort in the pre-defined comfort zone.

In this study, there are some limitations to be noted. First, there are limitations in the experimental results carried on in the laboratory. Since the ACMV system was uniquely designed and isolated from the school ACMV systems, the experimental results are limited for the laboratory so far, but the concept can be generally applied. Second, the experimental results are limited for equator climate regions, since the experiments were carried out in Singapore, a tropical season country. Third, the conceptual aim of this study is to optimize the whole buildings' air and ventilation controlled by ACMV systems. However, there is a presumption that every single room is identical for simplicity purpose. Therefore, there are zones-dividing techniques required for more comprehensively optimizing buildings' efficiency, which could also be future study areas as well.

4.3.3 Study 3: EEE under Bayesian Optimization and Augmented Firefly Algorithm with Passive PMV CSE

The experiments were carried out under different initial sizes of samples from 10 to 50. Due to the constraints of operating conditions of ACMV systems, the boundaries of operating conditions are set as 50 and 30 for upper and lower boundaries respectively.

AFA optimization is based on computational weight and distance learnings according to randomly distributed population. The pseudo-code is illustrated in Algorithm 11. The experimental parameters are presented in Table 4.5 and Table 4.6. The experiments were carried out under different initial sizes of samples ranging from 10 to 50. Due to the constraints of operating conditions of ACMV systems, the boundaries of operating conditions are set as 50 and 30 for the upper and lower boundaries. Gaussian distributions of randomness are selected due to better performances of earlier studies [94].

Table 4.5: Experimental Parameters of Bayesian Gaussian Process Optimization

Parameter	Sample	Boundary	θ_h
Value	10/20/30/40/50	50/30	1

Table 4.6: Experimental Parameters of Sparse Augmented Firefly Algorithms

Parameter	Sample	Boundary	α	β	γ	ϵ
Value	10/20/30/40/50	50/30	0.6	0.3	0.6	Gaussian $(0, 1)$

Following the application of the methodologies mentioned in the previous section, the experimental results of Bayesian Gaussian Process Optimization (BGPO) and Augmented Firefly Algorithm (AFA) optimization are shown in Figures A3.1 - A3.12 in Appendix A3. Both BGPO and AFA statistical analyses are tabulated in Table A3.1 - A3.3 in Appendix A3. Based on the statistical analyses, there are two groups for each of the two cases as Table 4.1 shows. The groups are classified by λ values. The thermal comfort preferred (TCP) group is classified as $\lambda \leq 0.3$. In addition, for $\lambda \geq 0.7$, the group is classified as energy efficiency preferred (EEP) group. Comparing Table A3.1 and A3.2, BGPO generally outperforms AFA in terms of searching for more optimal solutions, since the means of Energy Saving Rate (ESR) are around -21% and -10% for BGPO and AFA respectively for both Case 1 and Case 2. However,

AFA is better than BGPO in terms of consistency, and the standard deviations of ESR are around 0.02 and 0.006 for BGPO and AFA respectively. The increment of sample sizes improves searching precision and consistency as presented in Table A3.1 and A3.2. As seen in Table A3.3, the evaluations at a sample size of 50 reveals that AFA is superior to BGPO in terms of consistency. Moreover, BGPO searches more optimal solutions of ESR than AFA on Case 1 and Case 2. However, AFA locates more precise solutions of PMV than BGPO on Case 1 and Case 2. Furthermore, the ESR and PMV results of Case 1 are more optimal than those of Case 2, due to different environmental resistance to ACMV systems.

Based on the experimental results and analyses of BGPO and AFA above, we can draw the following conclusions.

First, BGPO outperforms AFA in terms of Energy Saving Rate (ESR) in EEP group. BGPO has an ESR of -21% for Case 1 and Case 2 in EEP group, while AFA has an ESR of -10% for Case 1 and Case 2 in EEP group. As the figures presented, BGPO can perform more energy-saving than AFA does on average. Generally, the experimental laboratory consumes 73.741 kWh per day for office hours. In terms of economical performances of these two methodologies, the Singapore Energy Market Authority announced that the electricity costs 21.56 cents per kWh, and it results in a saving of about S$1219.1 annually (equivalently 15% of total energy saving according to the current situation) for such single experimental room compared to general operation conditions without optimization algorithms applied. If all the rooms in the building were governed by the methodology, the electricity tariff could be significantly reduced and demonstrate a large number of economical benefits.

Second, AFA not only surpasses BGPO in terms of indoor thermal comfort (i.e. PMV index), but also in solution consistency in TCP group. The standard deviation of

BGPO is around 0.02 for Case 1 and Case 2. While the standard deviation of AFA is about 0.006 for Case 1 and Case 2. BGPO and AFA have PMV indices of 0.0087 and 0.0008 respectively for Case 1 with a sample size of 50. Similarly, BGPO and AFA have PMV indices at 0.3463 and 0.1524 respectively for Case 2 with a sample size of 50. As shown in the experimental results, although both of BGPO and AFA have located the PMV indices within the pre-defined comfort zone, AFA can locate around 10 times and 2 times better than BGPO does for Case 1 and Case 2 respectively.

Third, the improvements of ESR and PMV can be achieved by both BGPO and AFA with incremental sample sizes. The optimization results in Case 1 are slightly better than those in Case 2, due to different physiological parameters of the experimental occupant. The activity level and clothing factor in Case 1 are significantly lower than those in Case 2. Thus, the cooling demand in Case 2 is higher than that in Case 1, and the ACMV systems do more work to meet the cooling demand in Case 2.

4.4 Summary

In this chapter, the energy efficiency evaluations (EEE) based on three study topics have been presented. The EEE is evaluated under passive approaches of comfort sensation evaluations (CSE) from environmental parameters. The validity and effectiveness of the proposed modeling and optimization algorithms have been validated under various comparative studies of different schemes and methods. Several limitations in these studies can be summarized as follows: (1) the thermal laboratory is located in Singapore, so the ACMV systems only provide cooling capacity; (2) different rooms in buildings are normally different in terms of dimensions, solar radiations, positions and so forth. The experiments were however carried out under the assumption of identical room for different cases in our study due to limitations

of experimental platforms and for the purpose of simplicity. However, suitable room classification techniques can be developed for more comprehensive optimization of buildings' efficiency; (3) The indoor comfort actually consists of more than just thermal comfort, and there are luminous comfort and air quality as well. In this study, the lighting is always provided due to the situation of the thermal laboratory inside the ACMV laboratory of the School of Electrical and Electronic Engineering. In addition, since there is only one occupant in this thermal laboratory during each round of experiment, the air quality (mainly CO_2) was always within the acceptable range while experiments were conducted. Therefore, luminous comfort and air quality of the experimental room are not in the scope of this thesis, only indoor thermal comfort has been investigated. In the next chapter, the experimental results of EEE evaluated with CSE using active approaches will be discussed in details.

Chapter 5

Energy Efficiency Evaluation

- Using Active Approaches

5.1 Introduction

Currently, there are many studies on thermal comfort evaluations with active approaches. In the study of Zhang et al. [96], the thermal sensations of occupants were discussed on the mean skin temperature of 22 body locations. However, the approach was developed for an automobile setting, which could not be adopted into real building environments. Moreover, the approach had high measurement costs, and many measurements were also intrusive to occupants. In the study of Takada et al. [74], a mathematical expression of regression model was proposed. The model was built upon mean skin temperature of 7 body locations. Xiong et al.'s study of thermal sensations of occupants were analyzed from 7 locations of body skin temperature during transient processes of ambient air temperature [83]. Similarly, Liu et al. proposed a method of thermal comfort evaluation based on mean skin temperature of 10 body skin locations in sleeping mode [52]. Due to the constraints of Liu's work in sleeping mode, the skin temperature ranges were limited.

Sim et al. [71] analyzed the skin temperature of 4 skin locations near the hand. The study showed good results, but the validation of models was limited by small

sample sizes. The studies mentioned above are basically intrusive to occupants when measuring those temperatures and they may not be feasible for real applications. In our earlier studies, the thermal comfort sensations of occupants were evaluated and modeled by different approaches [17, 90, 91, 93, 94]. The overall analytic diagram of modeling and optimization is presented in Figure 5.1 with the controllable variables, such as ω_1 (operating frequency of supply air fan motor), ω_2 (operating frequency of compressor) and ω_3 (operating frequency of water pump).

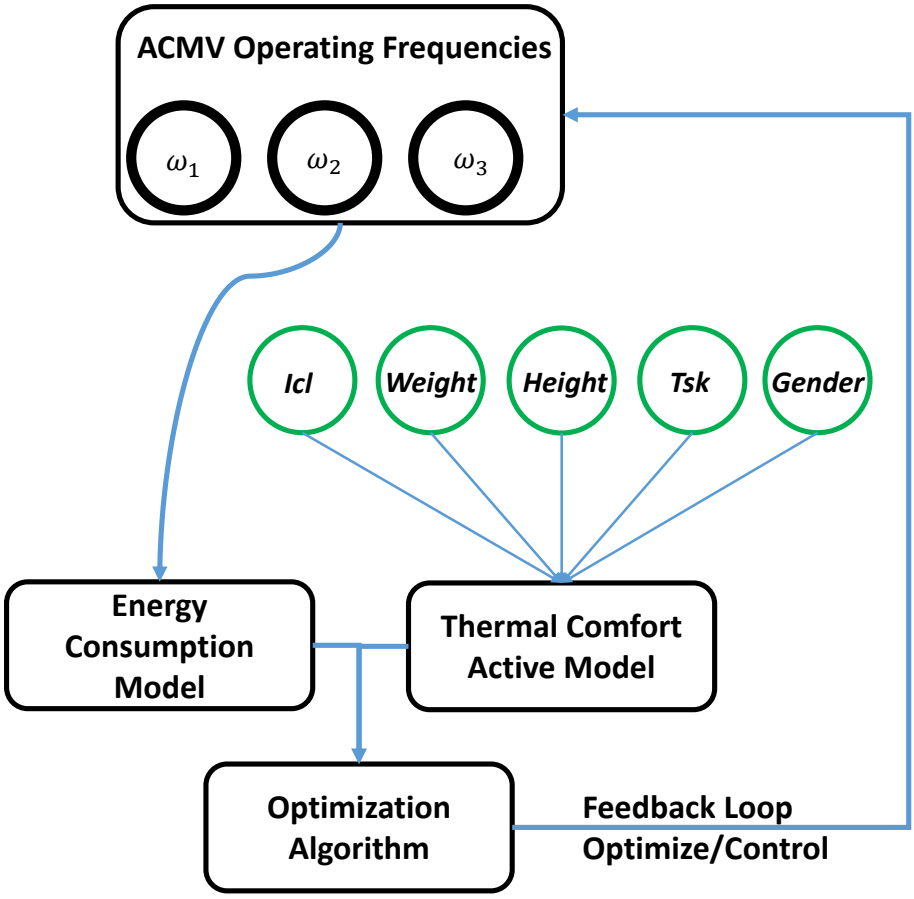

Figure 5.1: Overall Analytic Diagram for Active Approaches

In this study, a novel algorithm is proposed to improve Operating State (OS) of ACMV systems. It is integrated with the models of Predictive Thermal State (PTS) shown in Figure 5.2 and Figure 5.3. The input of PTS model is physiological pa-

rameters of occupants, such as height, weight, clothing and skin temperature. The output of PTS model is the thermal state of occupant, such as -1 (cool discomfort), 0 (neutral comfort) and 1 (warm discomfort). Considering ASHRAE Standard, the cool discomfort (-1) is equivalent to -3 and -2 (PMV), and the neutral comfort is equivalent to -1, 0 and +1 (PMV), and the warm discomfort is equivalent to +2 and +3 (PMV). The training features are selected as normalized skin temperature and normalized skin temperature gradient. The training processes are back-propagation with batch/stochastic gradient descent method.

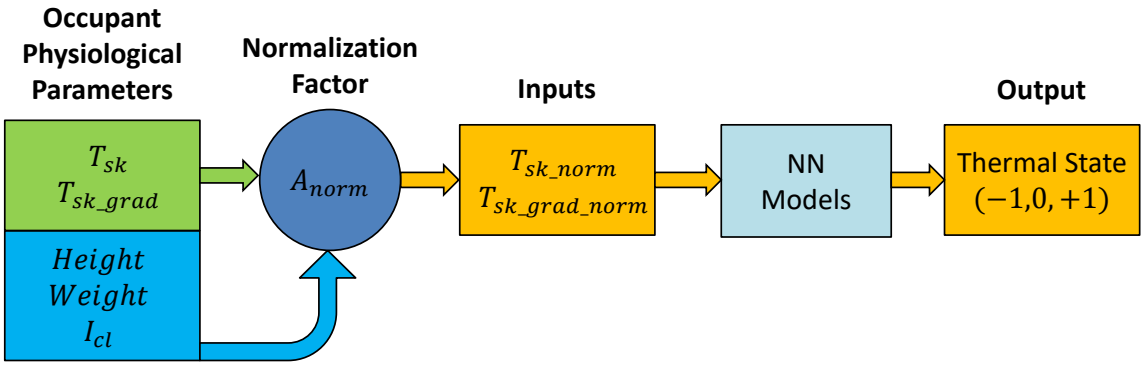

Figure 5.2: Predictive Thermal State (PTS) Models

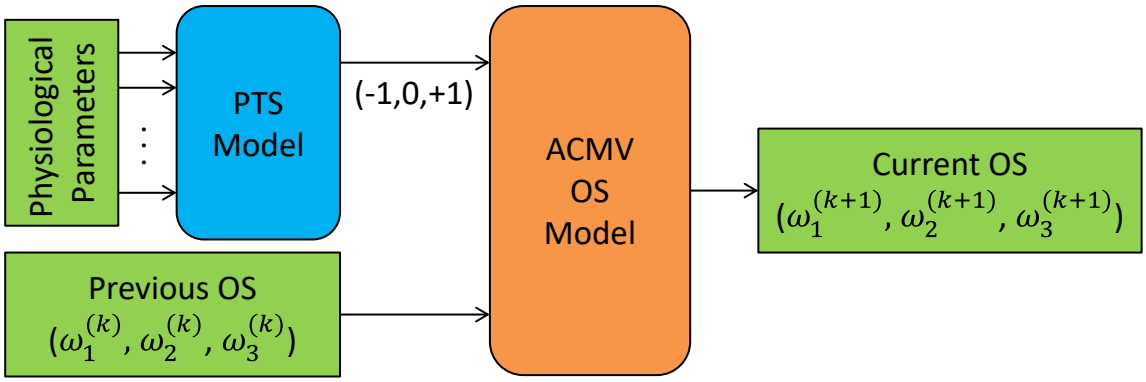

Figure 5.3: Overall Analytical Diagram ($t^{(k)} \rightarrow t^{(k+1)}$)

The OS algorithm of ACMV systems alternates OS considering thermal comfort levels

of occupants in real time, and the overall analytical diagram of this study is shown in Figure 5.3. The proposed PTS model in this study is trained by neural networks. The approach is non-intrusive by only using one spot of skin temperature located at the back of the hand. It could be more feasible for real applications.

5.2 Method - Active Approaches

In this section, methodologies of this study will be illustrated in details. First, PTS models are adopted and described. Second, OS algorithm of ACMV systems is proposed. Third, the energy consumption of ACMV systems embedded with ACMV OS algorithm is evaluated by three cases.

The PTS model shown in Figure 5.2 has been presented in details in our earlier studies [17] and [93], and the PTS model is adopted and applied. The inputs of PTS model are physiological parameters of occupants, and the models are trained by skin temperature. The PTS model then provides predictive thermal states of occupants based on the measurements. The skin temperature (T_{sk}) was recorded every second, therefore an extended feature "gradient of skin temperature (T_{sk_grad})" can be easily calculated. The proposed normalization factor of T_{sk} and T_{sk_grad} is governed by Eq. 2.44. In the ACMV OS algorithm, the ACMV systems acquire and alternate OS every $T_{sampling}$, and a modification factor in temperature is noted as ΔT (i.e. 0.1 $^{\circ}C$).

This problem can be formulated as a Markov Decision Process (MDP). Actions are taken only on the basis of previous states. The pseudo-code of ACMV OS algorithm is illustrated in Algorithm 12. This algorithm has two inputs, which are results of PTS models and Previous Operating State (POS), and the output is Current Operating State (COS).

In this algorithm, there are two important functions to bridge OS and air temperature T_a of the thermal room, namely $F_1(\cdot)$ and $F_2(\cdot)$ as shown in Figure 5.4. The $F_1(\cdot)$ is a function of forward associations of OS and T_a, while the $F_2(\cdot)$ is a function of backward searching OS with respect to T_a which is based on the proposed optimization algorithm, namely Augmented Firefly Algorithm (AFA) [94].

Algorithm 12 ACMV Operating State Algorithm

Input:
  $PMV = \{-3, -2, -1, 0, +1, +2, +3\}$ or $PTS = \{-1, 0, +1\}$
  $POS = (\omega_1(k), \omega_2(k), \omega_3(k))$
Output:
  $COS = (\omega_1(k+1), \omega_2(k+1), \omega_3(k+1))$
for every $T_{sampling}$:
  $if(PMV == 0) \quad or \quad (PTS == 0):$
    $COS \leftarrow POS$
  $elseif(PMV \leq -1) \quad or \quad (PTS == -1):$
    $T_a^{(k)} \leftarrow F_1(POS)$
    $T_a^{(k+1)} \leftarrow T_a^{(k)} + \Delta T$
    $COS \leftarrow F_2(T_a^{(k+1)})$
  $elseif(PMV \geq +1) \quad or \quad (PTS == +1):$
    $T_a^{(k)} \leftarrow F_1(POS)$
    $T_a^{(k+1)} \leftarrow T_a^{(k)} - \Delta T$
    $COS \leftarrow F_2(T_a^{(k+1)})$
Stop.

Derived from the earlier studies [92], the models between E and OS has been well developed and adopted and this virtual bridge is named as $F_3(\cdot)$ in Figure 5.4. This is the key linkage of constructing the objective function in AFA optimizations for $F_2(\cdot)$. Since there could be more than one possible OS solutions given a particular T_a, the optimal OS* is defined in Eq. 5.1:

$$OS^* = \underset{\forall OS|_{T_a}}{\arg\min} F_3(OS|_{T_a}) \tag{5.1}$$

The ACMV systems with ACMV OS algorithm can adjust OS responsively with respect to thermal comfort levels of occupants in real-time, therefore it could intelligently improve the energy efficiency of ACMV systems while taking the thermal comfort of occupants into considerations.

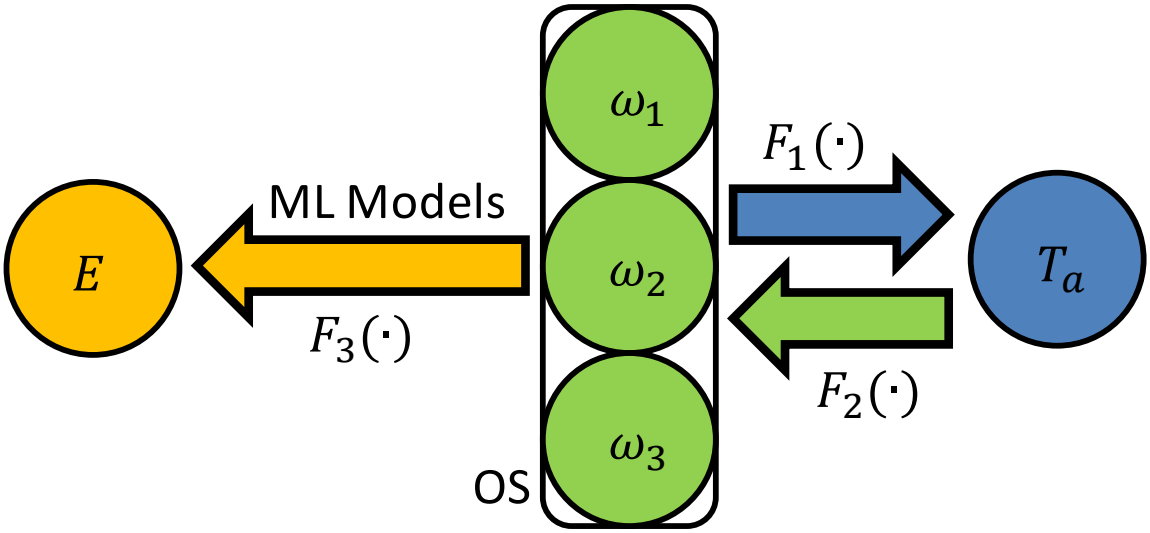

Figure 5.4: Illustrations of Functions F_1,F_2 and F_3

5.3 Experimental Result and Discussion

In this section, the experimental results of air-conditioning and mechanical ventilation (ACMV) systems are evaluated and the corresponding discussions are presented. The essential hardware parts of ACMV systems cannot be updated since manufactured. However, the performance of ACMV systems has been enhanced by the software parts, namely the proposed models and algorithms in this study. The experimental results with active approaches are elaborated in this section for energy efficiency evaluations (EEE) with k-means methods and neural networks modeling methods on comfort sensation evaluations (CSE).

For the active model of thermal comfort, the predictive thermal state (PTS) method is implemented. Based on experimental results, the validation results of PTS models are presented in Figure 5.5. With the ground truth data of occupant feedbacks, the validation results show that the prediction accuracies of PTS in cooling and neutral mode are 95% and 90% ,respectively.

5.3.1 Study 1: EEE under Augmented Firefly Algorithm with K-Means CSE

Since there is a strong correlation between skin temperature and ambient air temperature presented in Figure 5.6, the models of skin temperature are also based on neural networks. The input of the models is ambient air temperature. The output of the models is skin temperature. The activation function or transfer function of neurons is sigmoid function. The training parameters and the training MSE results are shown in Table 5.1 and 5.2 respectively.

Table 5.1: Training Parameters of NN Models

Model	# Hidden Neurons	# Iterations	Learning Rate
$Energy$	3	500	0.06
Ta	3	500	0.01
Ts	3	500	0.01
Ts_grad	3	500	0.01

Table 5.2: Accuracy Evaluations of Models

Model	Mean Squared Error (MSE)
$Energy$	0.023766527
Ta	0.000703694
Ts	0.059943429
Ts_grad	0.040547322

Several studies [20, 21] have shown that thermal comfort can be predicted using

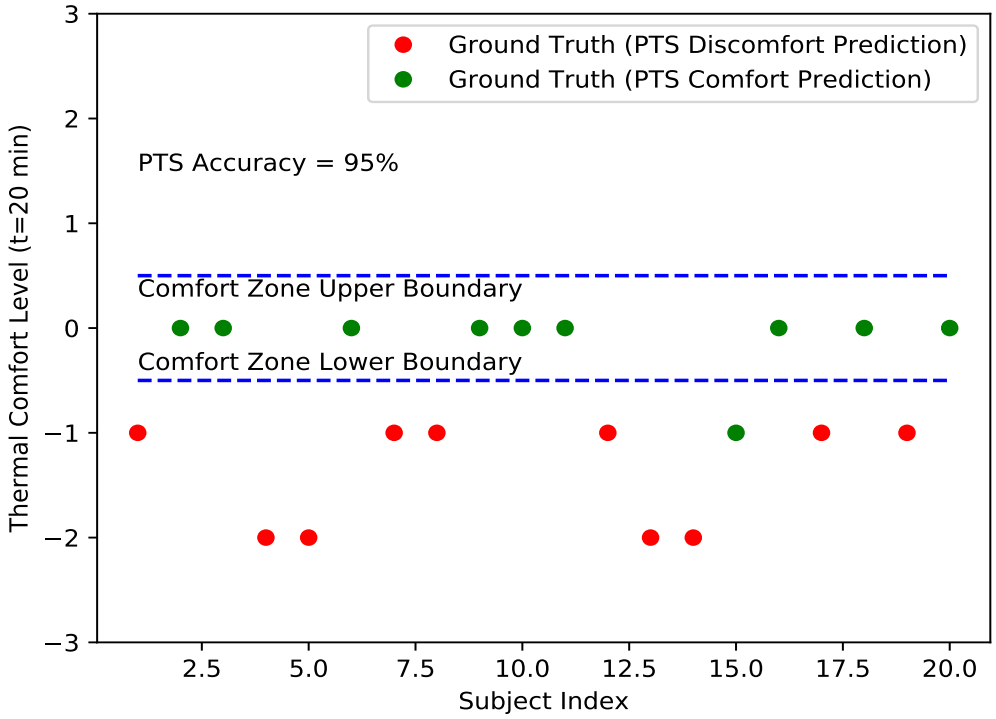

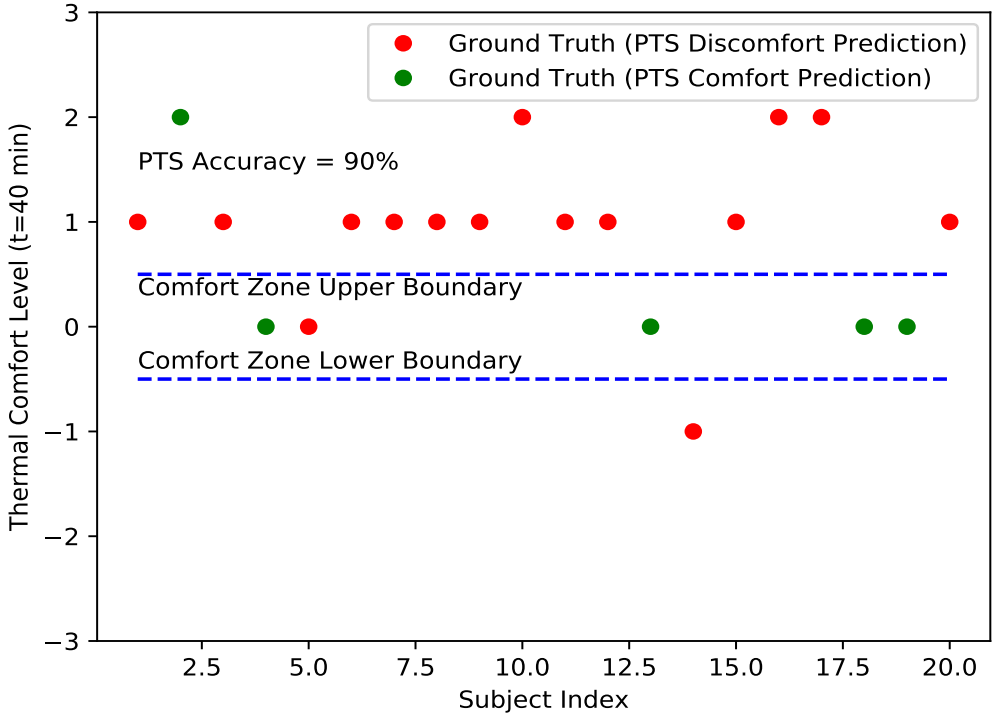

Figure 5.5: PTS Model Validation

peripheral skin temperature as they are strongly correlated. Moreover, the ambient air temperature and skin temperature are also strongly correlated as Figure 5.6 shows. We suggest a new approach for the prediction based on k-means clustering.

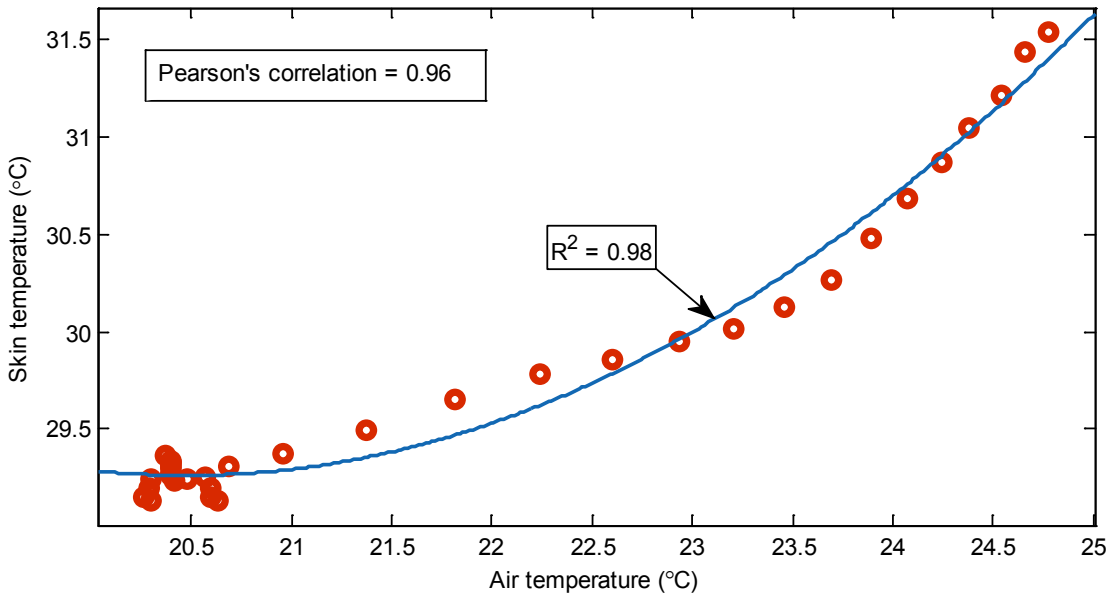

Figure 5.6: Correlations between Air Temperature and Skin Temperature

The k-means clustering works by dividing the observations into k distinct clusters depending on target variable, and assigning new observations to the cluster with shortest Euclidean distance from the cluster centroid. In our study, the thermal comfort model inputs are vectors of skin temperature and skin temperature gradient and the model output is a scalar thermal comfort state, namely "Discomfort (1)" and "Comfort (0)". Thus, k=2 clusters for the two states have been employed, and the optimization problem can be formulated as follows:

Let,

$$\begin{aligned} & g(\omega) \\ =& E(\omega) \cdot TC(T_s[T_a(\omega)], T_{s\_grad}[T_a(\omega), T_s(T_a(\omega))]) \end{aligned} \tag{5.2}$$

Then,

$$\begin{aligned} \text{Problem}: \omega^* &= \underset{\forall\omega}{argmin}(g(\omega)) \\ \text{Subject to}: 30 \leq \underset{\forall i}{\omega_i} &\leq 50 \\ g(\omega) &\neq 0 \end{aligned} \tag{5.3}$$

The energy saving ratio (ESR) is defined as follows:

$$ESR(\omega^*) = \frac{E(\omega^*) - E(\omega_{\mathbf{bench}})}{E(\omega_{\mathbf{bench}})} \times 100\% \tag{5.4}$$

where

ω^* is the optimal operating conditions from AFA optimization algorithm;

$\omega_{\mathbf{bench}}$ is the nominal benchmark operating conditions of ACMV systems (i.e. $\omega_{\mathbf{bench}}$=$[40, 40, 40]^T$);

$E(\omega)$ is the energy consumption NN model;

$Ta(\omega)$ is the air temperature NN model;

$T_s(T_a)$ is the skin temperature NN model;

$T_{s\_grad}(T_a, T_s)$ is the skin temperature gradient NN model; and

$TC(T_s, T_{s\_grad})$ is the thermal comfort k-means model.

Since the previous studies on Augmented Firefly Algorithm (AFA) show better optimization results under identical conditions (i.e. same models and environment) [90], the AFA is chosen as the optimization algorithm for solving this formulated problem. The optimization algorithm is previously presented in Algorithm 11. The comparisons

between uniform and Gaussian distribution randomness are presented in Figure 5.7 and Figure 5.8. As the results show, the optimal solutions can be obtained through larger number of population, and fewer iterations are required when the number of population is large enough. In comparisons, the results of uniform distribution are more consistent than those of Gaussian distribution for larger number of population. It is vice versa for small number of population.

The energy efficiency improvements are presented in Figure 5.9. According to the results, the optimizations with uniform distribution randomness are more consistent with larger population, whereas the optimizations with Gaussian distribution randomness are more consistent with smaller population. The trend of ESR is generally decreasing with the increase of population, and the ESR is generally below -21% (i.e. improving energy efficiency by 21% and more compared with benchmark operating conditions).

The results of the k-means approach applied to thermal comfort model are presented in Figure 5.10. The centroids (T_s, T_{s_grad}) for the Discomfort(1) and Comfort (0) states are found to be (30.0878, -0.0789) and (32.8751, 0.1358) respectively. The mean prediction accuracy is found to be 90%. It is to be noted that thermal comfort states have been predicted with even 100% accuracy for many subjects. Based on the experimental results, some key conclusions are drawn as follows:

- The skin temperature of occupants has strong correlations with ambient air temperature, and the highest R^2 value can be 0.98.
- The predictions of thermal comfort states can be non-intrusively and feasibly achieved by measuring skin temperature of occupants with a time interval. The use of skin temperature and its gradient as features can model thermal comfort

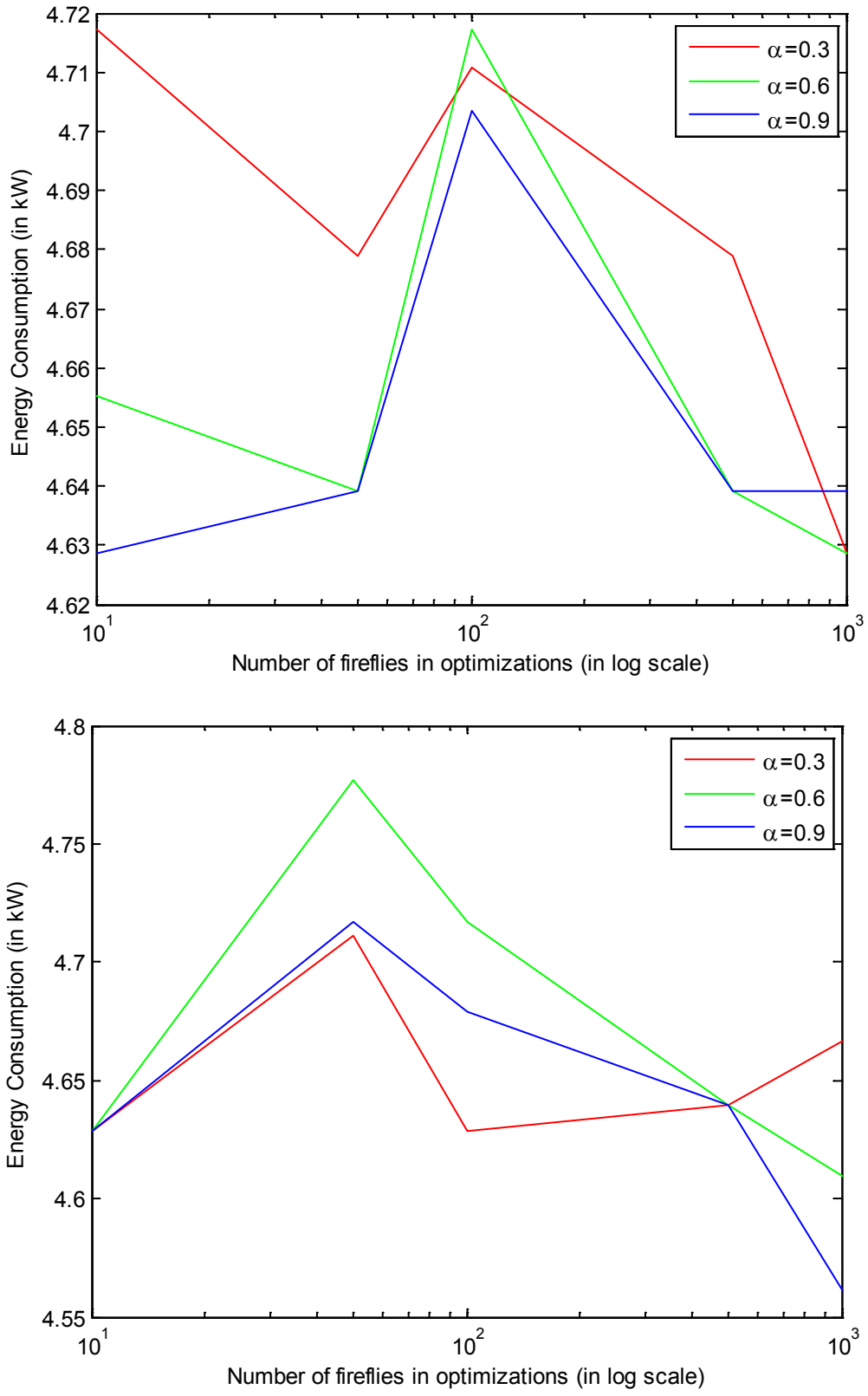

Figure 5.7: Energy Consumption Comparisons: Uniform (Upper) Distribution Randomness and Gaussian (Lower) Distribution Randomness

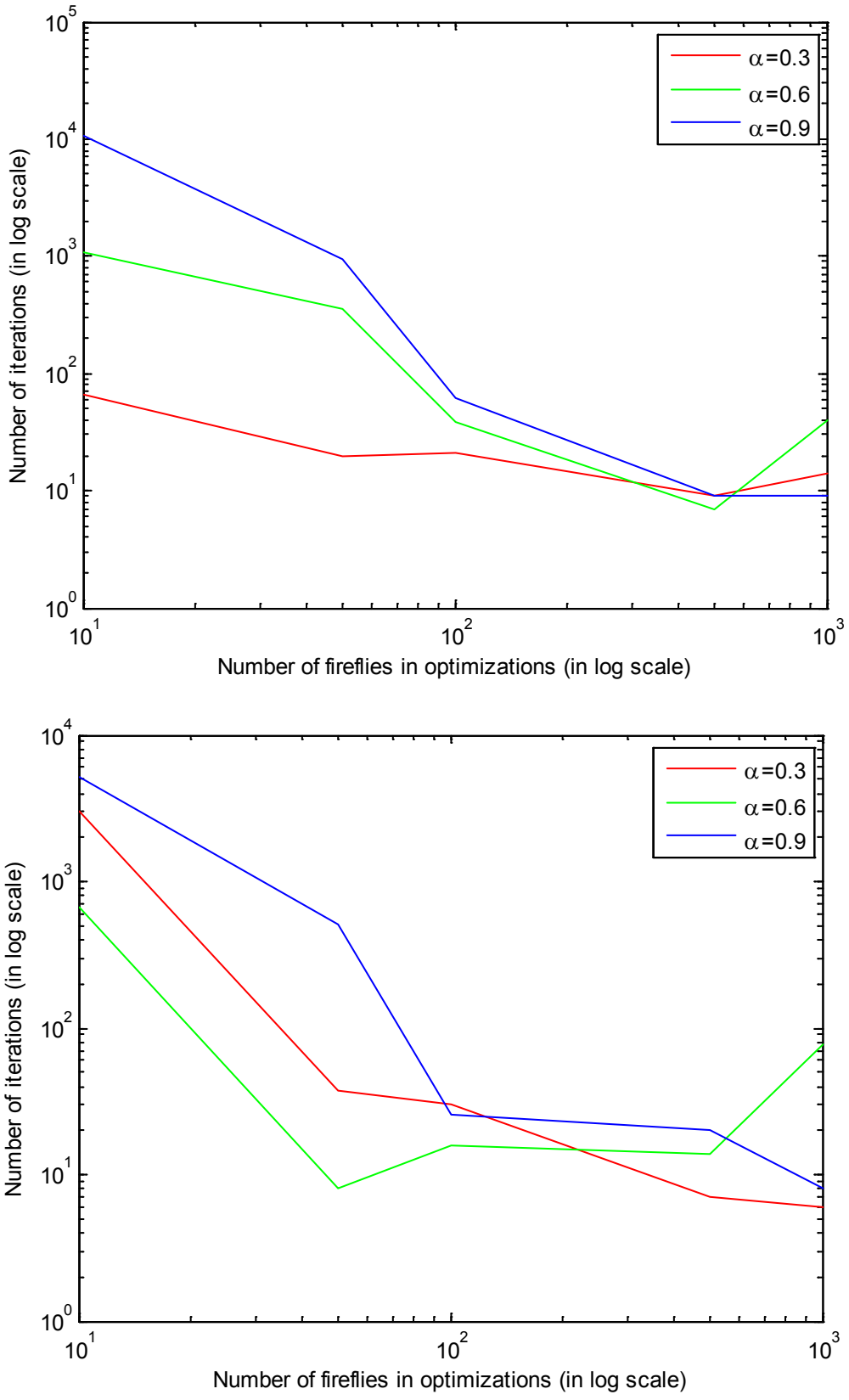

Figure 5.8: Iterations Comparisons: Uniform (Upper) Distribution Randomness and Gaussian (Lower) Distribution Randomness

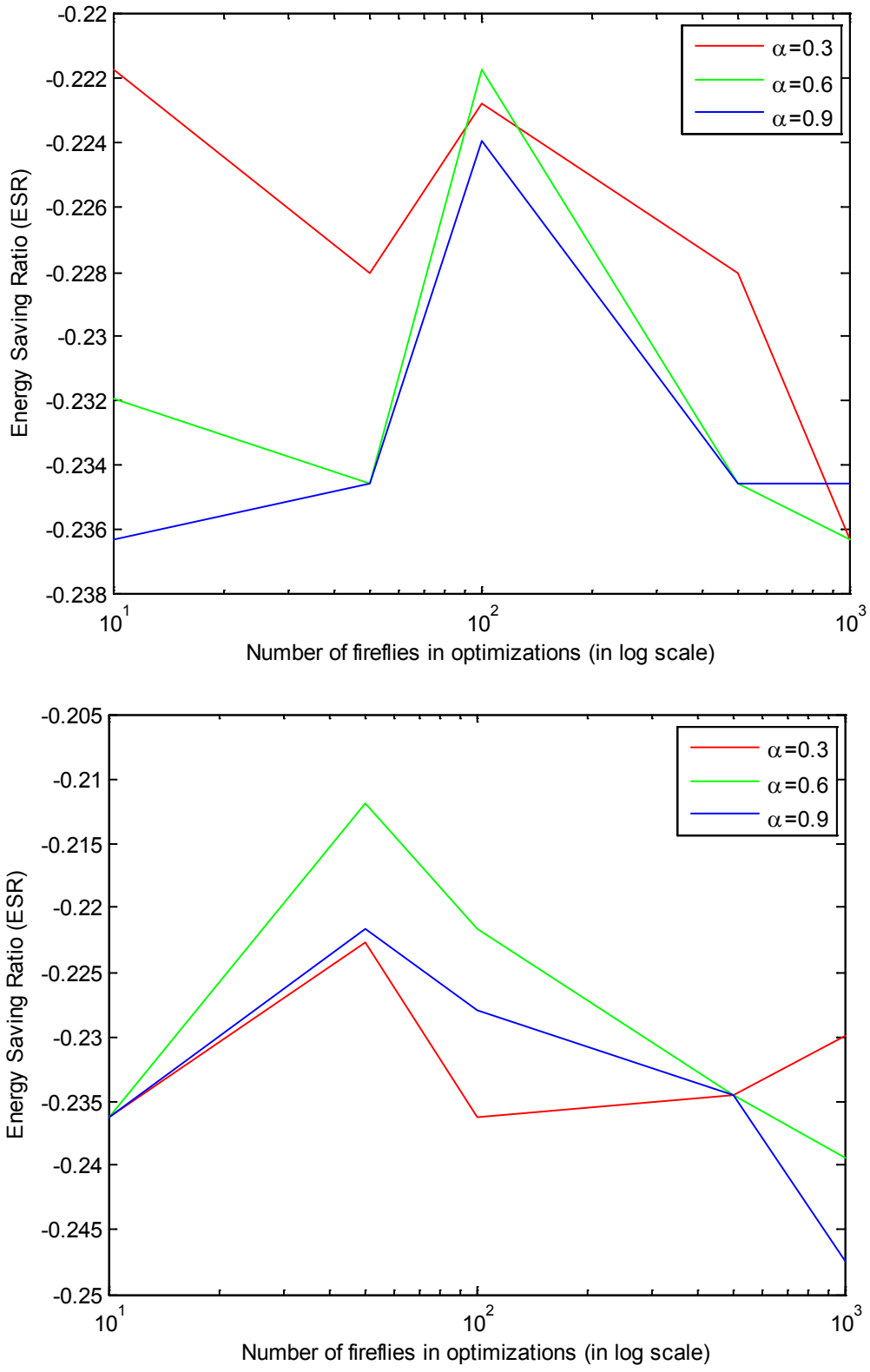

Figure 5.9: Energy Saving Ratio Comparisons: Uniform (Upper) Distribution Randomness and Gaussian (Lower) Distribution Randomness

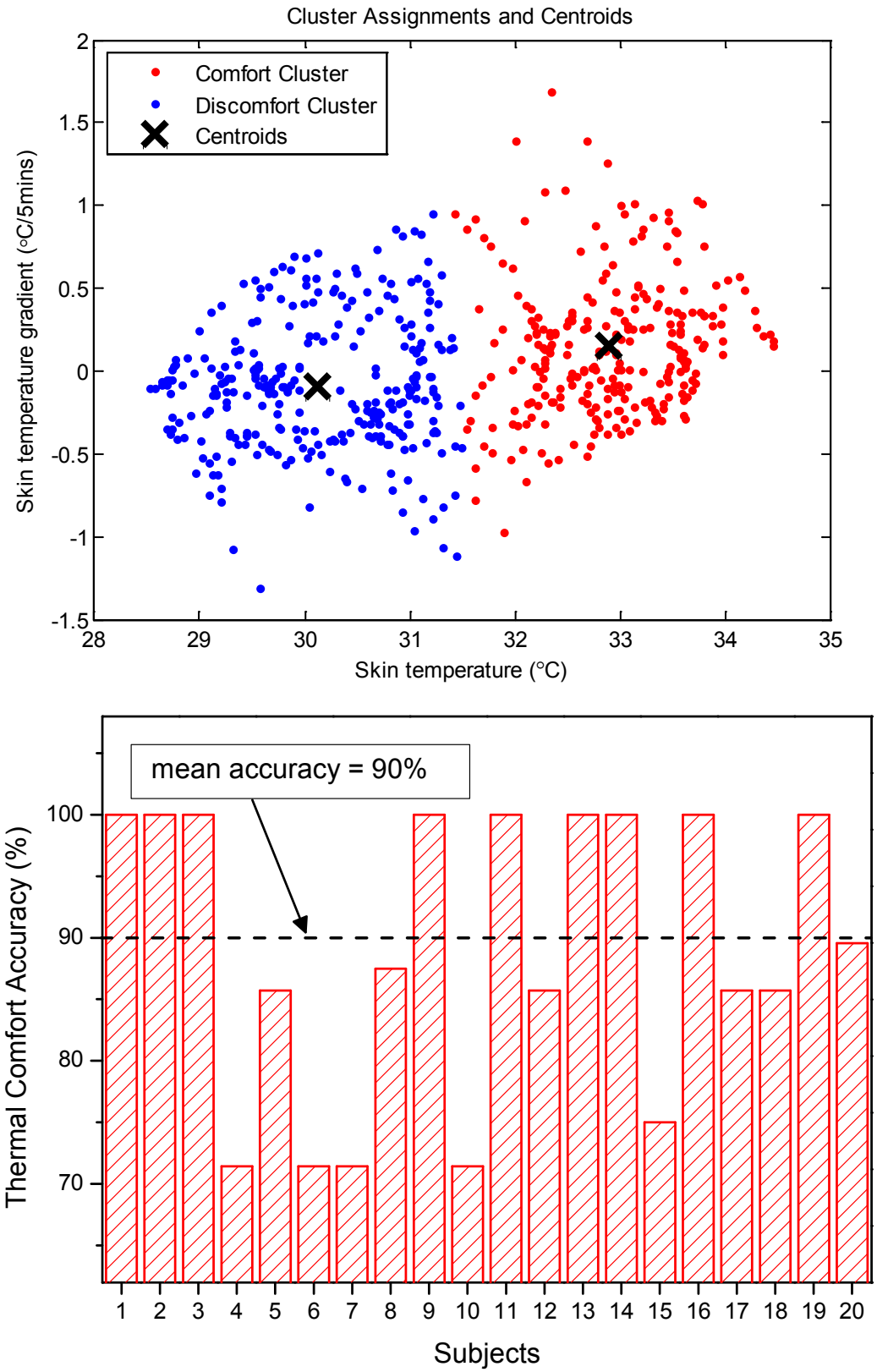

Figure 5.10: Results of K-Means Approach

states with accuracy of as high as 90% on average with k-means approach.

- According to the AFA optimization results, the energy efficiency can be improved by at least 21% when compared with the benchmark operating conditions. Furthermore, the number of iterations decreases when the number of population increases, and more optimal solutions can be obtained as the number of population increases as well. In general, the Gaussian distribution is more consistent than uniform distribution.

5.3.2 Study 2: EEE under Augmented Firefly Algorithm with Neural Networks CSE

Table 5.3: Physiological Parameters of Occupant

Occupant	Height (cm)	Weight (kg)	$I_{cl}(clo)$
Case 1			0.67
Case 2	174	60	0.42
Case 3			0.76

The thermal states of 3 individual cases are illustrated in Table 5.3 and Figure 5.13. The thermal states of occupants are defined into 3 categories of feelings in this study: cool discomfort (-1), neutral comfort (0) and warm discomfort (+1). The skin temperature of occupants was monitored from 8am to 8pm for 3 consecutive days (a full-day experiment for each case). From the data of skin temperature, Predictive Thermal State (PTS) model generated the thermal states of these 3 mutually exclusive cases. The PTS models, which are based on different training features, are evaluated. The validation results of prediction accuracy are presented in Figure 5.11 and Figure 5.12.

By considering gender differences, the developed PTS models have the best accuracies

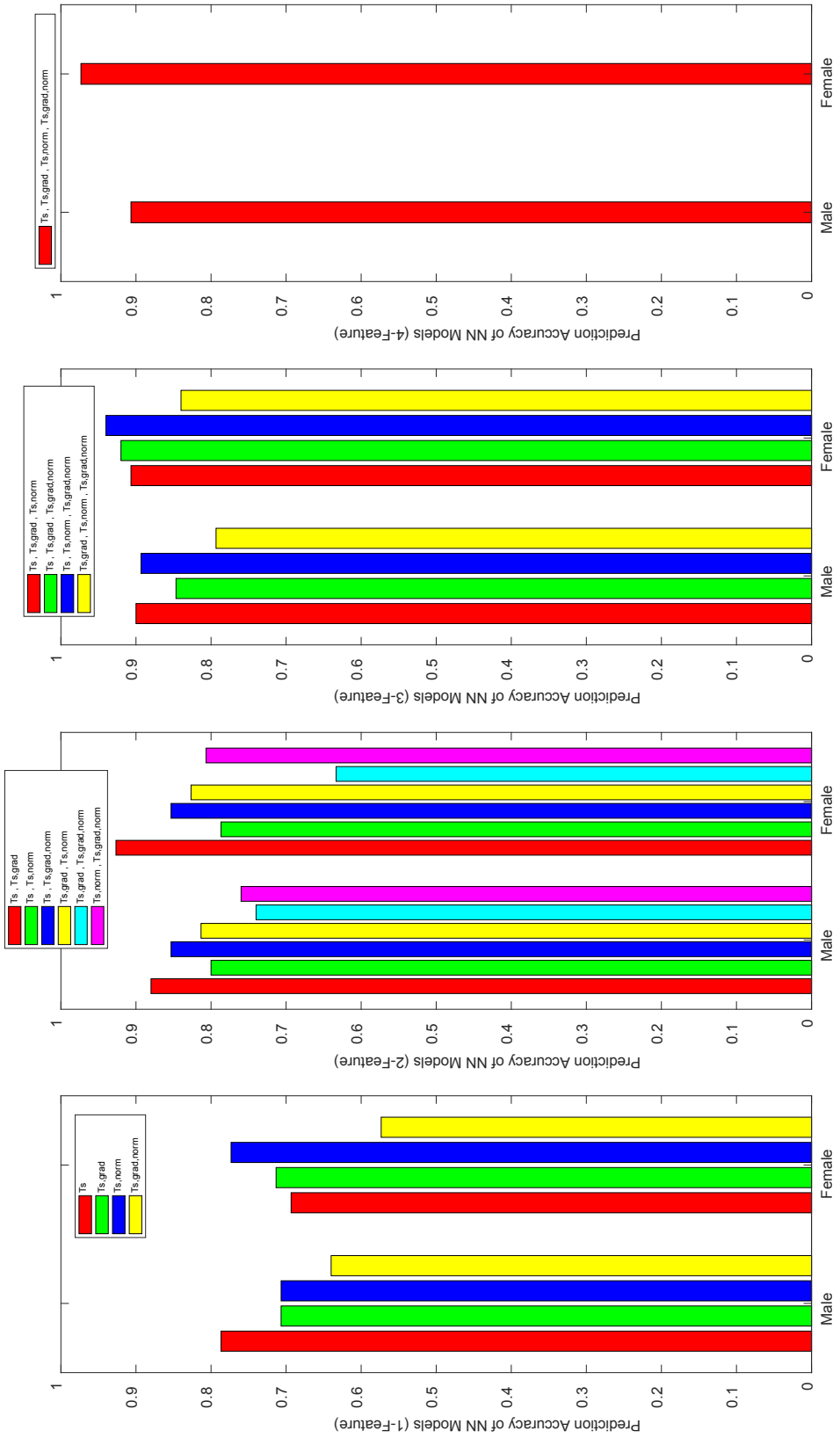

Figure 5.11: Prediction Accuracy of NN-based PTS Models (Iteration=30000, Learning Rate=0.1)

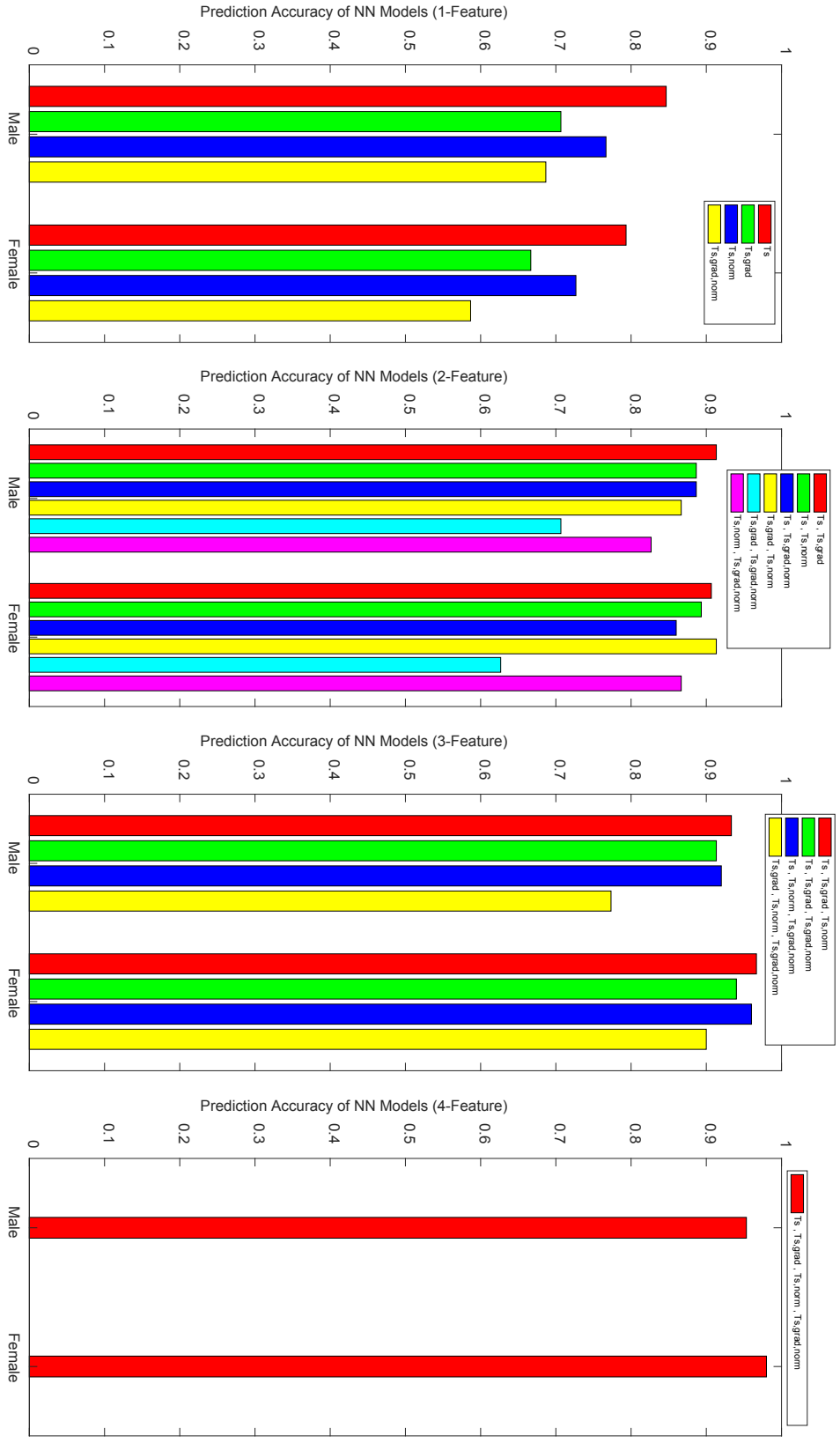

Figure 5.12: Prediction Accuracy of NN-based PTS Models (Iteration=100000, Learning Rate=0.6)

of 96% and 98% for male and female respectively through normalized datasets of skin temperatures. The training parameters are selected as follows (male/female): (1) number of neurons is 5/5; (2) number of iterations is 30000/100000; (3) learning rate is 0.1/0.6; (4) regularization factor is 0.01/0.01; (5) transfer function is sigmoid function; (6) standard Gaussian is used for data normalization. The PTS models are adopted from 4-feature models due to the best performances. Augmented firefly algorithms (AFA) are applied to obtain optimal solutions of operating states (OS) for feed-backing ACMV systems.

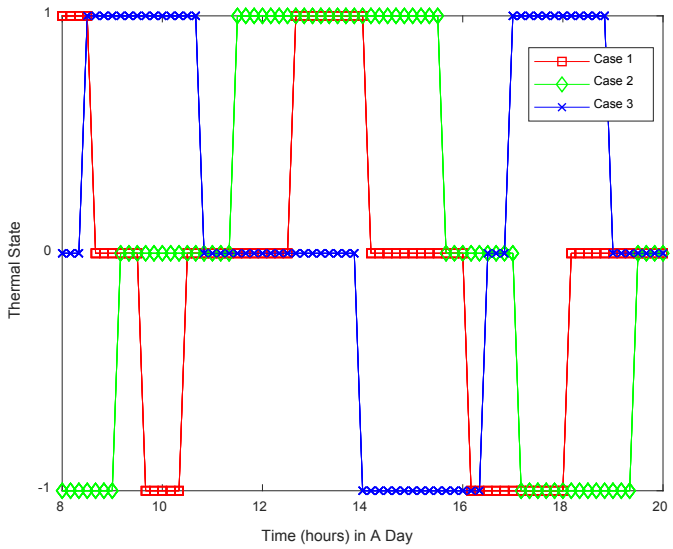

Figure 5.13: Thermal States of 3 Cases in A Day ($T_{sampling} = 10\ mins$)

Given PTS models of occupants, the ACMV systems can operate intelligently with the help of this pre-knowledge. The results of a typical sampling time (i.e. $T_{sampling} = 10$ $mins$) are illustrated in Figure 5.14 and the results of accumulated energy consumption are presented in Figure 5.15 for 3 different cases. The results of PTS models with different sampling time are shown in Figure 5.15 and Table 5.4.

As the Figure 5.14 and Figure 5.15 show, the energy changes of both cases took place in state transitions throughout the whole day. However, the significant changes

of prediction ($T_{sampling} = 5\ mins$) did not occur at the most demanding period of time (i.e. 14 hours or 2pm). The mis-prediction of PTS model is due to fast sampling, and the occupants had not stabilized yet that cannot be interpreted as correct information. For $T_{sampling} \geq 15\ mins$, the tracking sharpness of occupants' thermal states was heavily reduced due to long sampling period. The long sampling period leads to a linear growth in energy consumption throughout the whole day.

The energy consumed is tabulated in Table 5.4 for 3 mutually exclusive cases of full-day experiments with different $T_{sampling}$ from 8am to 8pm as ACMV systems operate. Compared with general operating states, the ACMV systems could be more energy efficient with PTS information incorporated. The improvement of this experimental room could save around 10 kWh per day ($T_{sampling} = 10\ mins$) or about 2.552 Singapore dollars per day without compromising the tracking sharpness of occupants between state changes. The longer time of $T_{sampling}$ could improve the energy efficiency of ACMV systems better. However, the systems can be lagging due to the slow responses of occupant thermal states that lead to uncomfortable sensations between state transitions.

Clearly, the ACMV systems can be more energy efficient when there are PTS models involved. Generally, the energy could be reduced by about 10 kWh (around 13.5% of total daily energy consumption) daily according to the scope of this study in the laboratory. Moreover, the optimal sampling time ($T_{sampling}$) of ACMV OS algorithm can be set as 10 $mins$ due to its significant changing in OS without losing sharpness of tracking the occupant thermal states. For $T_{sampling} < 10\ mins$, the issue is that the thermal states of occupant are not stabilized due to fast sampling, which leads to wrong predictions of thermal states. The wrong prediction may or may not cost more energy, but it does definitely reflect wrong information of occupants to the ACMV

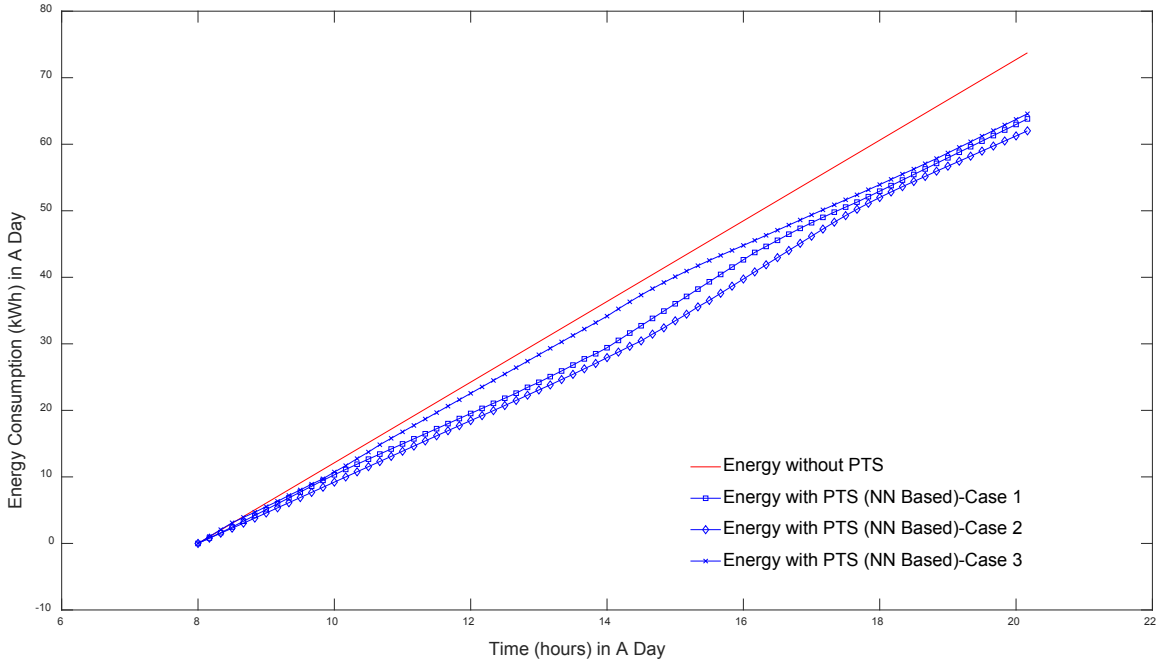

Figure 5.14: Energy Consumption in A Day ($T_{sampling} = 10\ mins$)

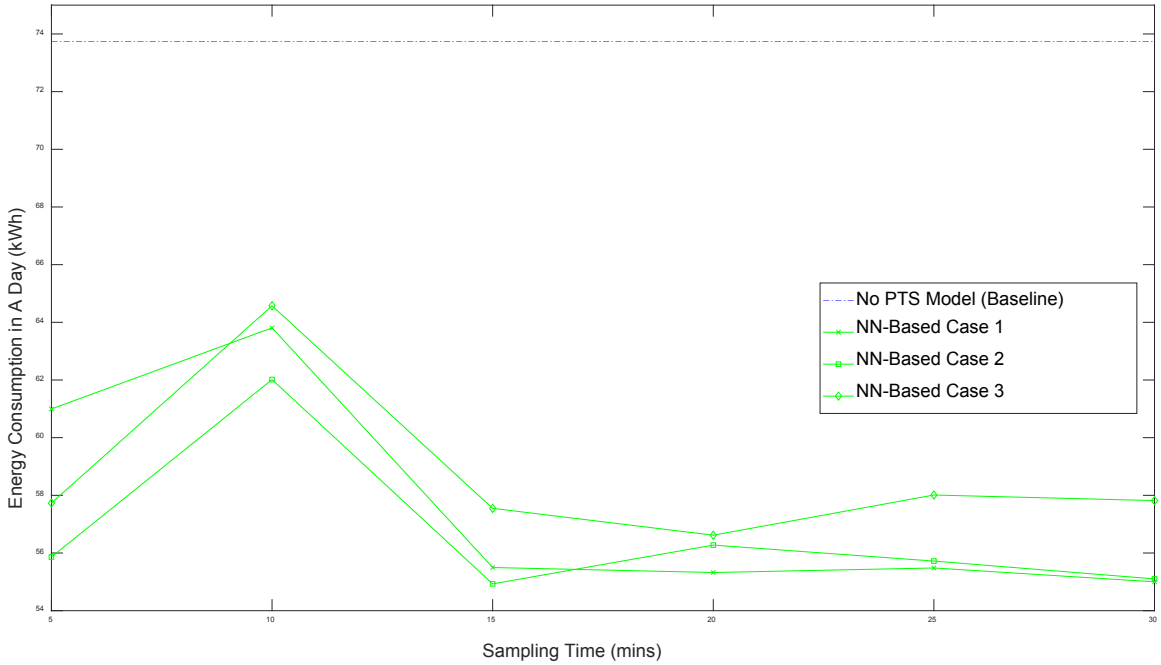

Figure 5.15: Energy Consumption in A Day

Table 5.4: Energy Consumption in A Day

Case - $T_{sampling}$	Baseline	PTS (NN Based)
Case 1-5 *mins*	73.741	60.994 (17.29%)
Case 2-5 *mins*	73.741	55.862 (24.25%)
Case 3-5 *mins*	73.741	57.732 (21.71%)
Case 1-10 *mins*	73.741	63.808 (13.47%)
Case 2-10 *mins*	73.741	62.015 (15.90%)
Case 3-10 *mins*	73.741	64.574 (12.43%)
Case 1-15 *mins*	73.741	55.497 (24.74%)
Case 2-15 *mins*	73.741	54.930 (25.51%)
Case 3-15 *mins*	73.741	57.549 (21.96%)
Case 1-20 *mins*	73.741	55.324 (24.98%)
Case 2-20 *mins*	73.741	56.275 (23.69%)
Case 3-20 *mins*	73.741	56.618 (23.22%)
Case 1-25 *mins*	73.741	55.481 (24.76%)
Case 2-25 *mins*	73.741	55.721 (24.44%)
Case 3-25 *mins*	73.741	58.011 (21.33%)
Case 1-30 *mins*	73.741	55.001 (25.41%)
Case 2-30 *mins*	73.741	55.102 (25.28%)
Case 3-30 *mins*	73.741	57.818 (21.59%)

Notes: Values in brackets are the percentages of energy saving. Other values are in the unit of kWh.

systems, which make the environment uncomfortable. For $T_{sampling} \geq 10\ mins$, the sharpness of tracking occupant thermal states can be heavily impacted. The ACMV systems cannot response in time for actions and hence result in lagging performance (i.e. the plots of energy consumption are more linear).

5.4 Summary

In this chapter, the energy efficiency evaluations (EEE) are examined by two case studies. The EEE is evaluated under active approaches of comfort sensation evaluations (CSE) from occupant physiological parameters. The validity and effectiveness of the proposed modeling and optimization algorithms have been tested and validated under two topics. Several limitations should be considered: (1) The ACMV Operating State (OS) algorithm is only based on the same single occupant in these case studies to mimic different occupant conditions. If there are more than one occupants in the laboratory, then the PTS model cannot predict the overall thermal states of all occupants. This would be the future direction of study. (2) The PTS model was developed for the Singapore local climate (i.e. tropical climate). Therefore, the PTS model may have limitations of applications on other climatic conditions. The PTS model should be re-trained with new datasets on newly-applied climatic conditions.

Chapter 6

Conclusion

In this chapter, the author shall draw some insightful conclusions based on the proposed algorithms and experimental studies in this thesis. Some limitations of the studies are also summarized. Several interesting and relevant extensions and problems are highlighted for future research.

6.1 Conclusion

In this study, the promising concepts of artificial intelligence (AI) and internet of things (IoT) have been integrated and validated in the platform of air-conditioning and mechanical ventilation (ACMV) systems in Nanyang Technological University, Singapore. The key contributions and main conclusions of this PhD study on smart and energy efficient buildings can be summarized below.

Key Contributions:

1. The author developed a systematic **data acquisition system** for acquiring environmental parameters of thermal laboratory and physiological parameters of occupants by Dell laptop (Windows 10 operating system), Matlab 2017a, Python 3.6, Arduino Uno, Raspberry Pi 2 (Debian operating system) and respective sensors (i.e. air temperature, air velocity, air relative humidity, human

skin temperature and surface temperature sensors). The author also developed a machine learning **control system** of ACMV systems to facilitate carrying out experiments in the laboratory platform.

2. The author developed and validated machine learning data-driven **models of energy consumption** of ACMV systems, and data-driven **models of thermal comfort** of occupants (i.e. passive and active approaches). The proposed passive approaches largely use environmental parameters, while the proposed active approaches use physiological parameters. For both passive and active approaches, an important normalization process has been proposed in this study for data pre-processing. The models have been validated by experimental results in the thermal laboratory and they show significant improvements on **prediction accuracy** with **70%** and **90%** for passive and active approaches, respectively.

3. The author formulated the aggregated models of energy consumption and models of thermal comfort sensations by proposing a **user-preference tuning parameter**. The tuning parameter has been verified to increase the flexibility of operations in ACMV systems on different customer demand profiles in real applications.

4. The author developed and validated the proposed algorithms by applying them on the formulated objective problems of this study. The author also accomplished the implementations and comparisons of algorithms, namely classic firefly algorithm (FA), newly proposed augmented firefly algorithm (AFA) and Bayesian algorithms (Bayesian Gaussian processes). The AFA is one of the key proposed algorithms in this study. Compared with classic FA, the **key modifications** of AFA are summarized as follows: (1) reduce the number of

inner for-loops, (2) introduce vortex coefficient, (3) introduce randomness mode switches, (4) introduce searching mode switches, (5) modify updating equations. The modifications of (1) and (5) reduce the computational complexity significantly, and the modifications of (2)-(4) help to locate high performance solutions without sub-optima trapping. The experimental results validated that the AFA followed a linear trend of computational complexity, while the classic FA has an exponential trend of computational complexity with the increase of population.

Main conclusions:

For passive approaches in comfort sensation evaluations (CSE), the energy efficiency evaluations (EEE) of different study topics are summarized as follows:

- **Data-driven models** of energy consumption and environmental parameters have been developed and examined by supervised learning techniques with back-propagation and batch gradient descent algorithms.

- Augmented firefly algorithm (AFA) has been proposed, examined and validated through a experimental platform of **ACMV systems** on energy efficiency and thermal comfort sensations.

- Evaluations of classic firefly algorithm (FA) and augmented firefly algorithm (AFA) show that **AFA** generally **outperforms** FA in terms of global optima searching capability, computational complexity and consistency.

- Evaluations of the six different schemes of AFA show that Large Region and Gaussian distribution Wandering (**LRGW**) generally outperforms the other schemes in the problems of PhD study.

- The best experimental results of **AFA** optimizations are demonstrated through thermal laboratory, and the maximum potentials of **energy saving** are about **-26.5%** for Case 1 (general offices) and **-9.83%** for Case 2 (lecture theatres/ conference rooms).

- The optimal solutions of **AFA** are more consistent than those of Bayesian Gaussian process optimization (BGPO) at given sample sizes. The maximum potential of **energy saving** by BGPO and AFA are around **-21%** and **-10%** respectively for Case 1 (general offices) and Case 2 (lecture theatres/ conference rooms).

For active approaches in comfort sensation evaluations (CSE), the energy efficiency evaluations (EEE) of different study topics are summarized as follows:

- The prediction of thermal comfort states via **k-means** approach has been implemented and it is based on features of skin temperature and skin temperature gradient. The **prediction accuracy** of differentiation using skin temperature and its gradient is up to **90%**. The experimental results show that the energy efficiency can be improved by **21%** with the predictive models of thermal comfort sensations.

- The predictive models of thermal comfort states through **neural networks (NN)** have been developed and examined. Based on skin temperature, height, weight, gender and clothing factors, the accuracy of male and female models can reach up to **96%** and **98%**, respectively. The optimal **sampling time** of **ACMV OS algorithm** is **10** $\boldsymbol{mins}$ without the issues of system lagging and sharpness losing for predictive thermal states of occupants, and it reduces the energy consumption of thermal laboratory by around **10** $\boldsymbol{kWh}$ out of **74**

kWh per day, namely about saving **S$2.55** in current electricity tariff rate of Singapore (about **13.5%** energy reduction).

6.2 Limitations

In this study, there are several limitations that should be highlighted as follows:

- The thermal laboratory is located in tropical Singapore. Therefore, the set-ups of air-conditioning and mechanical ventilation (ACMV) systems only provide the cooling capacity without the need for heating capacity, which are not general heating, ventilation and air-conditioning (HVAC) systems for all multi-season and multi-geographical situations.

- There is an assumption that the rooms in the buildings are identical for the purpose of experimental simplicity. However, in real applications, each room is different from its facing, location inside the building and many other factors. Therefore, there is a need for room classifications to be incorporated if we aim to comprehensively improve the energy efficiency of the whole building.

- The ACMV operating state algorithm is only based on a single occupant in these case studies to mimic different occupant conditions. If there were more than one occupants in thermal laboratory, then the PTS model may have to use some other techniques, for instance weighted states for each occupant, so to integrate the overall thermal state of all of the occupants.

6.3 Future Research Directions

Considering the limitations outlined, several future research directions are pointed as follows:

- The modeling and optimization approaches developed in this thesis can be further enhanced. The energy consumption modeling of operating air conditioning and mechanical ventilation (ACMV) systems can address different geographic locations that make the models more comprehensive, robust and adaptable. The optimization can be further investigated under the various factors of energy efficiency, thermal comfort sensations, air quality, system failure rates, maintenance costs, etc.

- Indoor zone differentiations and classifications are worthy of further study to investigate the handling algorithms of different zones. Occupant indoor positioning is essential under this research. The handling algorithms can utilize the inputs of occupant positions and zone classifications, so that they can precisely alter the operating conditions of lights, windows, doors and centralized air conditioning systems smartly.

- Multiple-occupant comfort sensation evaluations should also be future directions with the incorporation of zone handling algorithms to achieve energy efficient smart buildings. With the non-intrusive information from the proposed thermal comfort models, a general zone thermal comfort model can be investigated and examined for centralized air conditioning systems.

Appendix A1

Comprehensive comparisons of six schemes of sparse Augmented Firefly Algorithms (AFA) based on passive Predicted Mean Vote (PMV) are examined on energy efficient evaluations in the figures below. The different schemes are about small/large regions and Gaussian/uniform wanderings. The algorithms are examined under two cases, such as general offices (Case 1) and lecture theatres/conference rooms (Case 2).

Study 1: EEE under Six Schemes of AFA

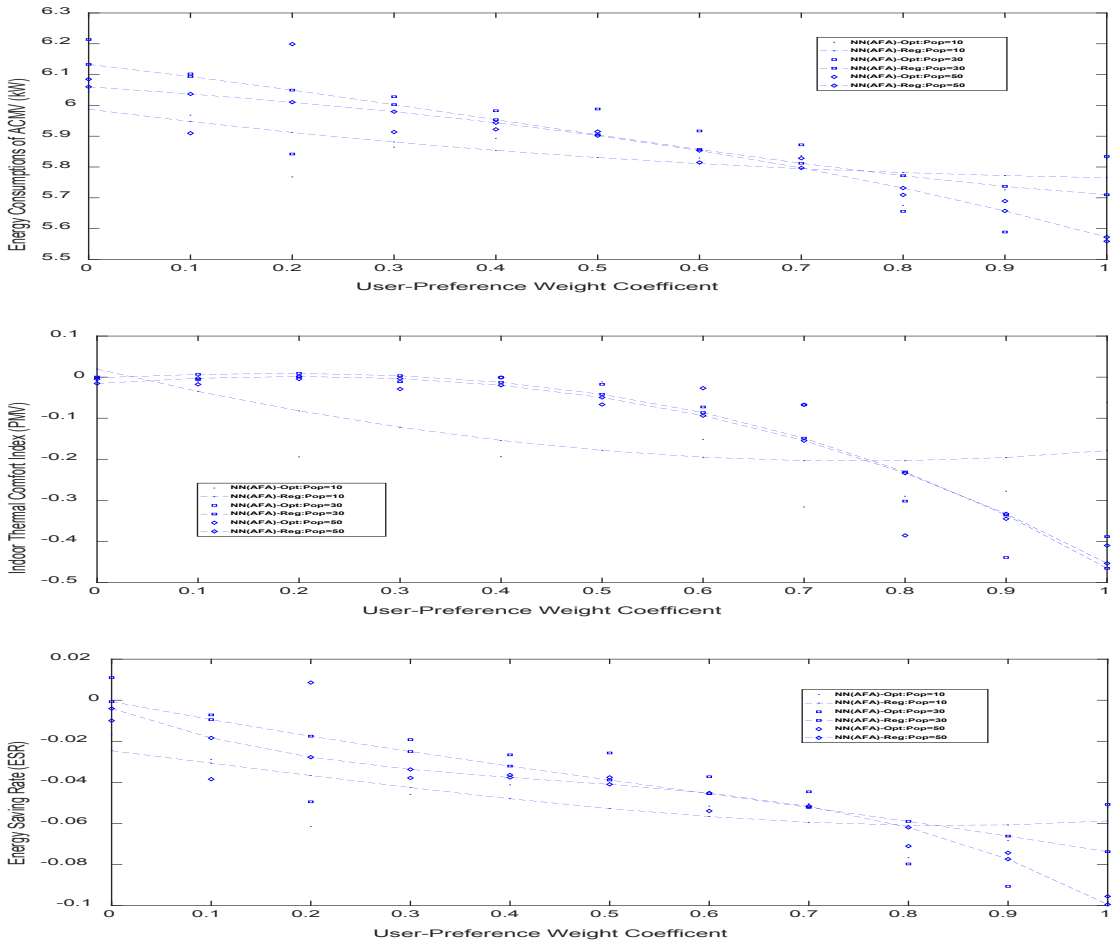

Figure A1.1: Optimizations Results via AFA-SRUW $(-0.5, +0.5)$ on Case 1

Study 1: EEE under Six Schemes of AFA

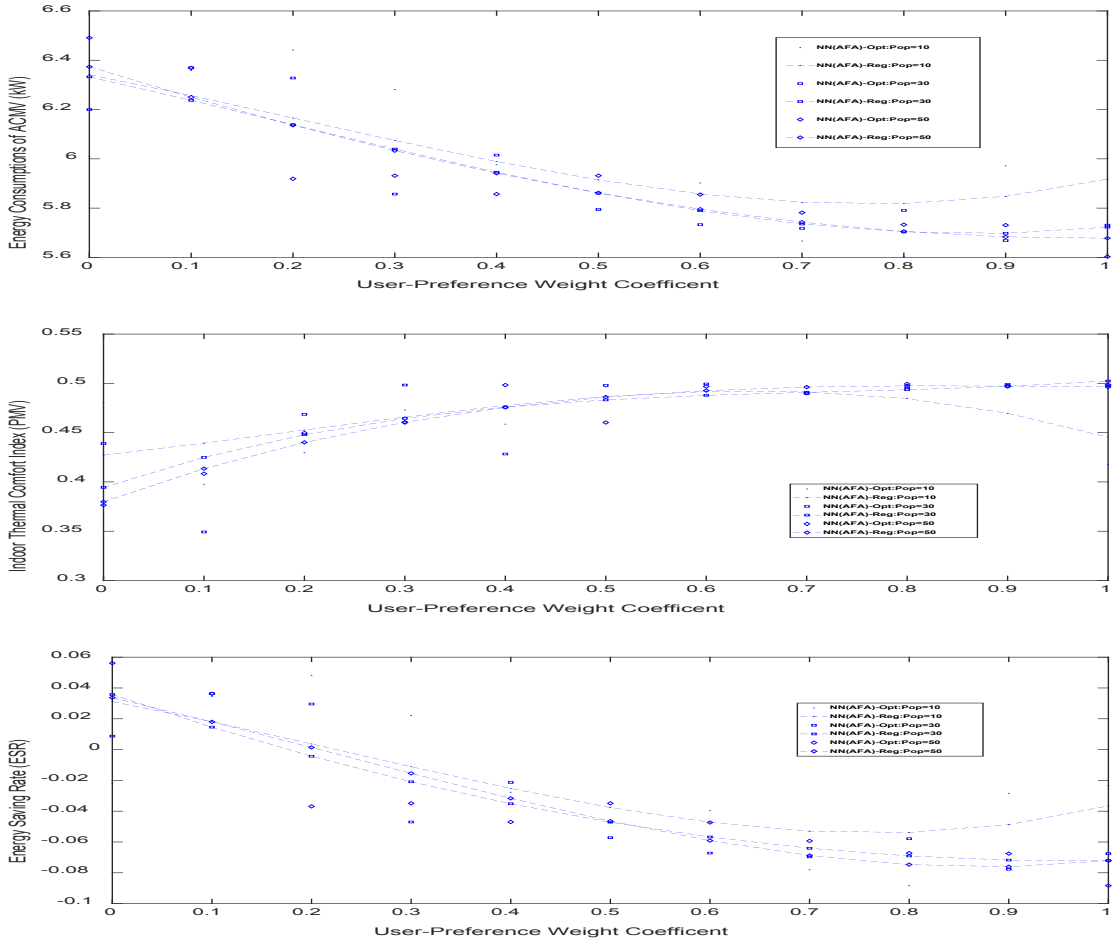

Figure A1.2: Optimizations Results via AFA-SRUW $(-0.5, +0.5)$ on Case 2

Study 1: EEE under Six Schemes of AFA

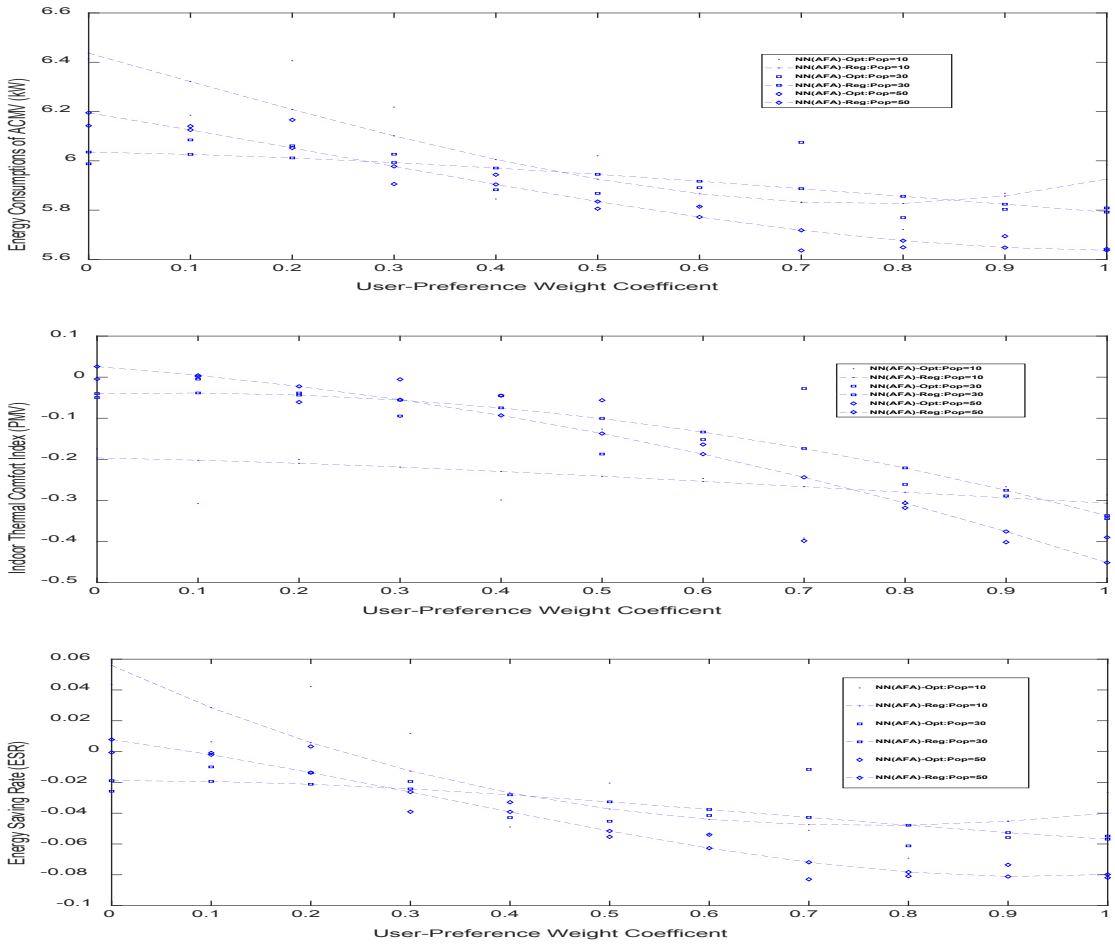

Figure A1.3: Optimizations Results via AFA-LRUW $(-0.5, +0.5)$ on Case 1

Study 1: EEE under Six Schemes of AFA

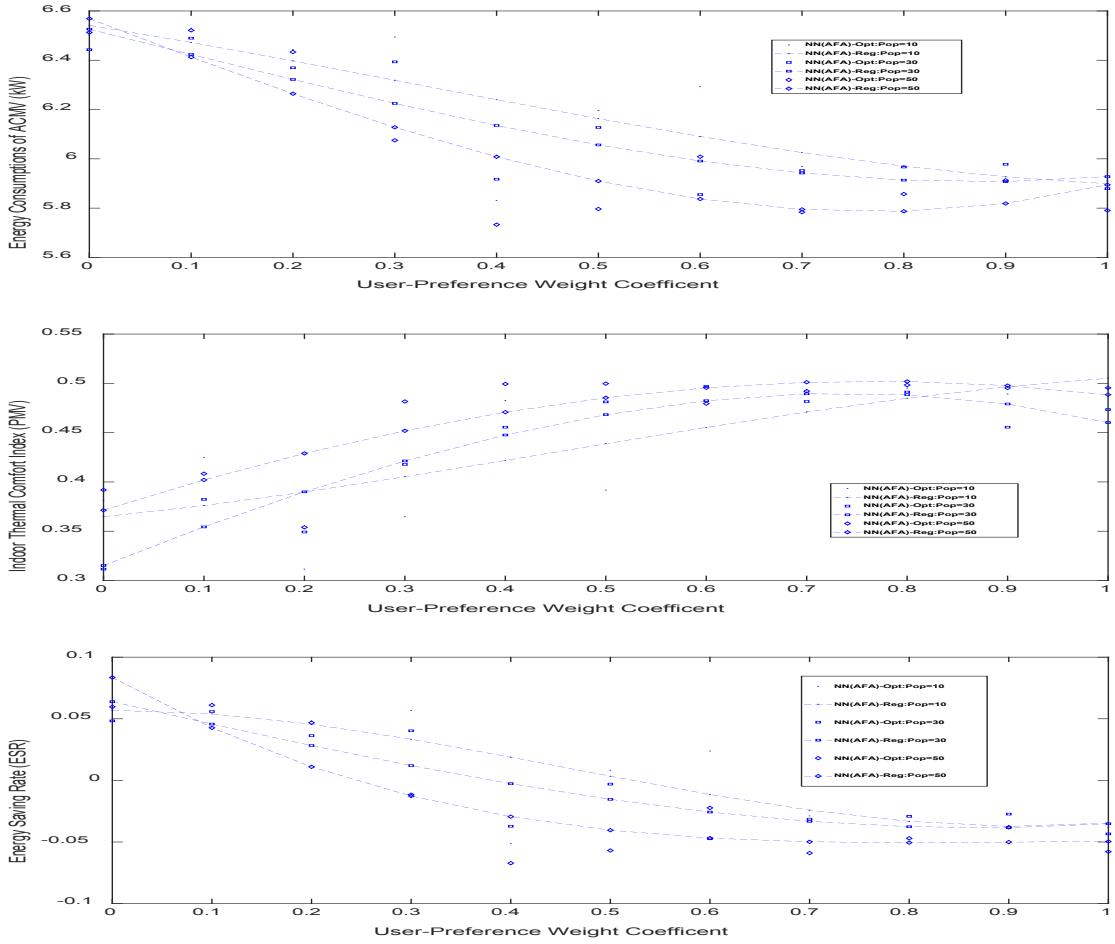

Figure A1.4: Optimizations Results via AFA-LRUW $(-0.5, +0.5)$ on Case 2

Study 1: EEE under Six Schemes of AFA

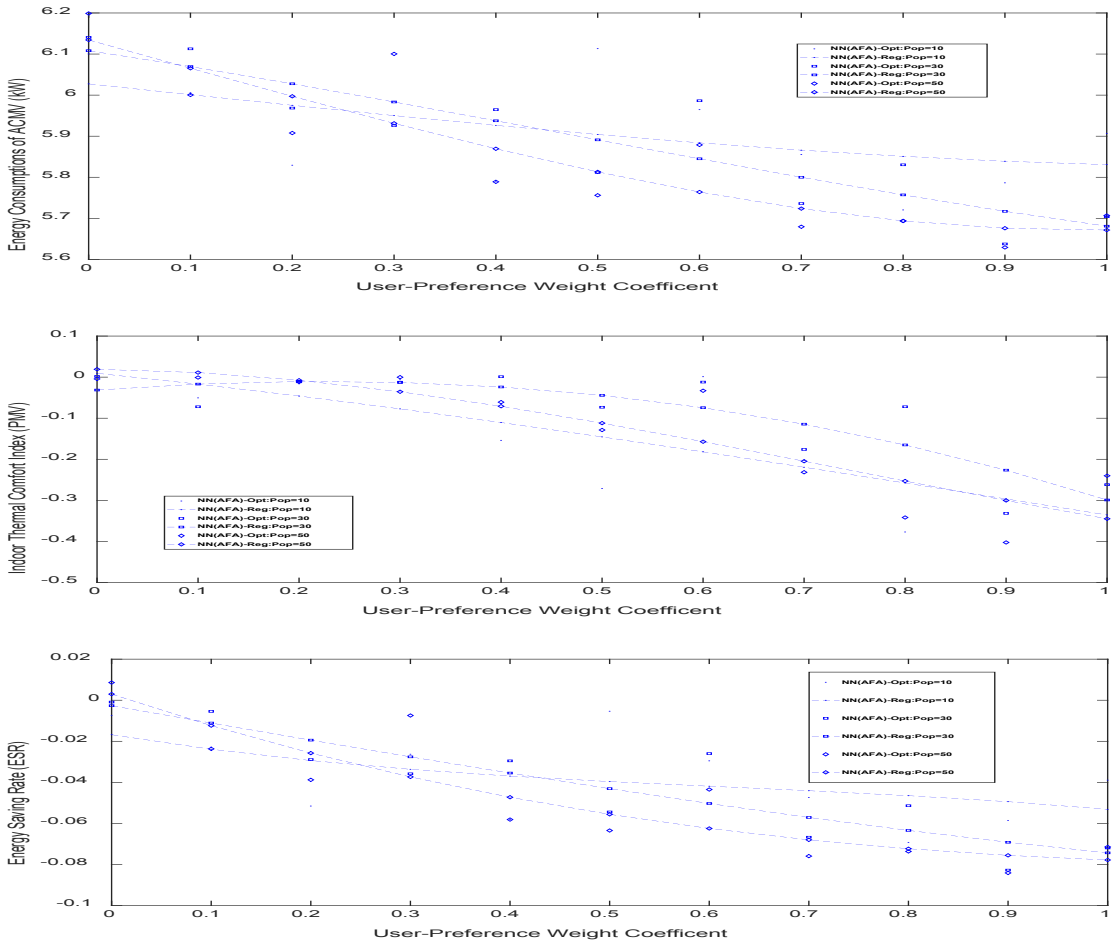

Figure A1.5: Optimizations Results via AFA-SRGW-I ($\mu = 0, \sigma = 0.1$) on Case 1

Study 1: EEE under Six Schemes of AFA

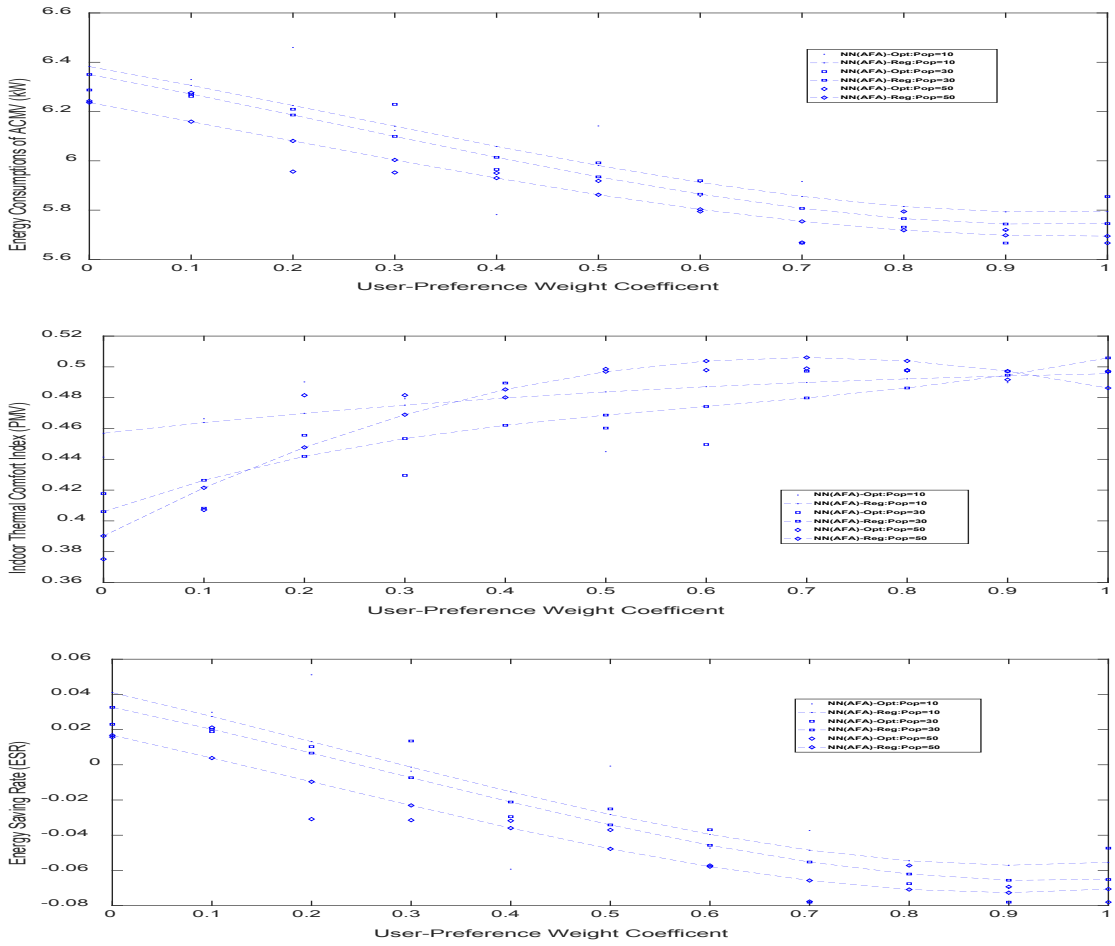

Figure A1.6: Optimizations Results via AFA-SRGW-I ($\mu = 0, \sigma = 0.1$) on Case 2

Study 1: EEE under Six Schemes of AFA

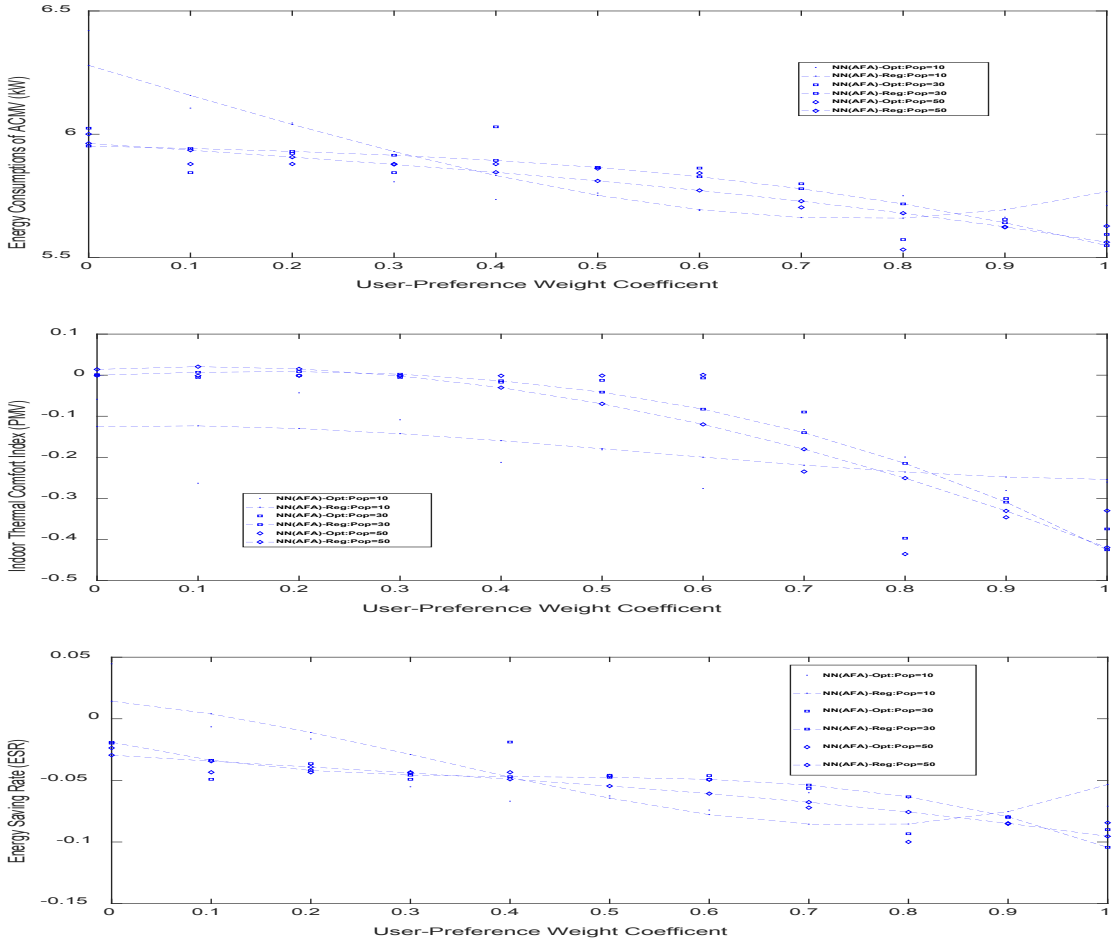

Figure A1.7: Optimizations Results via AFA-LRGW-I ($\mu = 0, \sigma = 0.1$) on Case 1

Study 1: EEE under Six Schemes of AFA

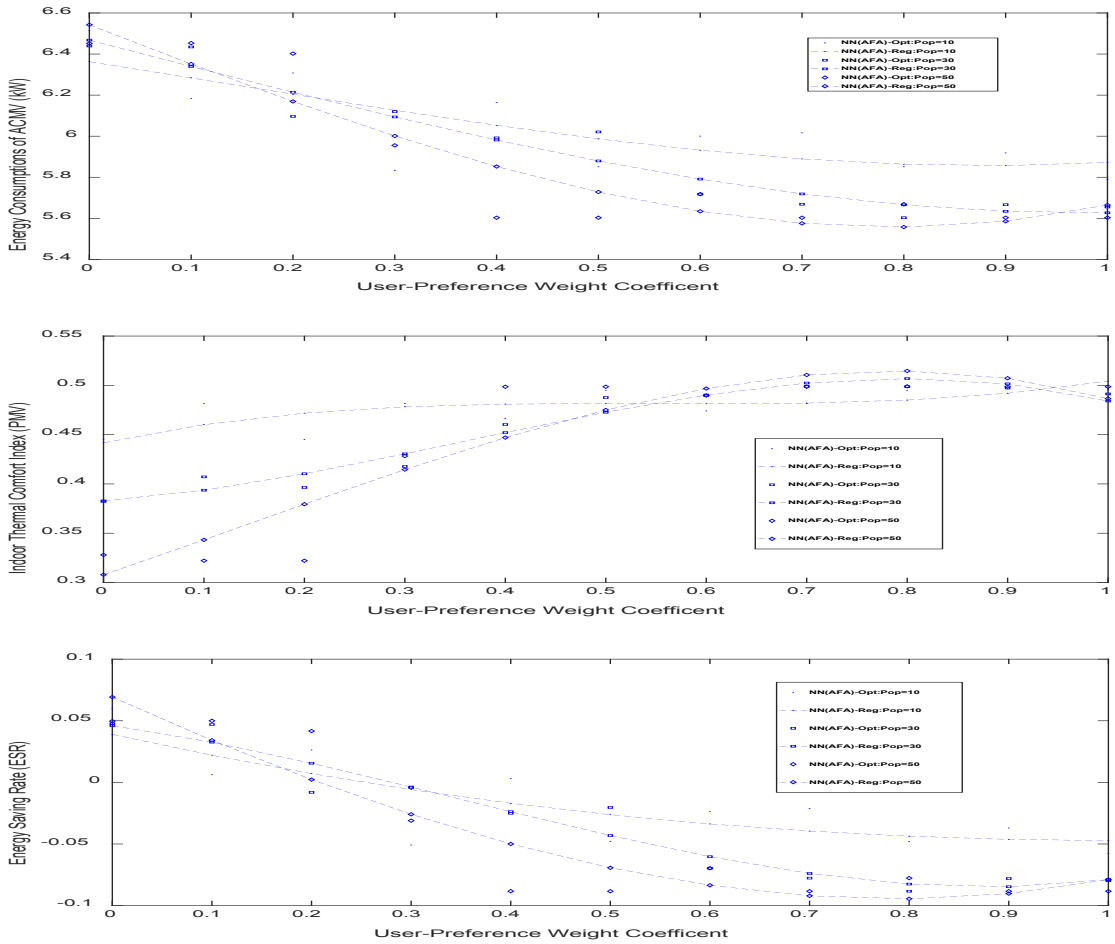

Figure A1.8: Optimizations Results via AFA-LRGW-I ($\mu = 0, \sigma = 0.1$) on Case 2

Study 1: EEE under Six Schemes of AFA

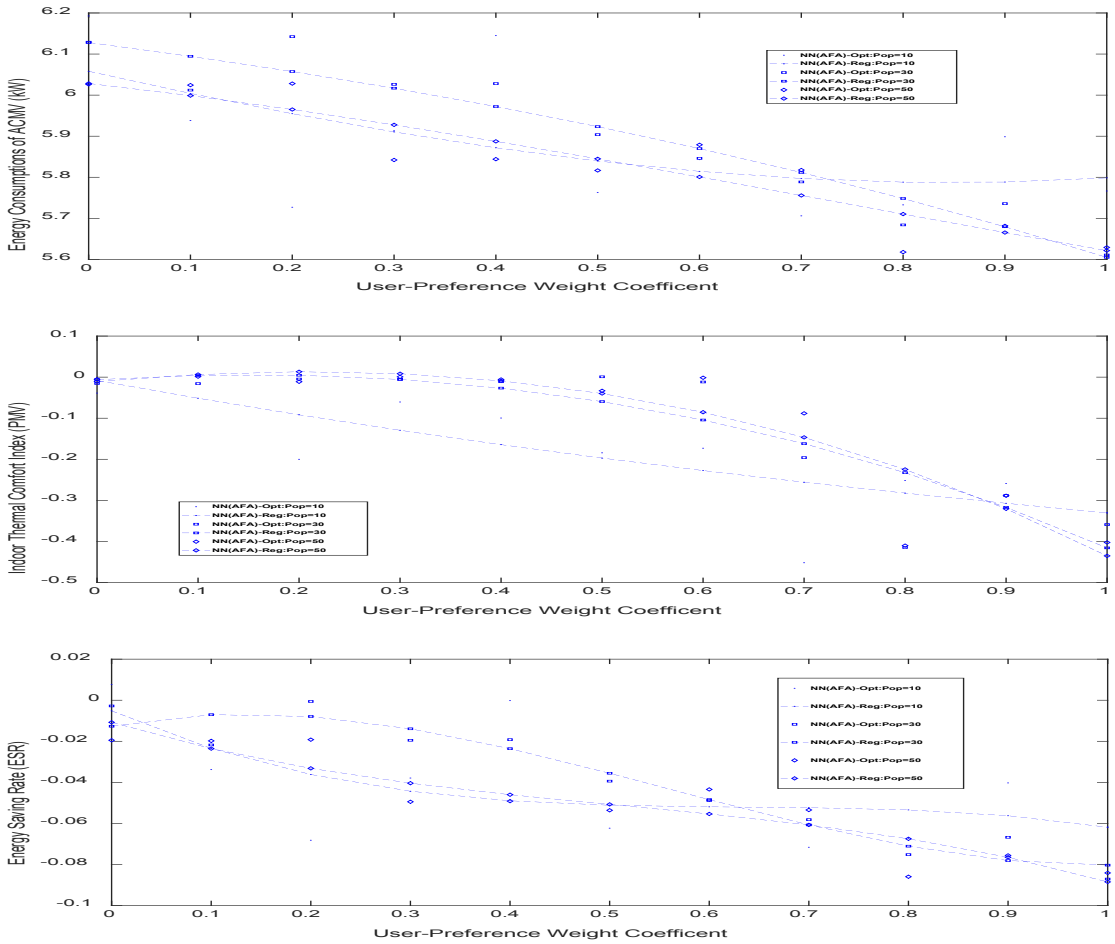

Figure A1.9: Optimizations Results via AFA-SRGW-II ($\mu = 0, \sigma = 1$) on Case 1

Study 1: EEE under Six Schemes of AFA

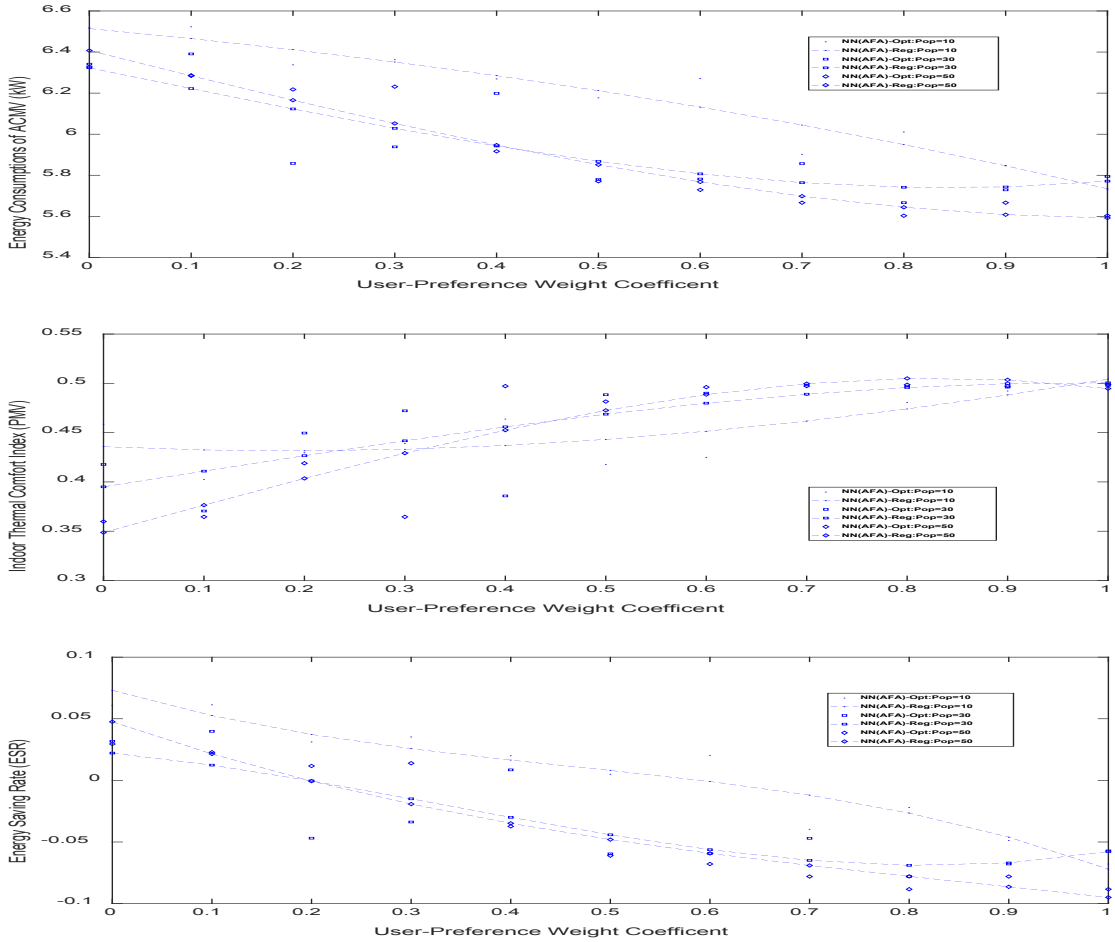

Figure A1.10: Optimizations Results via AFA-SRGW-II ($\mu = 0, \sigma = 1$) on Case 2

Study 1: EEE under Six Schemes of AFA

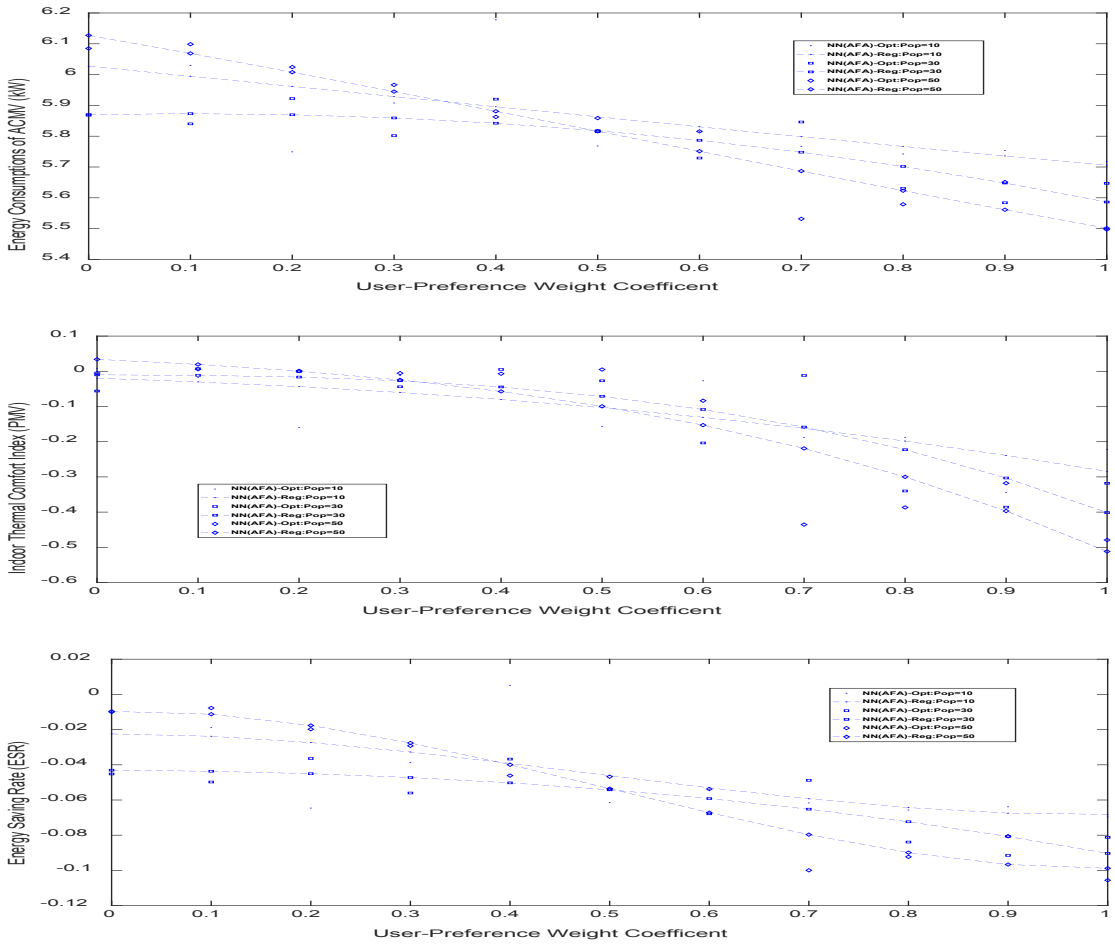

Figure A1.11: Optimizations Results via AFA-LRGW-II ($\mu = 0, \sigma = 1$) on Case 1

Study 1: EEE under Six Schemes of AFA

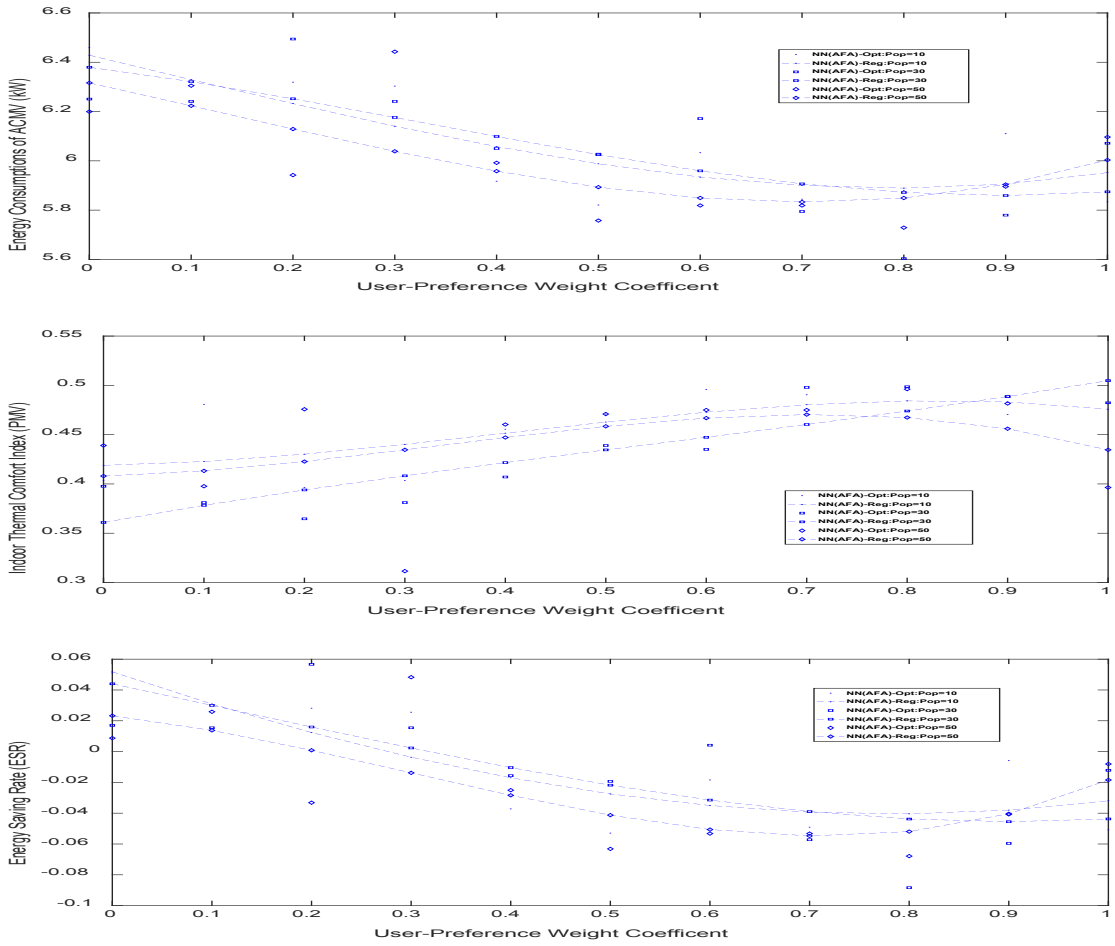

Figure A1.12: Optimizations Results via AFA-LRGW-II ($\mu = 0, \sigma = 1$) on Case 2

Appendix A2

Energy efficiency evaluations of classic Firefly Algorithms (FA) and Augmented Firefly Algorithm (AFA) with passive Predicted Mean Vote (PMV) are presented in the figures below. The algorithms are examined under two cases, such as general offices (Case 1) and lecture theatres/conference rooms (Case 2).

Study 2: EEE under Classic FA and AFA

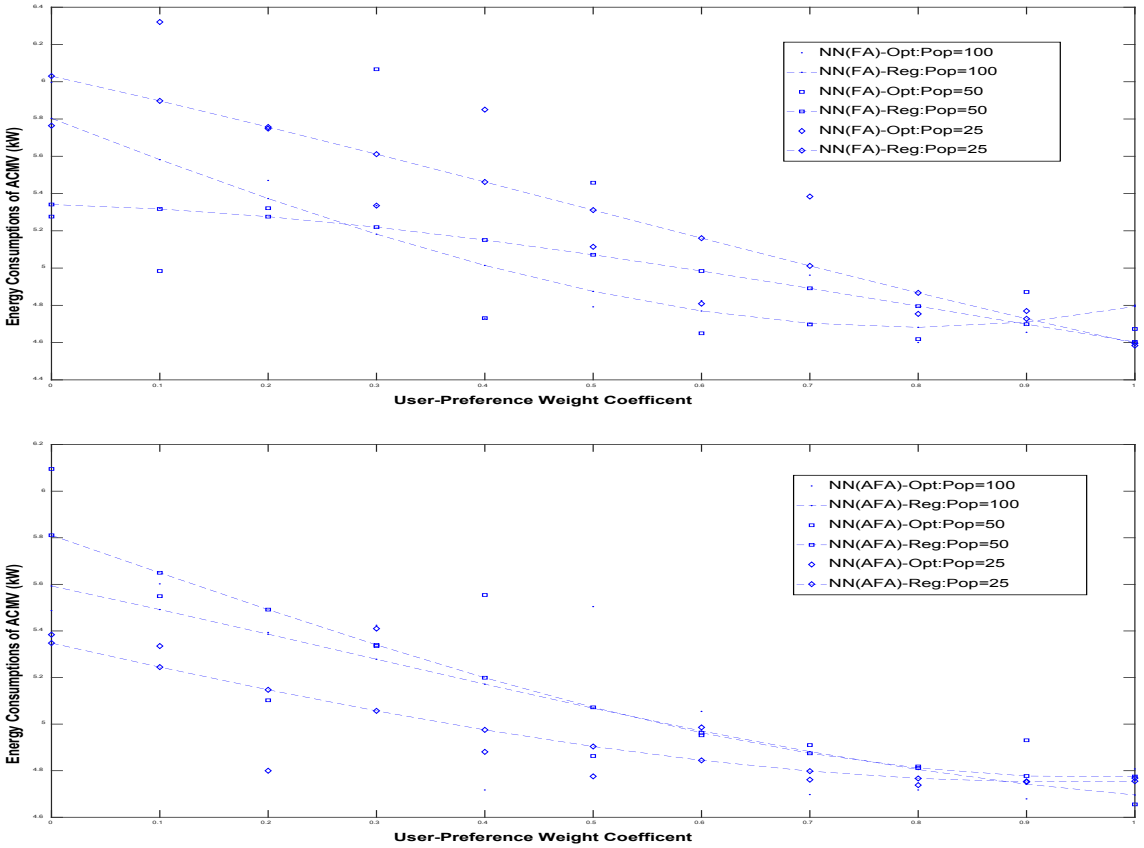

Figure A2.1: Sparse FA and AFA Optimizations on Energy Consumption of ACMV Systems (Case 1: Sedentary Activities, e.g. General Offices)

Study 2: EEE under Classic FA and AFA

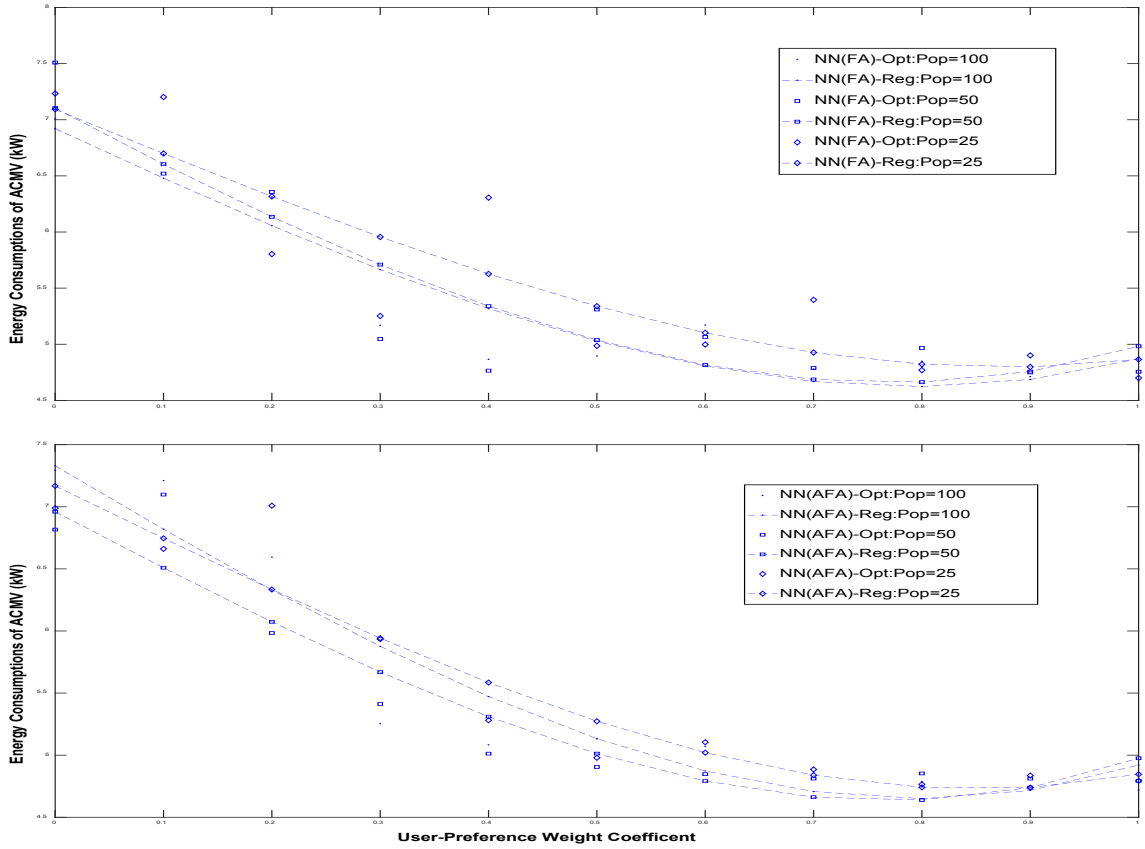

Figure A2.2: Sparse FA and AFA Optimizations on Energy Consumption of ACMV Systems (Case 2: Light Activities, e.g. Lecture Theatres and Conference Rooms)

Study 2: EEE under Classic FA and AFA

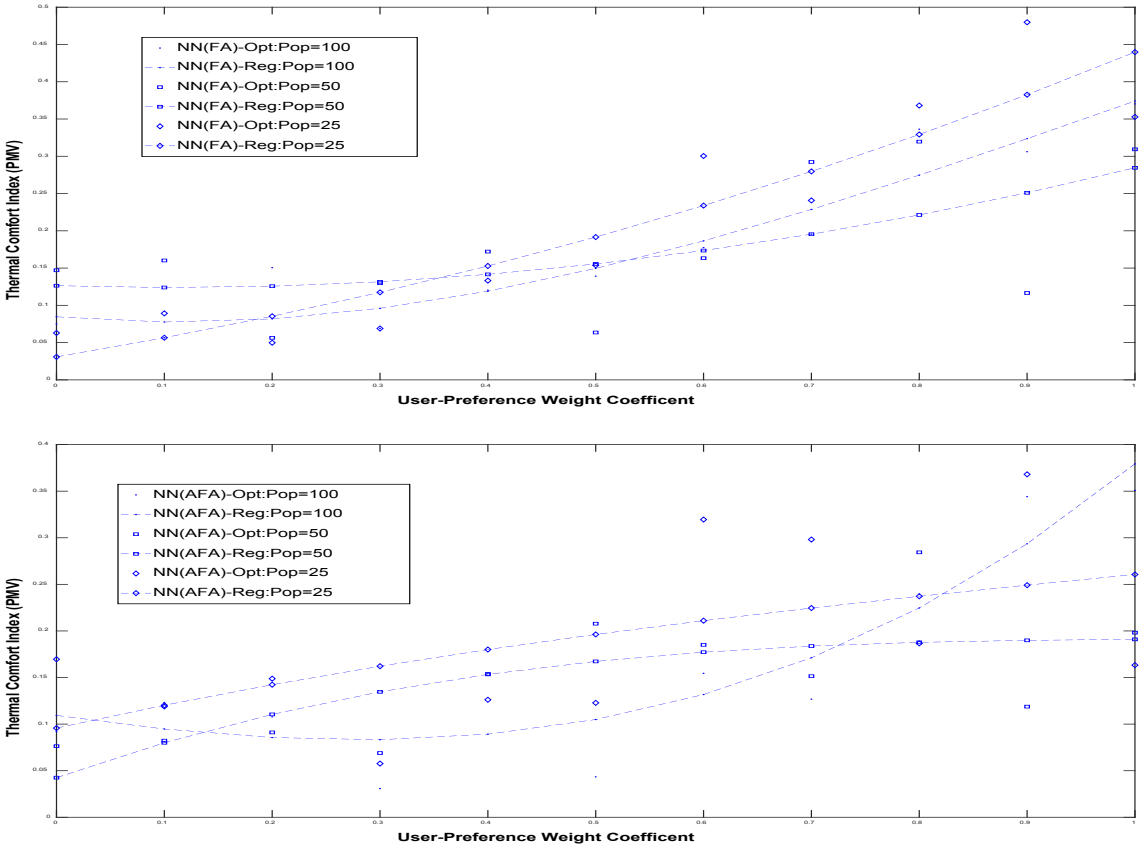

Figure A2.3: Sparse FA and AFA Optimizations on Indoor Thermal Comfort (Case 1: Sedentary Activities, e.g. General Offices)

Study 2: EEE under Classic FA and AFA

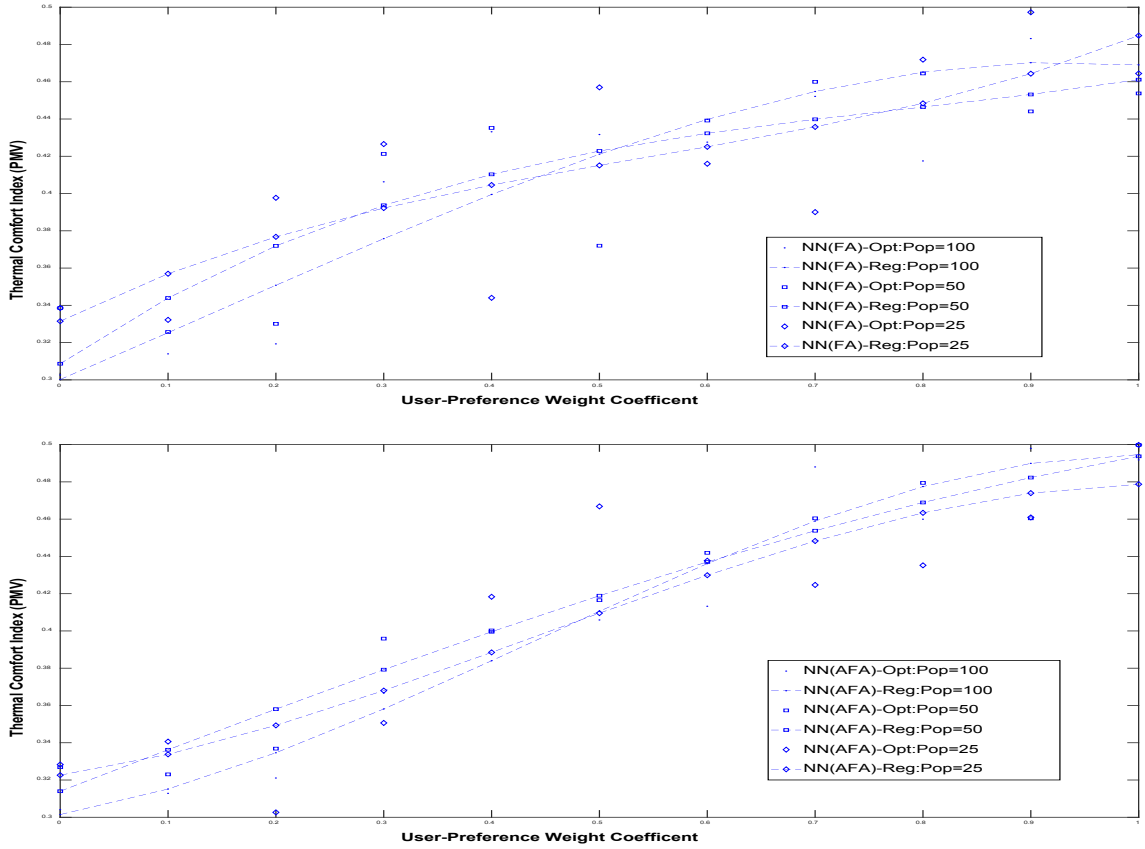

Figure A2.4: Sparse FA and AFA Optimizations on Indoor Thermal Comfort (Case 2: Light Activities, e.g. Lecture Theatres and Conference Rooms)

Study 2: EEE under Classic FA and AFA

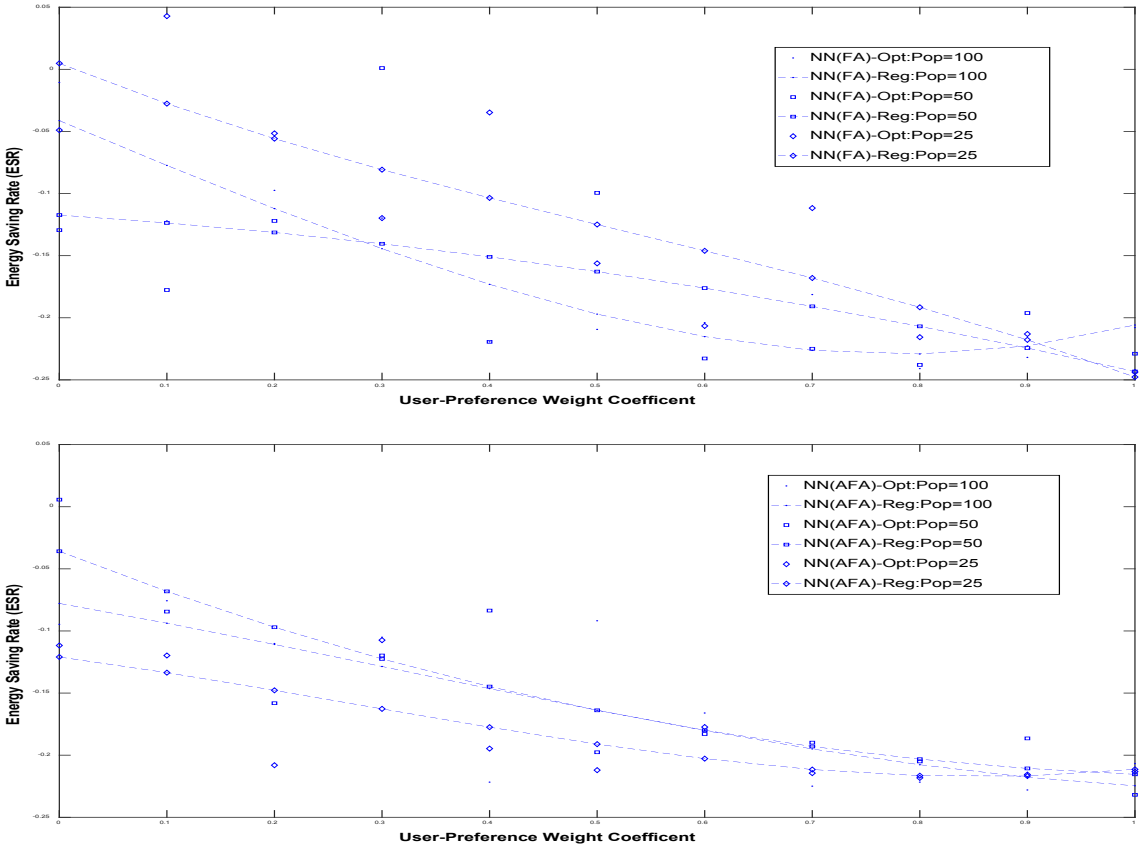

Figure A2.5: Sparse FA and AFA Optimizations on Energy Saving Rate (ESR) (Case 1: Sedentary Activities, e.g. General Offices)

Study 2: EEE under Classic FA and AFA

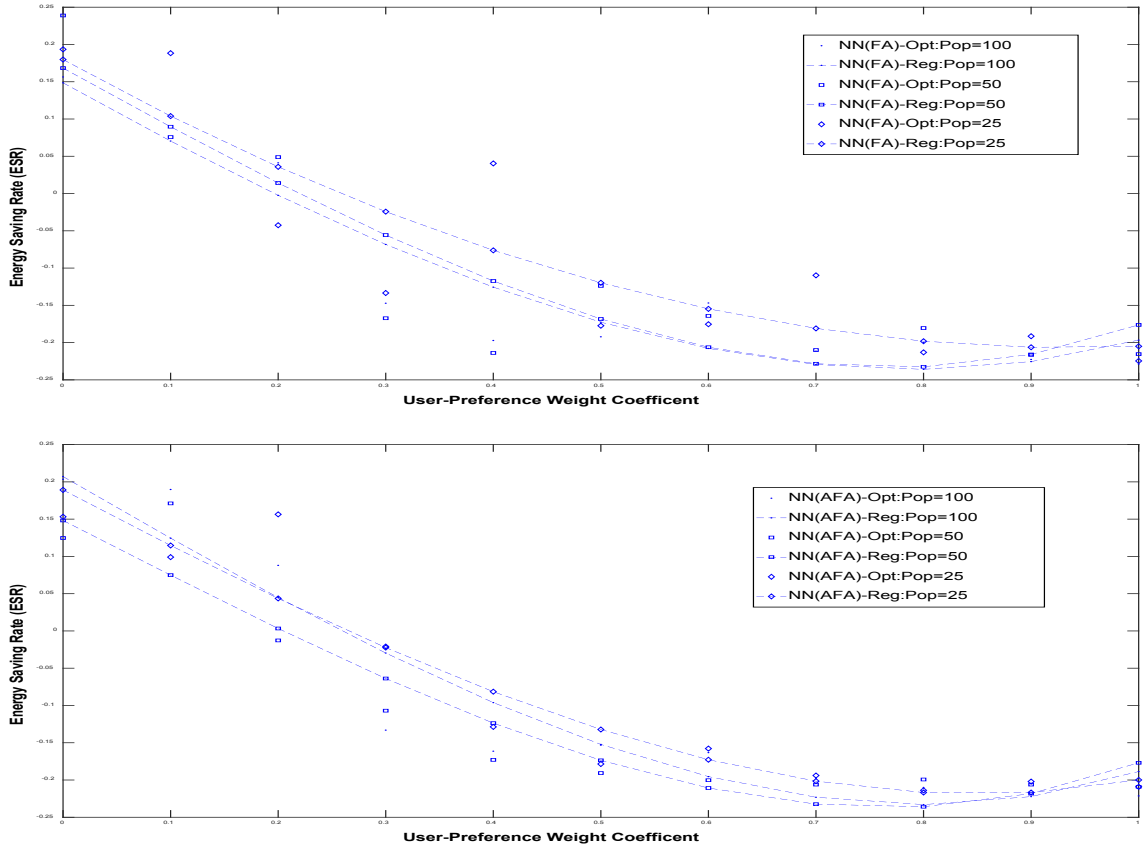

Figure A2.6: Sparse FA and AFA Optimizations on Energy Saving Rate (ESR) (Case 2: Light Activities, e.g. Lecture Theatres and Conference Rooms)

Appendix A3

Energy efficiency evaluations of Augmented Firefly Algorithm (AFA) and Bayesian Optimization with passive Predicted Mean Vote (PMV) are presented in the figures below. The algorithms are examined under two cases, such as general offices (Case 1) and lecture theatres/conference rooms (Case 2).

Study 3: EEE under BGPO and AFA

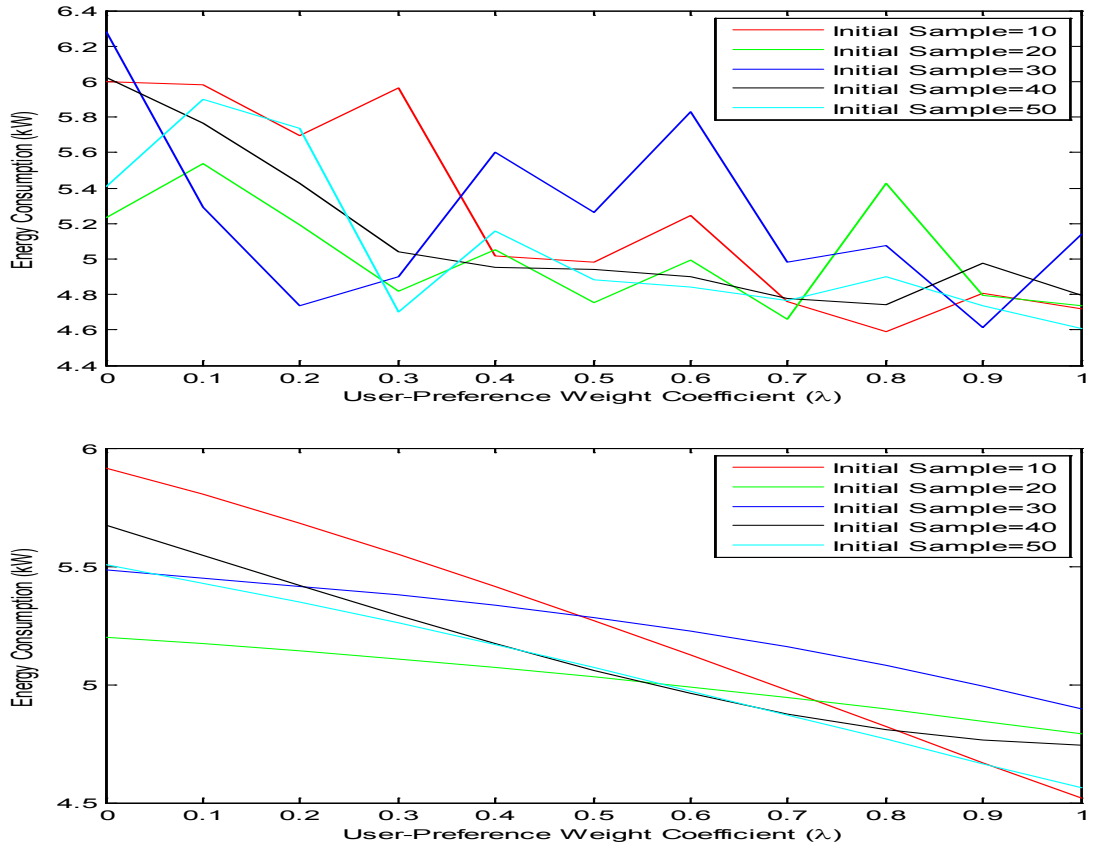

Figure A3.1: Energy Consumption BGPO Case 1 - Discrete(Upper) / Regression (Lower)

Study 3: EEE under BGPO and AFA

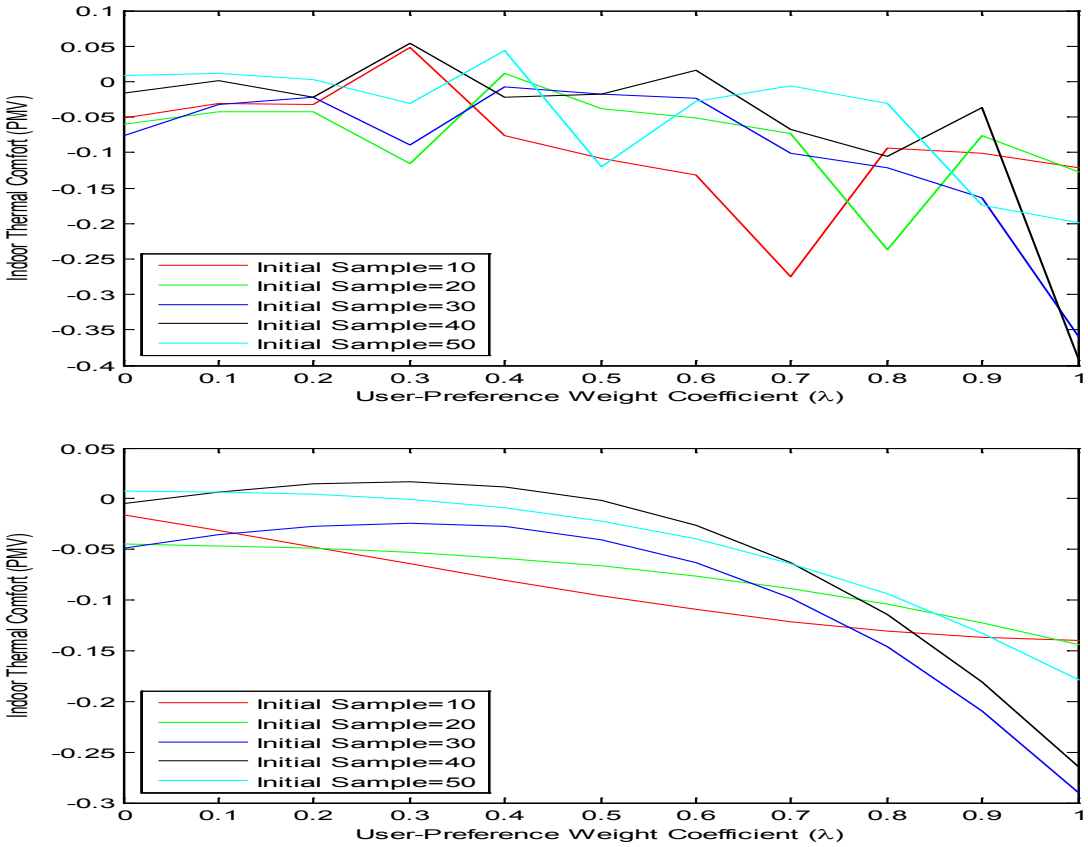

Figure A3.2: Indoor Thermal Comfort BGPO Case 1 - Discrete(Upper) / Regression (Lower)

Study 3: EEE under BGPO and AFA

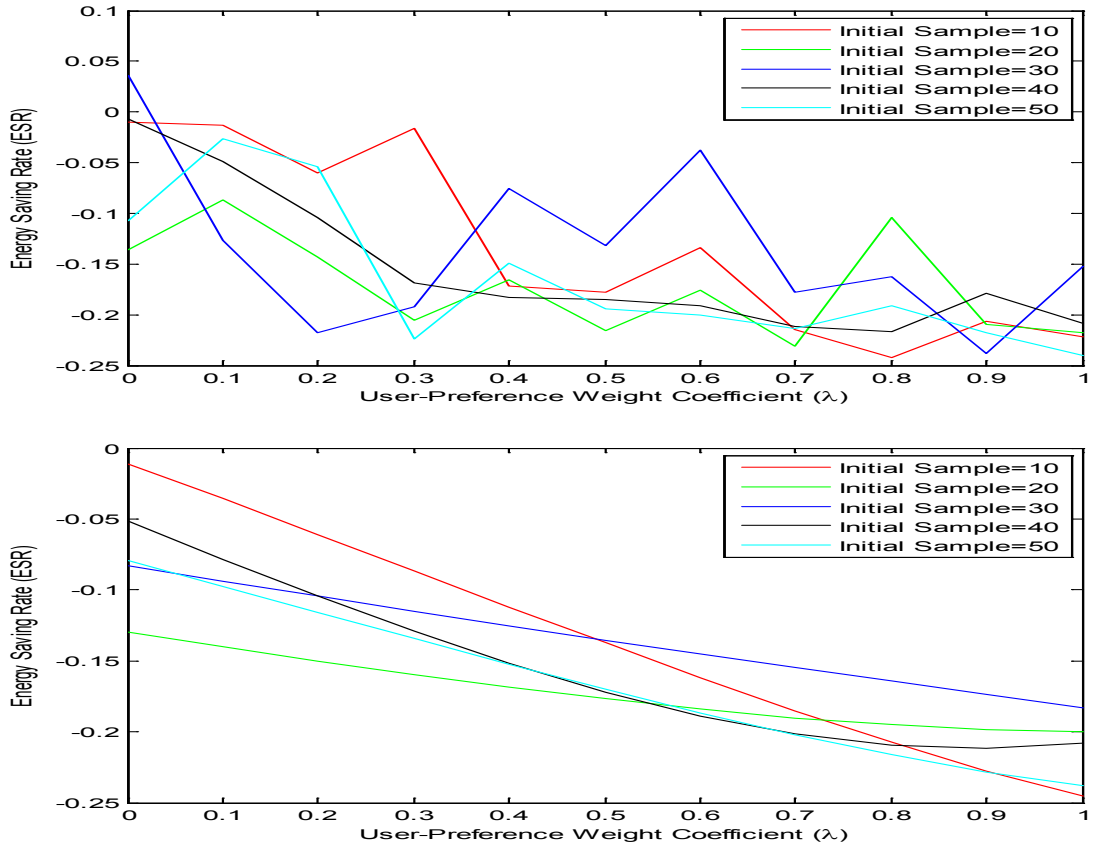

Figure A3.3: Energy Saving Rate BGPO Case 1 - Discrete(Upper) / Regression (Lower)

Study 3: EEE under BGPO and AFA

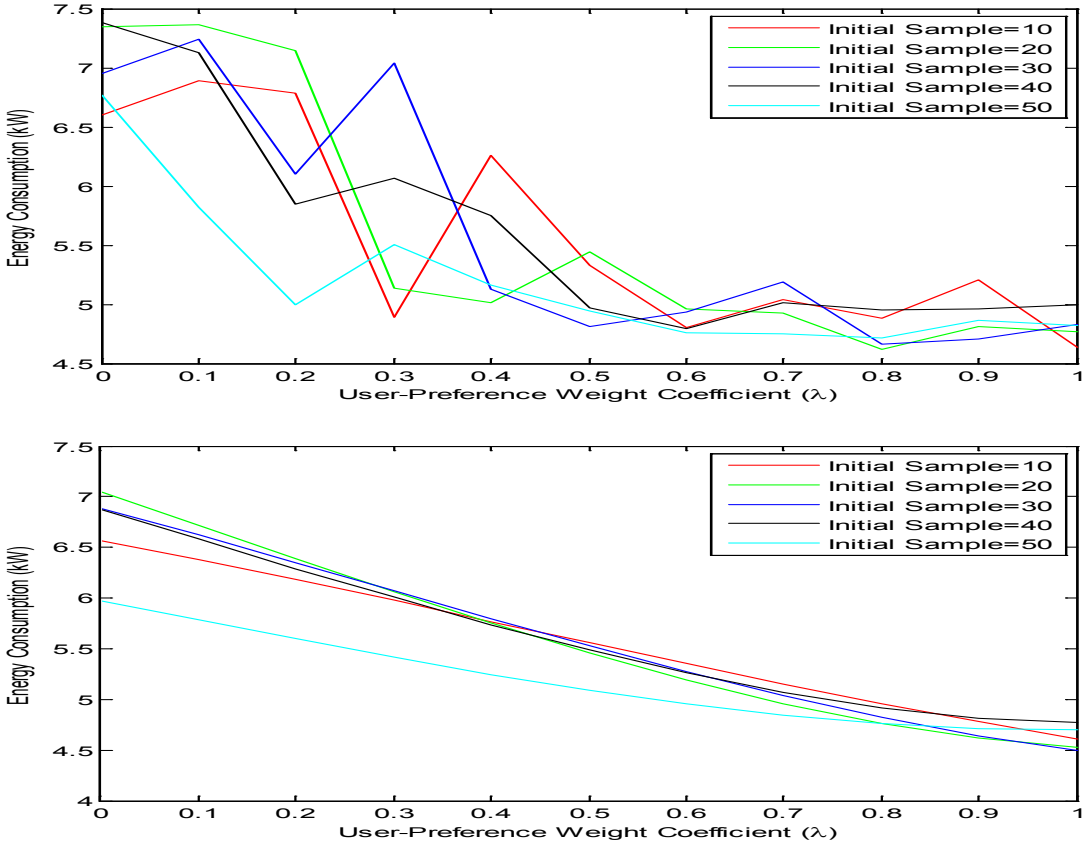

Figure A3.4: Energy Consumption BGPO Case 2 - Discrete(Upper) / Regression (Lower)

Study 3: EEE under BGPO and AFA

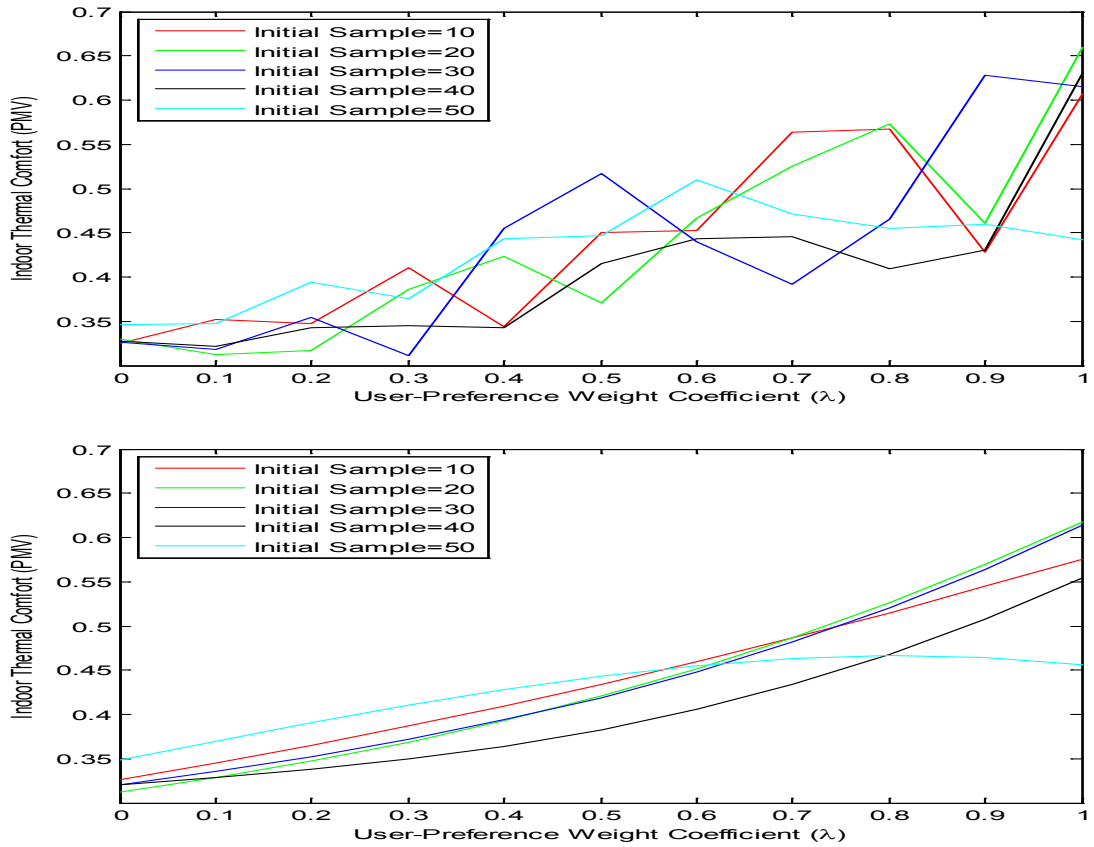

Figure A3.5: Indoor Thermal Comfort BGPO Case 2 - Discrete(Upper) / Regression (Lower)

Study 3: EEE under BGPO and AFA

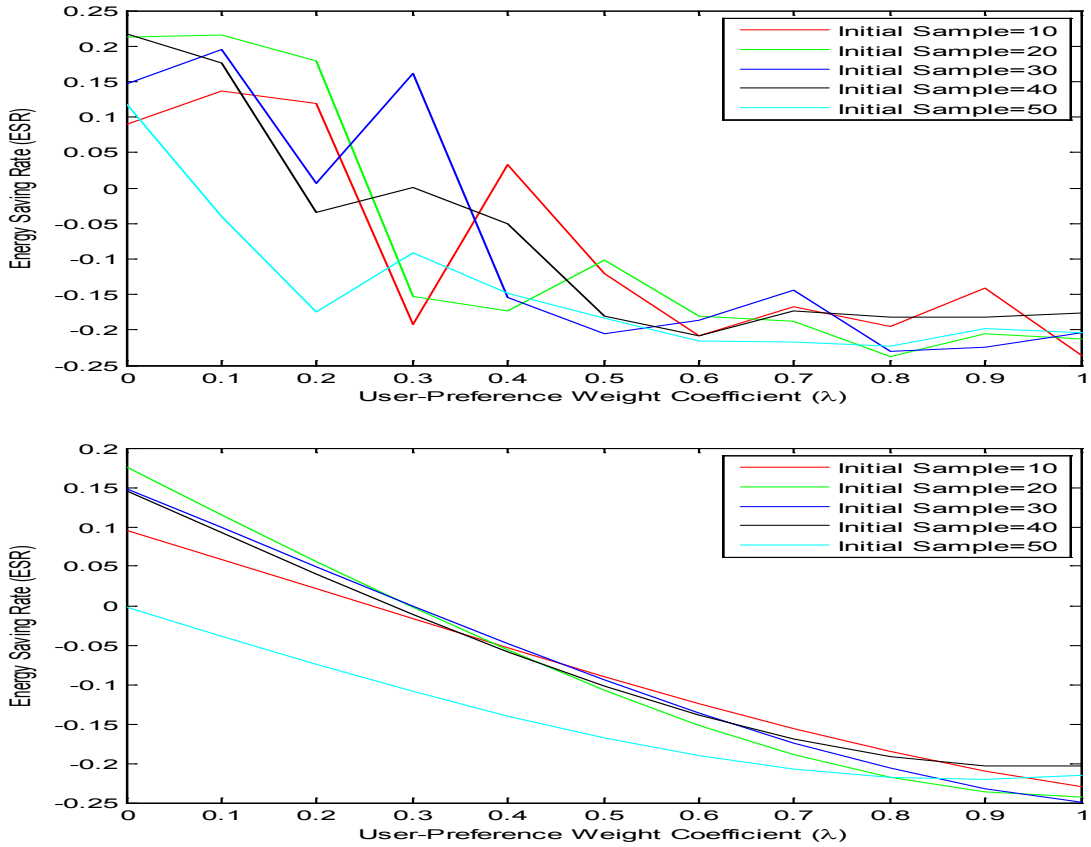

Figure A3.6: Energy Saving Rate BGPO Case 2 - Discrete(Upper) / Regression (Lower)

Study 3: EEE under BGPO and AFA

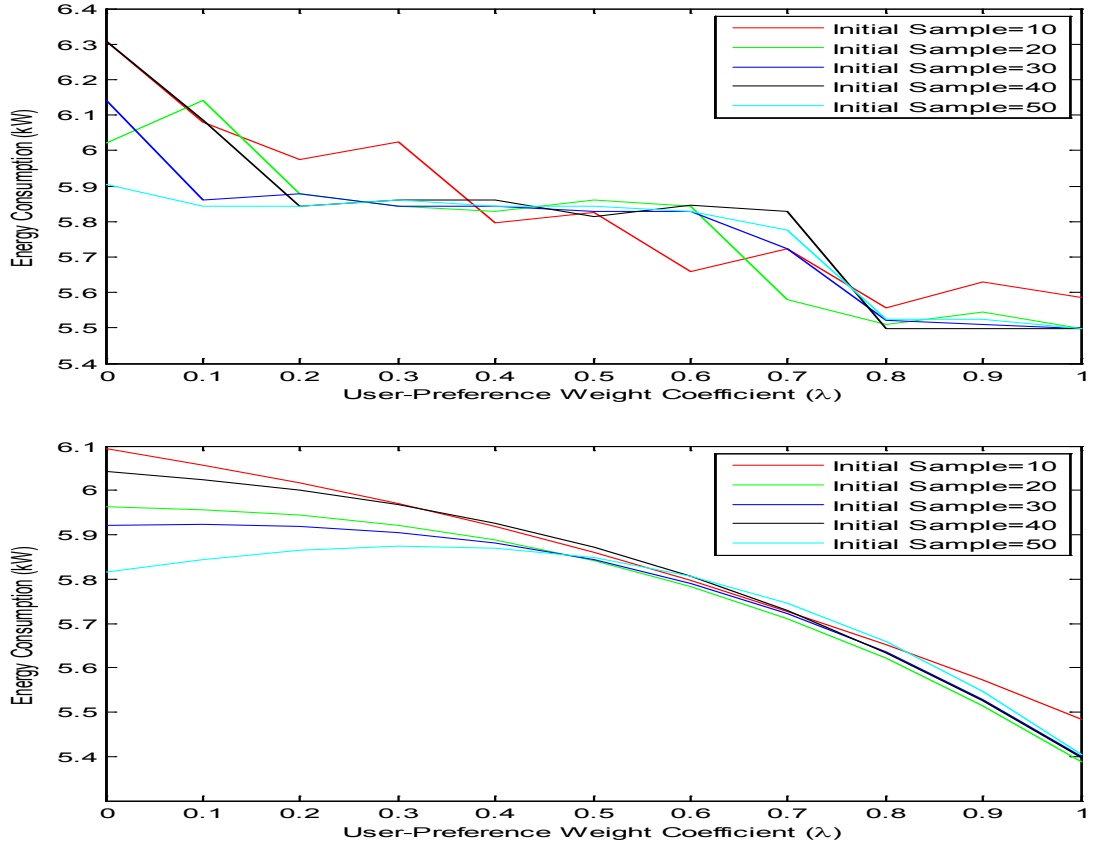

Figure A3.7: Energy Consumption AFA Case 1 - Discrete(Upper) / Regression (Lower)

Study 3: EEE under BGPO and AFA

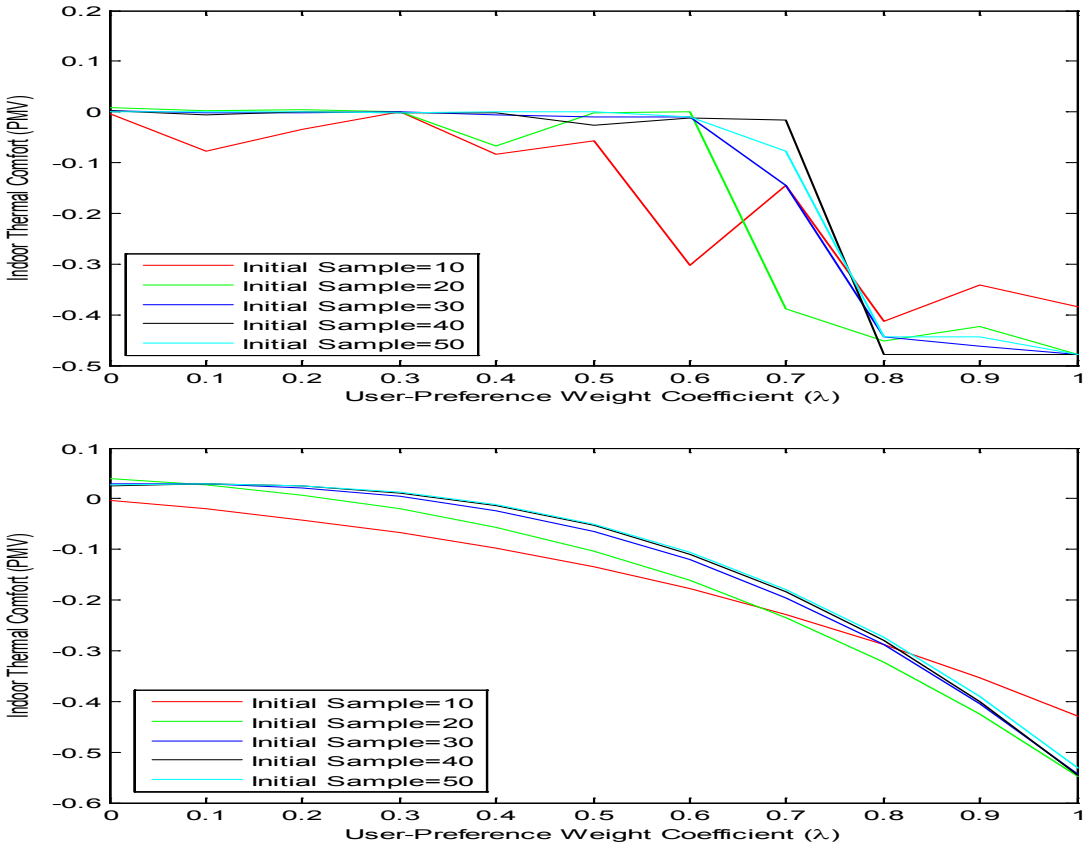

Figure A3.8: Indoor Thermal Comfort AFA Case 1 - Discrete(Upper) / Regression (Lower)

Study 3: EEE under BGPO and AFA

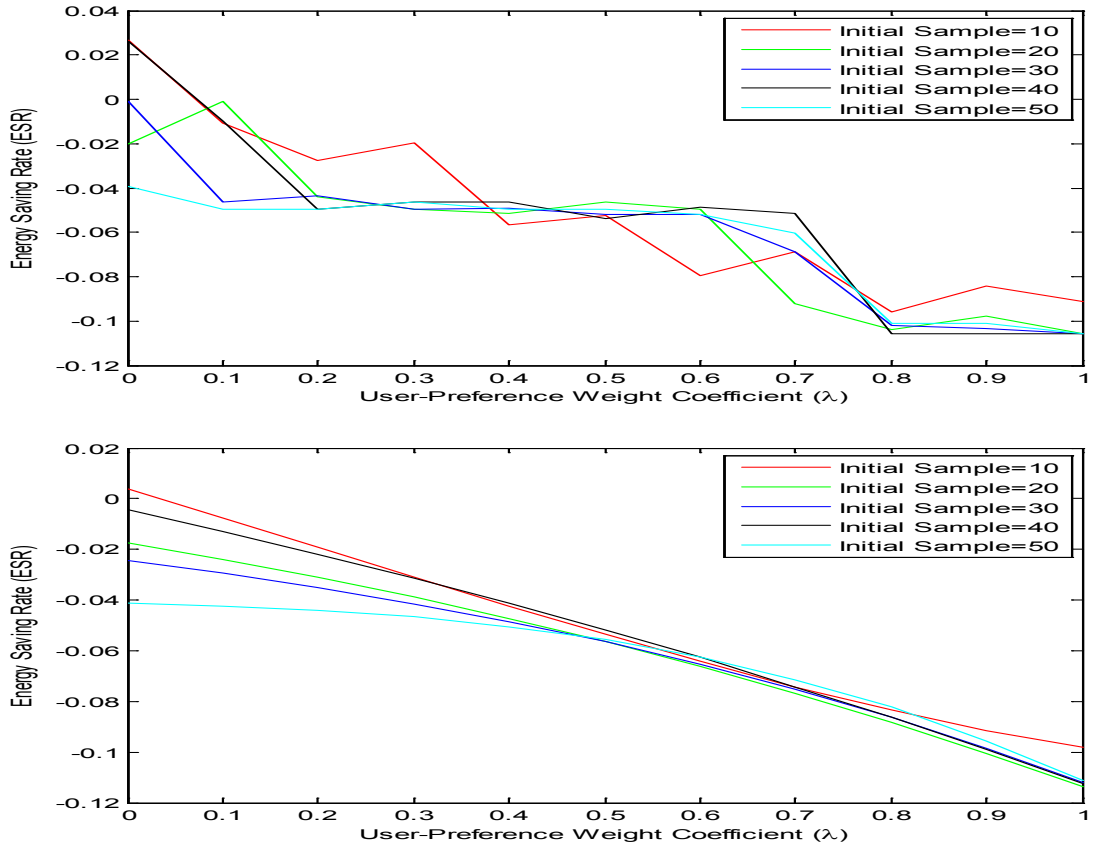

Figure A3.9: Energy Saving Rate AFA Case 1 - Discrete(Upper) / Regression (Lower)

Study 3: EEE under BGPO and AFA

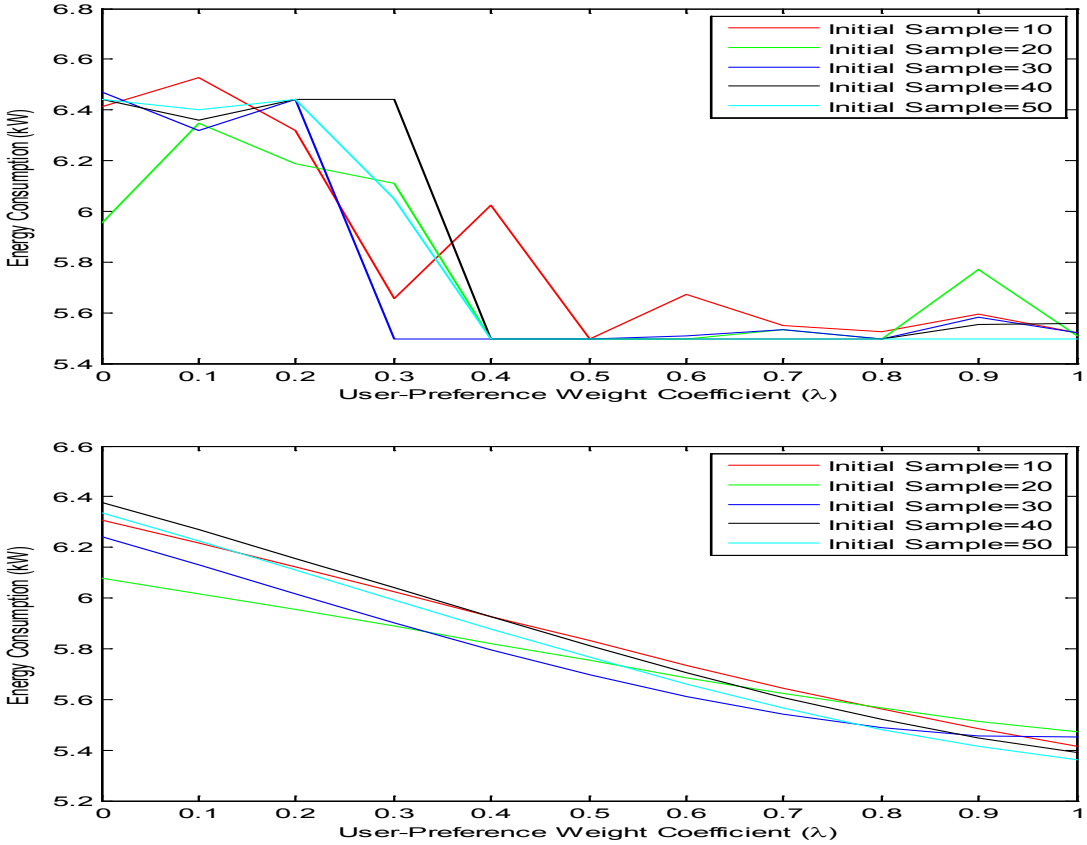

Figure A3.10: Energy Consumption AFA Case 2 - Discrete(Upper) / Regression (Lower)

Study 3: EEE under BGPO and AFA

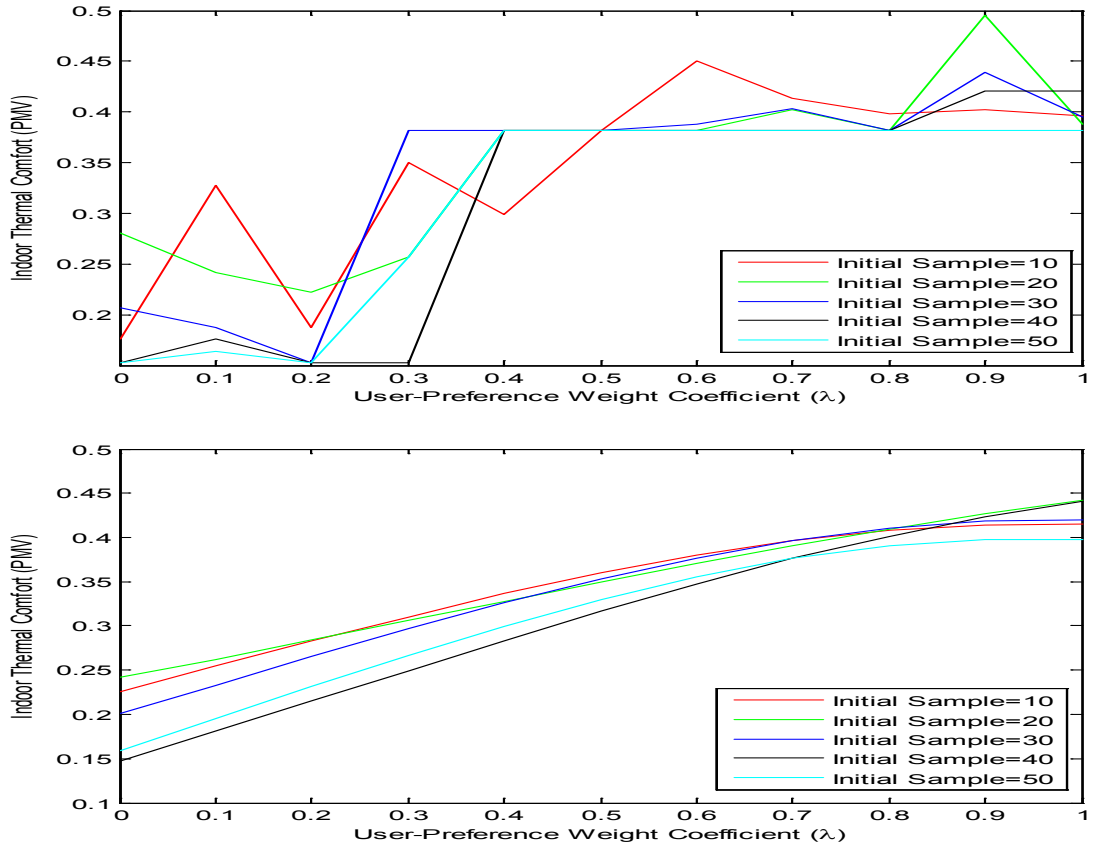

Figure A3.11: Indoor Thermal Comfort AFA Case 2 - Discrete(Upper) / Regression (Lower)

Study 3: EEE under BGPO and AFA

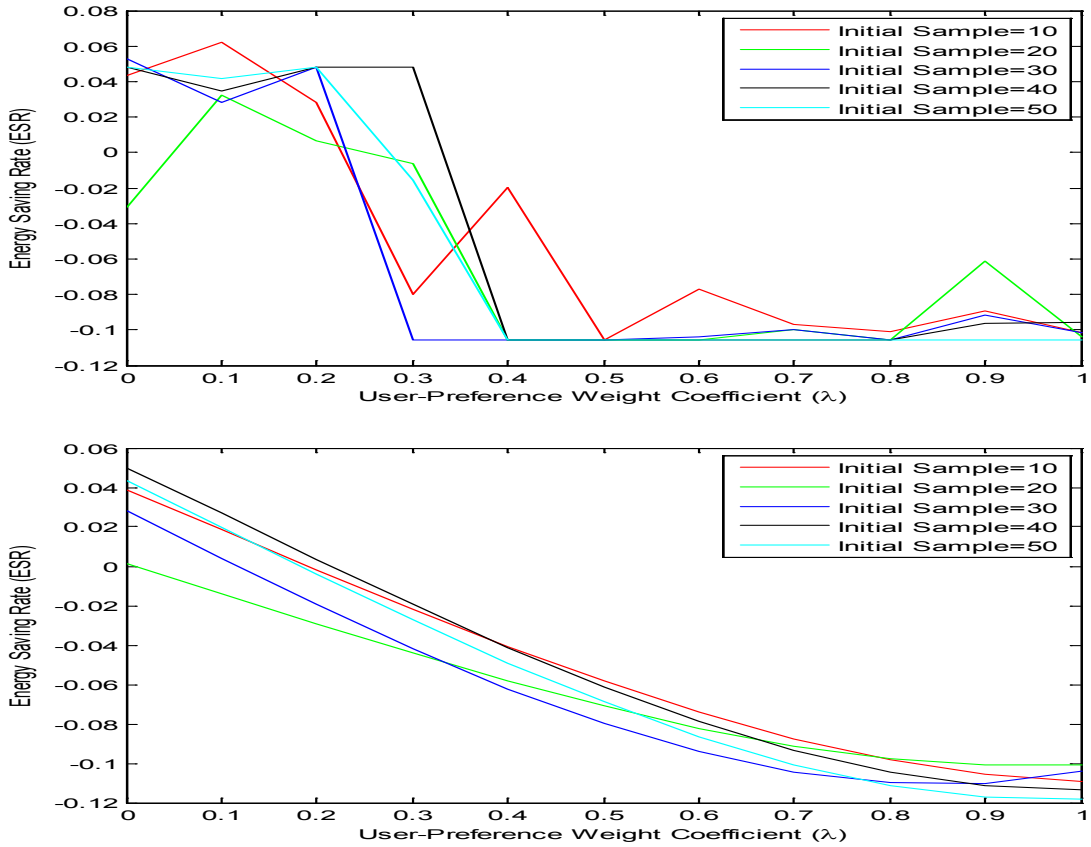

Figure A3.12: Energy Saving Rate AFA Case 2 - Discrete(Upper) / Regression (Lower)

Table A3.1: BGPO Evaluations for Case 1 and Case 2 (Note: Bold values are optimal results for each sample size.)

Sample	ESR Mean (Case 1)		ESR Mean (Case 2)		Sample	ESR Std Dev (Case 1)		ESR Std Dev (Case 2)	
	$\lambda \leq 0.3$	$\lambda \geq 0.7$	$\lambda \leq 0.3$	$\lambda \geq 0.7$		$\lambda \leq 0.3$	$\lambda \geq 0.7$	$\lambda \leq 0.3$	$\lambda \geq 0.7$
10	-0.0248	**−0.2213**	0.0382	-0.1847	10	0.0237	**0.0154**	0.1549	0.0405
20	-0.1429	-0.1907	0.1135	**−0.2112**	20	0.0487	0.0581	0.1784	**0.0209**
30	-0.1252	-0.1827	0.1274	**−0.2007**	30	0.1141	**0.0387**	0.0833	0.0392
40	-0.0820	**−0.2043**	0.0899	-0.1783	40	0.0700	0.0170	0.1253	**0.0047**
50	-0.1029	**−0.2158**	-0.0475	-0.2102	50	0.0874	0.0200	0.1229	**0.0114**
BGPO Mean Evaluations					BGPO Standard Deviation Evaluations				

Table A3.2: AFA Evaluations for Case 1 and Case 2 (Note: Bold values are optimal results for each sample size.)

Sample	ESR Mean (Case 1)		ESR Mean (Case 2)		Sample	ESR Std Dev (Case 1)		ESR Std Dev (Case 2)	
	$\lambda \leq 0.3$	$\lambda \geq 0.7$	$\lambda \leq 0.3$	$\lambda \geq 0.7$		$\lambda \leq 0.3$	$\lambda \geq 0.7$	$\lambda \leq 0.3$	$\lambda \geq 0.7$
10	-0.0079	-0.0850	0.0134	**−0.0973**	10	0.0239	0.0119	0.0637	**0.0056**
20	-0.0286	**−0.0998**	0.0005	-0.0926	20	0.0224	**0.0061**	0.0265	0.0210
30	-0.0351	-0.0949	0.0058	**−0.0996**	30	0.0229	0.0175	0.0750	**0.0060**
40	-0.0199	-0.0921	0.0449	**−0.1007**	40	0.0356	0.0270	0.0067	**0.0056**
50	-0.0462	-0.0920	0.0306	**−0.1056**	50	0.0047	0.0213	0.0310	**0.0000**
AFA Mean Evaluations					AFA Standard Deviation Evaluations				

Table A3.3: BGPO and AFA Evaluations for Case 1 and Case 2 at Sample=50 (Note: Bold values are optimal results.)

λ			0	0.1	0.2	0.3	0.4	0.5	0.6	0.7	0.8	0.9	1
Case 1	BGPO	ESR	-0.1074	-0.0265	-0.0537	-0.2239	-0.1496	-0.1947	-0.2007	-0.2133	-0.1914	-0.2183	**−0.2401**
		PMV	0.0087	0.0110	**0.0027**	-0.0313	0.0438	-0.1204	-0.0282	-0.0058	-0.0305	-0.1738	-0.1984
	AFA	ESR	-0.0394	-0.0495	-0.0495	-0.0464	-0.0495	-0.0495	-0.0519	-0.0602	-0.1011	-0.1011	**−0.1056**
		PMV	0.0008	**0.0007**	0.0007	-0.0011	0.0007	0.0007	-0.0098	-0.0778	-0.4442	-0.4442	-0.4792
Case 2	BGPO	ESR	0.1170	-0.0403	-0.1750	-0.0914	-0.1489	-0.1838	-0.2154	-0.2166	**−0.2224**	-0.1974	-0.2044
		PMV	**0.3463**	0.3472	0.3944	0.3758	0.4437	0.4469	0.5103	0.4715	0.4550	0.4595	0.4417
	AFA	ESR	0.0483	0.0416	0.0483	-0.0156	-0.1056	-0.1056	-0.1056	-0.1056	-0.1056	-0.1056	**−0.1056**
		PMV	**0.1524**	0.1640	0.1524	0.2570	0.3813	0.3813	0.3813	0.3813	0.3813	0.3813	0.3813

Table A3.4: Energy, Air Temperature and Air Velocity NN Model Evaluations

Entity	Model/Index	Number of Neurons									
		100	200	300	400	500	600	700	800	900	1000
Energy	NN/MSE	0.519825	0.479765	0.450205	0.431532	0.419206	0.410991	0.405697	0.40265	0.40143	0.40175
T_a		0.3143	0.297706	0.297414	0.296973	0.296671	0.29693	0.297347	0.297862	0.298474	0.299152
V_a		0.535912	0.496723	0.463521	0.436087	0.41408	0.396237	0.381513	0.369187	0.358755	0.349851

Learning Rate=0.01, Iteration=100 per epoch, Sigmoid Transfer Function.

Author's Publications

Journal Papers

1. **D. Zhai**, Y. C. Soh and X. Ou, "A Data-Driven Approach for Modeling Predictive Thermal State of Occupants," IEEE Transactions on Industrial Electronics (2019). [To be submitted]

2. **D. Zhai** and Y. C. Soh, "Data Driven Model-based Predictive Control and Bayesian Optimization for Energy Efficient ACMV Systems," Applied Energy (2019). [To be submitted]

3. **D. Zhai**, T. Chaudhuri and Y. C. Soh, "Modeling and optimization of different sparse augmented firefly algorithms for acmv systems under two case studies," Building and Environment, vol. 125, pp. 129-142, 2017.

4. **D. Zhai** and Y. C. Soh, "Balancing indoor thermal comfort and energy consumption of acmv systems via sparse swarm algorithms in optimizations," Energy and Buildings, vol. 149, pp. 1-15, 2017.

5. T. Chaudhuri, **D. Zhai**, Y. C. Soh, H. Li and L. Xie "Random forest based thermal comfort prediction from gender-specific physiological parameters using

wearable sensing technology," Energy and Buildings, vol. 166, pp. 391-406, 2018.

6. T. Chaudhuri, **D. Zhai**, Y. C. Soh, H. Li and L. Xie "Thermal comfort prediction using normalized skin temperature in a uniform built environment," Energy and Buildings, vol. 159, pp. 426-440, 2017.

7. X. Ou, W. Cai, X. He and **D. Zhai**, "Experimental investigations on heat and mass transfer performances of a liquid desiccant cooling and dehumidification system," Applied Energy, vol. 220, pp. 164-175, 2018.

8. X. Ou, W. Cai, X. He, X. Wang and **D. Zhai**, "A dynamic modeling of liquid desiccant cooling and dehumidification system for control and optimization," Energy and Buildings, vol. 163, pp. 44-57, 2017.

9. C. Jiang, Y. C. Soh, H. Li, M. K. Masood, Z. Wei, X. Zhou and **D. Zhai**, "CFD results calibration from sparse sensor observations with a case study for indoor thermal map," Building and Environment, vol. 117, pp. 166-177, 2017.

Conference Papers

1. **D. Zhai**, T. Chaudhuri, Y. C. Soh, X. Ou and C. Jiang, "Improvement of Energy Efficiency of Markov ACMV Systems based on PTS Information of Occupants," IEEE World Congress on Computational Intelligence (WCCI), Rio de Janeiro, Brazil, 2018.

2. **D. Zhai**, T. Chaudhuri and Y. C. Soh, "Energy efficiency improvement with k-means approach to thermal comfort for acmv systems of smart buildings," IEEE Asian Conference on Energy, Power and Transportation Electrification (ACEPT), pp. 203-208, Singapore, 2017.

3. **D. Zhai** and Y. C. Soh, "Balancing indoor thermal comfort and energy consumption of air-conditioning and mechanical ventilation systems via sparse Firefly algorithm optimization," IEEE 30th International Joint Conference on Neural Networks (IJCNN), pp. 1488-1494, Anchorage, Alaska, U.S.A., 2017.

4. **D. Zhai**, Y. C. Soh and W. Cai, "Operating points as communication bridge between energy evaluation with air temperature and velocity based on extreme learning machine (ELM) models," IEEE 11th International Conference on Industrial Electronics and Applications (ICIEA), pp. 712-716, Hefei, Anhui, China, 2016.

5. **D. Zhai** and Y. C. Soh, "Research on indoor air-flow measurements and predictions with different methods," International OSA Network of Students (IONS), The Optical Society, pp. 52-56, Nanjing, Jiangsu, China, 2015.

6. T. Chaudhuri, **D. Zhai**, Y. C. Soh, H. Li, L. Xie and X. Ou, "Convolutional Neural Network and Kernel Methods for Occupant Thermal State Detection

using Wearable Technology," IEEE World Congress on Computational Intelligence (WCCI), Rio de Janeiro, 2018.

Bibliography

[1] The paris protocol - a blueprint for tackling global climate change beyond 2020. *European Commission, 2015.*

[2] Herve Abdi and Lynne J. Williams. Principal component analysis. *Computational Statistics, Wiley*, 2, 2010.

[3] Adriana Acosta, Ana I. Gonzalez, Jesus M. Zamarreno, and Victor Alvarez. Energy savings and guaranteed thermal comfort in hotel rooms through nonlinear model predictive controllers. *Energy and Buildings, ELSEVIER*, 129:59–68, 2016. doi: 10.1016/j.enbuild.2016.07.061.

[4] Ahmed Qasim Ahmed, Shian Gao, and Ali Khaleel Kareem. Energy saving and indoor thermal comfort evaluation using a novel local exhaust ventilation system for office rooms. *Applied Thermal Engineering, ELSEVIER*, 110:821–834, 2017.

[5] A. Arabali, M. Ghofrani, M. Etezadi-Amoli, M. S. Fadali, and Y. Baghzouz. Genetic-algorithm-based optimization approach for energy management. *IEEE Transactions on Power Delivery*, 28:162–170, 2012. doi: 10.1109/TPWRD.2012.2219598.

[6] ASHRAE. Standard 55-2013 : Thermal environmental conditions for human occupancy. 2013.

[7] Ruben Baetens, Roel De Coninck, Juan Van Roy, Bart Verbruggen, Johan Driesen, Lieve Helsen, and Dirk Saelens. Assessing electrical bottlenecks at feeder level for residential net zero-energy buildings by integrated system simulation. *Applied Energy, ELSEVIER*, 96:74–83, 2012.

[8] Saadia Barbhuiya and Salim Barbhuiya. Thermal comfort and energy consumption in a uk educational building. *Building and Environment, ELSEVIER*, 68: 1–11, 2013.

[9] Christopher M. Bishop. *Neural networks for pattern recognition.* Oxford university press, 1995.

[10] Christopher M. Bishop. *Pattern Recognition and Machine Learning.* Springer, 2006.

[11] Stephen P. Boyd and Lieven Vandenberghe. *Convex Optimization.* Cambridge University Press, 2004.

[12] Eric Brochu, Vlad M. Cora, and Nando de Freitas. A tutorial on bayesian optimization of expensive cost functions, with application to active user modeling and hierarchical reinforcement learning. *arXiv.org*, 2010. doi: arxiv.org/abs/1012.2599.

[13] Edited by Geoffrey Hinton and Terrence J. Sejnowski. *Unsupervised Learning: Foundations of Neural Computation.* The MIT Press, 1999.

[14] C.G. Cassandras and S. Lafortune. *Introduction to Discrete Event Systems.* SpringerLink Engineering (2009). ISBN 9780387333328.

[15] Kristen S. Cetin, Lance Manuel, and Atila Novoselac. Effect of technology-enabled time-of-use energy pricing on thermal comfort and energy use in

mechanically-conditioned residential buildings in cooling dominated climates. *Building and Environment, ELSEVIER*, 96:118–130, 2016. doi: 10.1016/j.buildenv.2015.11.012.

[16] N Charkoudian. Skin blood flow in adult human thermoregulation: how it works, when it does not, and why. In *Mayo Clinic Proceedings*, pages 603–612, 2003. doi: 10.4065/78.5.603.

[17] Tanaya Chaudhuri, Deqing Zhai, Yeng Chai Soh, Hua Li, and Lihua Xie. Thermal comfort prediction using normalized skin temperature in a uniform built environment. *Energy and Buildings, ELSEVIER*, 159:426 – 440, 2018. doi: 10.1016/j.enbuild.2017.10.098.

[18] Xiao Chen, Qian Wang, and Jelena Srebric. Occupant feedback based model predictive control for thermal comfort and energy optimization: A chamber experimental evaluation. *Applied Energy, ELSEVIER*, 164:341–351, 2016. doi: 10.1016/j.apenergy.2015.11.065.

[19] Joon-Ho Choi and Vivian Loftness. Investigation of human body skin temperatures as a bio-signal to indicate overall thermal sensations. *Building and Environment, ELSEVIER*, 58:258–269, 2012. doi: 10.1016/j.buildenv.2012.07.003.

[20] Joon-Ho Choi and Vivian Loftness. Investigation of human body skin temperatures as a bio-signal to indicate overall thermal sensations. *Building and Environment, ELSEVIER*, 58:258–269, 2012.

[21] Changzhi Dai, Hui Zhang, Edward Arens, and Zhiwei Lian. Machine learning approaches to predict thermal demands using skin temperatures: Steady-state conditions. *Building and Environment, ELSEVIER*, 114:1–10, 2017. doi: 10.1016/j.buildenv.2016.12.005.

[22] Lyrian Daniel, Terence Williamson, and Veronica Soebarto. Comfort-based performance assessment methodology for low energy residential buildings in australia. *Building and Environment, ELSEVIER*, 111:169–179, 2017. doi: 10.1016/j.buildenv.2016.10.023.

[23] Wenyong Dong and MengChu Zhou. Gaussian classifier-based evolutionary strategy for multimodal optimization. *IEEE Transactions on Neural Networks and Learning Systems*, 25:1200–1216, 2014.

[24] Jean-Michel Dussault, Maarten Sourbron, and Louis Gosselin. Reduced energy consumption and enhanced comfort with smartwindows: Comparison between quasi-optimal, predictive andrule-based control strategies. *Energy and Buildings, ELSEVIER*, 127:680–691, 2016. doi: 10.1016/j.enbuild.2016.06.024.

[25] Andries P. Engelbrecht. *Computational Intelligence: An Introduction.* Wiley Publishing 2007, 2007.

[26] P.O. Fanger. *Thermal comfort: Analysis and applications in environmental engineering.* Danish Technical Press, 1970.

[27] Mohammad Hassan Fathollahzadeh, Ghassem Heidarinejad, and Hadi Pasdarshahri. Prediction of thermal comfort, iaq, and energy consumption in a dense occupancy environment with the under floor air distribution system. *Building and Environment, ELSEVIER*, 90:96–104, 2015. doi: 10.1016/j.buildenv.2015.03.019.

[28] Clifford Conrad Federspiel. User-adaptable and minimum-power thermal comfort control. *Massachusetts Institute of Technology*, 1992.

[29] P.M. Ferreira, A.E. Ruano, S. Silva, and E.Z.E. Conceicao. Neural networks

based predictive control for thermal comfort and energy savings in public buildings. *Energy and Buildings, ELSEVIER*, 55:238–251, 2012.

[30] Antonio Figueiredo, Jose Figueira, Romeu Vicente, and Rui Maio. Thermal comfort and energy performance: Sensitivity analysis to apply the passive house concept to the portuguese climate. *Building and Environment, ELSEVIER*, 103: 276–288, 2016.

[31] Katarzyna Gadyszewska-Fiedoruk. Correlations of air humidity and carbon dioxide concentration in the kindergarten. *Energy and Buildings, ELSEVIER*, 62: 45–50, 2013.

[32] Ali Ghahramani, Guillermo Castro, Burcin Becerik-Gerber, and Xinran Yu. Infrared thermography of human face for monitoring thermoregulation performance and estimating personal thermal comfort. *Building and Environment, ELSEVIER*, 109:1–11, 2016. doi: 10.1016/j.buildenv.2016.09.005.

[33] Ian Goodfellow, Yoshua Bengio, and Aaron Courville. *Deep Learning*. The MIT Press, 2016. `http://www.deeplearningbook.org`.

[34] David J. Hand. Principles of data mining. *Drug safety*, 30(7):621–622, 2007.

[35] Yingdong He, Nianping Li, Linxuan Zhou, Kuan Wang, and Wenjie Zhang. Thermal comfort and energy consumption in cold environment with retrofitted huotong (warm-barrel). *Building and Environment, ELSEVIER*, 112:285–295, 2017. doi: 10.1016/j.buildenv.2016.11.044.

[36] Yueer He, Meng Liu, Thomas Kvan, and Shini Peng. An enthalpy-based energy savings estimation method targeting thermal comfort level in naturally ventilated

buildings in hot-humid summer zones. *Applied Energy, ELSEVIER*, 187:717–731, 2017. doi: 10.1016/j.apenergy.2016.11.098.

[37] J. C. Ho, G. Jindal, and M. Low. Singapore's intended nationally determined contribution for cop21 climate conference in paris. *Energy Studies Institute, 2015.*

[38] John Henry Holland. *Adaptation in Natural and Artificial Systems.* University of Michigan Press, 1975.

[39] David W. Hosmer and Stanley Lemeshow. *Applied Logistic Regression.* A Wiley-Interscience Publication, 2000.

[40] Tapas Kanungo, David M. Mount, Nathan S. Netanyahu, Christine D. Piatko, Ruth Silverman, and Angela Y. Wu. An efficient k-means clustering algorithm: Analysis and implementation. *IEEE Transactions on Pattern Analysis and Machine Intelligence*, 24(7):881–892, 2002.

[41] James Kennedy and Russell Eberhart. Particle swarm optimization. In *IEEE international conference on neural networks*, pages 1942–1948, 1995. doi: 10.1109/ICNN.1995.488968.

[42] Jeong Tai Kim, Ji Hyun Lim, Sun Ho Cho, and Geun Young Yun. Development of the adaptive pmv model for improving prediction performances. *Energy and Buildings, ELSEVIER*, 98:100–105, 2015.

[43] Jimin Kim, Taehoon Hong, Jaemin Jeong, Choongwan Koo, and Kwangbok Jeong. An optimization model for selecting the optimal green systems by considering the thermal comfort and energy consumption. *Applied Energy, ELSEVIER*, 169:682–695, 2016. doi: 10.1016/j.apenergy.2016.02.032.

[44] N. Klepeis. The national human activity pattern survey (nhaps) - a resource for assessing exposure to environmental pollutants. *National Exposure Research Laboratory, U.S. Environmental Protection Agency.*

[45] Andrew Kusiak. Intelligent manufacturing systems. *PRENTICE HALL PRESS, 200 OLD TAPPAN ROAD, OLD TAPPAN, NJ 07675, USA, 1990, 448*, 1990.

[46] Andrew Kusiak and Mingyang Li. Cooling output optimization of an air handling unit. *Applied Energy, ELSEVIER*, pages 901–909, 2010. doi: 10.1016/j.apenergy.2009.06.010.

[47] Ranald Lawrence and Charlotte Keime. Bridging the gap between energy and comfort: Post-occupancy evaluation of two higher-education buildings in sheffield. *Energy and Buildings, ELSEVIER*, 130:651–666, 2016.

[48] A. Leavey, Y. Fu, M. Sha, A. Kutta, C. Lu, W. Wang, B. Drake, Y. Chen, and P. Biswas. Air quality metrics and wireless technology to maximize the energy efficiency of hvac in a working auditorium. *Building and Environment, ELSEVIER*, pages 287–297, 2015.

[49] Jiajia Li, Botao Wang, and Guoren Wang. Elm based efficient probabilistic threshold query on uncertain data. In *Proceedings of ELM-2014 Volume 1-Algorithms and Theories*, pages 71–80, 2014. doi: 10.1007/978-3-319-14063-6_7.

[50] Kangji Li, Chenglei Hu, Guohai Liu, and Wenping Xue. Building's electricity consumption prediction using optimized artificial neural networks and principal component analysis. *Energy and Buildings, ELSEVIER*, 108:106–113, 2015. doi: 10.1016/j.enbuild.2015.09.002.

[51] Shin-Yeu Lin, Shih-Ching Chiu, and Wei-Yuan Chen. Simple automatic supervisory control system for office building based on energy-saving decoupling indoor comfort control. *Energy and Buildings, ELSEVIER*, 86:7–15, 2015.

[52] Weiwei Liu, Zhiwei Lian, and Qihong Deng. Use of mean skin temperature in evaluation of individual thermal comfort for a person in a sleeping posture under steady thermal environment. *Indoor and Built Environment, ELSEVIER*, 24: 489–499, 2014. doi: 10.1177/1420326X14527975.

[53] Weiwei Liu, Zhiwei Lian, and Qihong Deng. Use of mean skin temperature in evaluation of individual thermal comfort for a person in a sleeping posture under steady thermal environment. *Indoor and Built Environment*, 24(4):489499, 2015. doi: 10.1177/1420326X14527975.

[54] Ning Mao, Mengjie Song, and Shiming Deng. Application of topsis method in evaluating the effects of supply vane angle of a task/ambient air conditioning system on energy utilization and thermal comfort. *Applied Energy, ELSEVIER*, 180:536–545, 2016.

[55] Jin Woo Moon and Sung Kwon jung. Development of a thermal control algorithm using artificial neural network models for improved thermal comfort and energy efficiency in accommodation buildings. *Applied Thermal Engineering, ELSEVIER*, 103:1135–1144, 2016.

[56] NEA and Singapore. Stricter energy performance standards for air-conditioners from september 2016. `http://www.nea.gov.sg/corporate-functions/newsroom/news-releases/stricter-energy-performance-standards-for-air-conditioners-from-september-2016`, Accessed: 2016-12-20.

[57] Andrew Ng and Dan Boneh. Cs229: Machine learning, 2017. URL `http://cs229.stanford.edu/`.

[58] Adam ODonovan, P.D. OSullivan, and Michael D. Murphy. A field study of thermal comfort performance for a slotted louvreventilation system in a low energy retrofit. *Energy and Buildings, ELSEVIER*, 135:312–323, 2017.

[59] Omkar M Parkhi, Andrea Vedaldi, C. V. Jawahar, and Andrew Zisserman. The truth about cats and dogs. In *Proceedings of IEEE International Conference on Computer Vision*, pages 1427–1434, 2011.

[60] Marco Pritoni, Kiernan Salmon, Angela Sanguinetti, Joshua Morejohn, and Mark Modera. Occupant thermal feedback for improved efficiency in university buildings. *Energy and Buildings, ELSEVIER*, 144:241–250, 2017. doi: 10.1016/j.enbuild.2017.03.048.

[61] C. E. Rasmussen and C. K. I. Williams. *Gaussian Processes for Machine Learning*. MIT Press, Cambridge, Massachusetts,, 2006.

[62] John O. Rawlings, Sastry G. Pantula, and David A. Dickey. *Applied Regression Analysis*. Springer, 1988.

[63] Frank Rosenblatt. The perceptron - a perceiving and recognizing automaton. *Report, Cornell Aeronautical Laboratory*, pages 85–460–1, 1957.

[64] Antonio E. Ruano, Shabnam Pesteh, Sergio Silva, Helder Duate, Goncalo Mestre, Pedro M. Ferreira, Hamid R. Khosravani, and Ricardo Horta. The imbpc hvac system: A complete mbpc solution for existing hvac systems. *Energy and Buildings, ELSEVIER*, 120:145–158, 2016.

[65] Dirk Saelens, Jan Carmeliet, and Hugo Hens. Energy performance assessment of multiple-skin facades. *HVACR Research*, 9:167–185, 2003.

[66] Dirk Saelens, Wout Parys, and Ruben Baetens. Energy and comfort performance of thermally activated building systems including occupant behavior. *Building and Environment*, 46:835–848, 2011.

[67] Sally Shahzad, John Brennan, Dimitris Theodossopoulos, Ben Hughes, and John Kaiser Calautit. Energy and comfort in contemporary open plan and traditional personal offices. *Applied Energy, ELSEVIER*, 185:1542–1555, 2017.

[68] Max H. Sherman. Simplified model of thermal comfort. *Energy and Buildings, ELSEVIER*, 8, 1985.

[69] Jonathon Shlens. A tutorial on principal component analysis. *arXiv*, 2014.

[70] David Silver, Julian Schrittwieser, Karen Simonyan, Ioannis Antonoglou, Aja Huang, Arthur Guez, Thomas Hubert, Lucas Baker, Matthew Lai, Adrian Bolton, Yutian Chen, Timothy Lillicrap, Fan Hui, Laurent Sifre, George van den Driessche, Thore Graepel, and Demis Hassabis. Mastering the game of go without human knowledge. *Nature*, 550:354–359, 2017. doi: 10.1038/nature24270.

[71] Soo Young Sim, Myung Jun Koh, Kwang Min Joo, Seungwoo Noh, Sangyun Park, Youn Ho Kim, and Kwang Suk Park. Estimation of thermal sensation based on wrist skin temperatures. *Sensors (Basel)*, 16, 2016. doi: 10.3390/s16040420.

[72] Adrian Streinu-Cercel, Sergiu Costoiu, Maria Mrza, Anca Streinu-Cercel, and Monica Mrza. Models for the indices of thermal comfort. *Journal of Medicine and Life*, X, 2017.

[73] Richard S. Sutton and Andrew G. Barto. *Reinforcement Learning: An Introduction*. The MIT Press, 1998.

[74] Satoru Takada, Sho Matsumoto, and Takayuki Matsushita. Prediction of whole-body thermal sensation in the non-steady state based on skin temperature. *Building and Environment, ELSEVIER*, 68:123–133, 2013. doi: 10.1016/j.buildenv.2013.06.004.

[75] Toolbox. Clothing and thermal insulation. `http://www.engineeringtoolbox.com/clo-clothing-thermal-insulation-d_732.html`, Accessed: 2017-06-20.

[76] Toolbox. Metabolic rate. `http://www.engineeringtoolbox.com/met-metabolic-rate-d_733.html`, Accessed: 2017-06-20.

[77] Allen M. Turing. Computing machinery and intelligence. *Mind*, 1950.

[78] Ali Vedavarz, Sunil Kumar, and Muhammed Iqbal Hussain. *HVAC: Handbook of Heating, Ventilation and Air Conditioning for Design and Implementation*. SpringerLink Engineering (2009). ISBN 0831131632,9780831131630.

[79] Yang Wang, Jens Kuckelkorn, Fu-Yun Zhao, Di Liu, Alexander Kirschbaum, and Jun-Liang Zhang. Evaluation on classroom thermal comfort and energy performance of passive school building by optimizing hvac control systems. *Building and Environment, ELSEVIER*, 89:86–106, 2015. doi: 10.1016/j.buildenv.2015.02.023.

[80] D. Randall Wilson and Tony R. Martinez. The general inefficiency of batch training for gradient descent learning. *Neural Networks, ELSEVIER*, 16:1429–1451, 2003.

[81] D.H. Wolpert and W.G. Macready. No free lunch theorems for optimization. *IEEE Transactions on Evolutionary Computation*, 1:67–82, 1997.

[82] L. T. Wong, K. W. Mui, and C. T. Cheung. Bayesian thermal comfort model. *Building and Environment, ELSEVIER*, 82:171–179, 2014. doi: 10.1016/j.buildenv.2014.08.018.

[83] Jing Xiong, Xin Zhou, Zhiwei Lian, Jianxiong You, and Yanbing Lin. Thermal perception and skin temperature in different transient thermal environments in summer. *Energy and Buildings, ELSEVIER*, 128:155–163, 2016. doi: 10.1016/j.enbuild.2016.06.085.

[84] Xin Yan and Xiaogang Su. *Linear regression analysis: theory and computing*. World Scientific, 2009.

[85] Xin-She Yang. *Nature-inspired metaheuristic algorithms*. 1st ed. Frome, UK: Luniver Press, 2008.

[86] Xin-She Yang. Firefly algorithms for multimodal optimisation. In *Proceedings fifth symposium on stochastic algorithms, foundations and applications*, pages 169–178, 2009.

[87] Xin-She Yang. *Nature-Inspired Optimization Algorithms*. ELSEVIER, 2014.

[88] Wei Yu, Baizhan Li, Hongyuan Jia, Ming Zhang, and Di Wang. Application of multi-objective genetic algorithm to optimize energy efficiency and thermal comfort in building design. *Energy and Buildings, ELSEVIER*, 88:135–143, 2015. doi: 10.1016/j.enbuild.2014.11.063.

[89] Wim Zeiler, Michal Vesely, Derek Vissers, and Rongling Li. Thermal response of different body parts: The fingertip as control sensor for personalized heating.

Energy Procedia, ELSEVIER, 78:2766–2771, 2015. doi: 10.1016/j.egypro.2015.11.622.

[90] Deqing Zhai and Yeng Chai Soh. Balancing indoor thermal comfort and energy consumption of acmv systems via sparse swarm algorithms in optimizations. *Energy and Buildings, ELSEVIER*, 149:1–15, 2017. doi: 10.1016/j.enbuild.2017.05.019.

[91] Deqing Zhai and Yeng Chai Soh. Balancing indoor thermal comfort and energy consumption of air-conditioning and mechanical ventilation systems via sparse firefly algorithm optimization. In *Proceedings of IEEE Joint Conference on Neural Networks*, pages 1488–1494, 2017. doi: 10.1109/IJCNN.2017.7966028.

[92] Deqing Zhai, Yeng Chai Soh, and Wenjian Cai. Operating points as communication bridge between energy evaluation with air temperature and velocity based on extreme learning machine (elm) models. In *Proceedings of IEEE Conference on Industrial Electronics and Applications*, pages 712–716, 2016. doi: 10.1109/ICIEA.2016.7603675.

[93] Deqing Zhai, Tanaya Chaudhuri, and Yeng Chai Soh. Energy Efficiency Improvement with k-means Approach to Thermal Comfort for ACMV Systems of Smart Buildings. In *IEEE Asian Conference on Energy, Power and Transportation Electrification (ACEPT)*, pages 203–208, October 2017.

[94] Deqing Zhai, Tanaya Chaudhuri, and Yeng Chai Soh. Modeling and optimization of different sparse augmented firefly algorithms for acmv systems under two case studies. *Building and Environment, ELSEVIER*, 125:129–142, 2017. doi: 10.1016/j.buildenv.2017.08.032.

[95] Deqing Zhai, Tanaya Chaudhuri, Yeng Chai Soh, Xianhua Ou, and Chaoyang Jiang. Improvement of energy efficiency of markov acmv systems based on pts information of occupants. In *IEEE World Congress on Computational Intelligence (WCCI)*, pages 3303–3309, July 2018.

[96] Hui Zhang, Edward Arens, Charlie Huizenga, and Taeyoung Han. Thermal sensation and comfort models for non-uniform and transient environments, part iii: Whole-body sensation and comfort. *Building and Environment, ELSEVIER*, 45:299 – 410, 2010. doi: 10.1016/j.buildenv.2009.06.020.

[97] Weiwei Zhang, Jian Sun, and Xiaoou Tang. Cat head detection - how to effectively exploit shape and texture features. In *Proceedings of European Conference on Computer Vision*, pages 802–816, 2008.

[98] Yuanhui Zhang. *Indoor Air Quality Engineering*. CRC Press, 2004.

[99] MengChu Zhou and Kurapati Venkatesh. *Modeling, Simulation, And Control Of Flexible Manufacturing Systems: A Petri Net Approach*. World Scientific Publishing Co Pte Ltd, 1999.